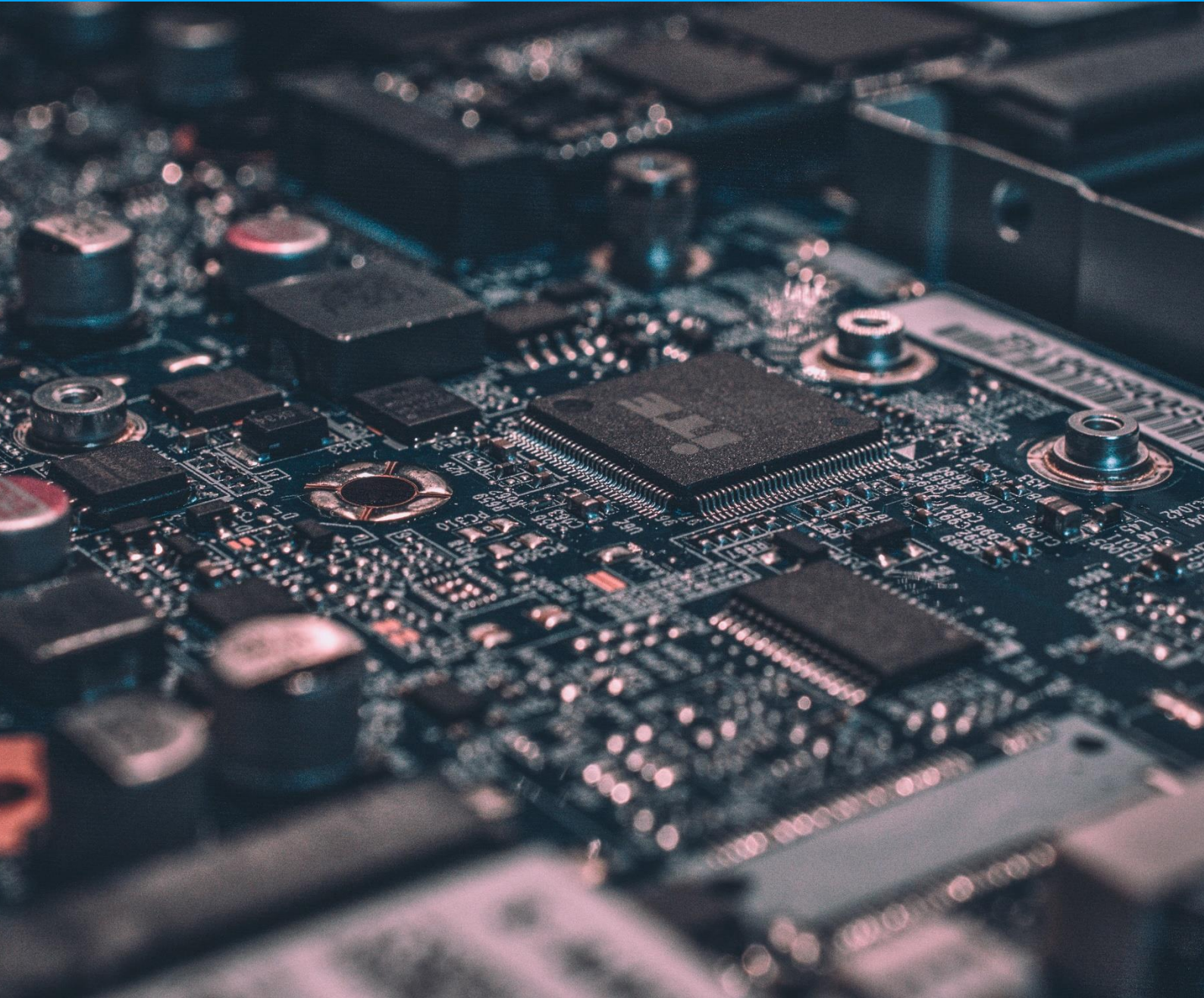# BOARD LEVEL VIBRATION TESTING AND QUALIFICATION FOR AUTOMOTIVE APPLICATIONS

Chinghsuan Chou

TUDelft

BOARD LEVEL VIBRATION TESTING AND QUALIFICATION FOR AUTOMOTIVE APPLICATIONS

In partial fulfillment of the requirements for the degree of

Master of Science

In
Electrical Engineering
At the Delft University of Technology
To be defended on October 20, 2021 at 09:00AM

by

Chinghsuan Chou

Student number:	4997182
Project duration:	September 21, 2020 - September 7, 2021
Supervisor	Prof.dr.ir. GuoQi Zhang
	Mr. Varun Thukral
Thesis committee:	Prof.dr.ir. GuoQi Zhang
	Prof.dr.ir. Rob Ross
	Prof.dr.ir. Willem van Driel

ACKNOWLEDGEMENTS

CONTENTS

LIST OF FIGURES

LIST OF TABLES

ACRONYMS

1 | INTRODUCTION

In this chapter, available vibration test methods and industrial specifications are presented. The electronic package is explained firstly, following with reliability theory and recent studies on vibration test methods at board level and module level. Vibration measurement method, hardware design consideration, failure monitoring techniques and environment factors are included in this section. Some appropriate failure analysis techniques for the test board are introduced. In the end, the research objectives and motivation are drawn.

1.1 ELECTRONIC PACKAGING AND RELIABILITY

Electronic Packaging:
Electronic packaging consists of the design and production of packages. Functions such as signal distribution, heat dissipation, and power distribution must be provided for microelectronic devices [19]. Also, the package should be able to support and protect the circuit for better reliability. In the past 60 years, packaging has enormously evolved. The improvements in technologies and the explosion of electronic devices have pushed this evolution. In general, packages can be classified into two categories, through-hole and Surface Mount Device (SMD). In this thesis, Ball Grid Array (BGA) and advanced Chip Scale Package (CSP) are analyzed. When comparing to the through-hole device, SMD involve much higher density because components can be soldered at both sides of the Printed Circuit Board (PCB). While pins of the through-hole device need to go through a multilayered PCB. SMD creates less parasitic inductance and capacitance due to shorter pins.
BGA is a type of package, often used to mount integrated circuits (microprocessors). There is a different kind of BGA, depending on the materials used for the substrate such as ceramic, plastic, or metal [11]. Solder joints are balls are arranged in a grid on the surface of the package to increase the area connected. The substrate carrier of this package is made up of plastic laminated, designed specifically for one package. The PCB is needed to connect the components to the solder balls. The material composing used for building such a PCB, is chosen to improve signal quality. The substrate material needed is selected to

meet the signal integrity requirements, for example, a special material should be used for processing RF signals to ensure that the substrate does not reduce the signal quality.

CSP is defined by J-STD-012 standard [14] that the edge length of the package should be within 1.2 times than the chip and the area should be 1.5 times less than the chip. It provides a smaller footprint which can offer more pins per unit area (typical outline is mentioned above) compare with the BGA package. Besides, CSP has better heat dissipation due to smaller thickness and smaller effective contact area with PCB. The parasitic effect is reduced due to the wiring is shorter from chip to the board which increases the performance at high frequency.

Reliability Theory:
Reliability engineering plays an important role in the current technology due to the safety issue. To evaluate mechanical and thermo-mechanical reliability, accelerated experiments such as thermal cycling, shock test, drop test, and vibration test are used for inducing failures and access electronic product reliability. The service life of components can be predicted by applying failure distribution functions on the reliability data generated by experimental testing. To characterize material in a certain environmental condition, and to analyze its capacity to resist mechanical or electrical, reliability analysis is needed to define the behavior in every phase of life. This analysis is important to measure the impact of a stressed condition, shape, sample size, and understand the nature of failures in a given component. In mathematics, the reliability function is based on a cumulative density function. The probability can be given by the following equations [18]:

$$F(t) = \int_t^0 f(s) \cdot ds \tag{1.1}$$

In reliability, the probability represents the probability of a unit failing at a given time interval t and $0 \le s \le t$. F is the probability of failure. In the tests, there are only 2 possibilities for the product: either fail or stay. Those are exclusives events. Therefore, from basic laws of probability:

$$(t) + R(t) = 1 \tag{1.2}$$

$$R(t) = 1 - Q(t) \tag{1.3}$$

$$R(t) = 1 - \int_t^0 f(s) \cdot ds \tag{1.4}$$

$$R(t) = \int_t^\infty f(s)ds \qquad (1.5)$$

Where R(t) is the reliability function. The figure 1.1 illustrates the relationship between the reliability function and the unreliability function.
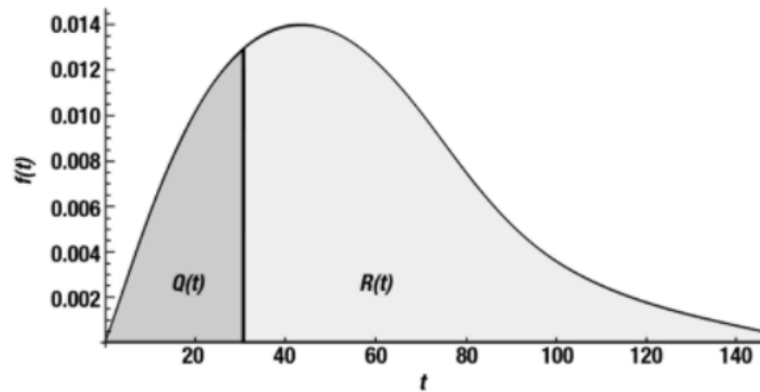
Figure 1.1: Probability density function [18]

Reliability Classification:
When it comes to micro-electronic-based reliability, it can be discussed by assessing the interaction among chip, package, and PCBs [31]. It can be categorized into four different levels, package (1st) level, board level (2nd), module (3rd) level and system (4th) level. In each level, the main purpose of the reliability test is distinct.
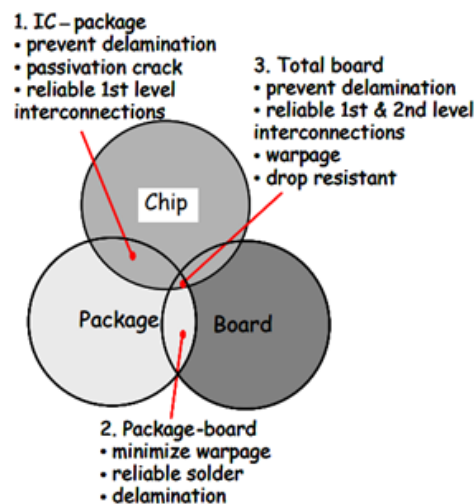
Figure 1.2: Focus area of reliability [31]

Component level (first level) reliability is intended to investigate the robustness of the packaging stresses under environmental tests. Therefore, it does not consider the solder joint reliability when it is mounted

on some PCB. During board-level reliability testing is aimed at mimicking situations such as shipment, IC mounting, and field application environments. Normally, mechanical, electrical, thermal-mechanical, and humidity are the four main stressed loadings for package reliability tests. In Board Level Reliability (BLR), which is typically considered as second-level reliability, characterizes the mechanical and thermo-mechanical robustness of the solder joint interconnect that is formed in between component and PCB. Common mechanical or thermo-mechanical tests such as thermal cycling, drop test, shock test, or vibration are conducted to induce failures on the solder joints. An electronic module in this thesis is defined as a single unit in a system that can function independently, such as a power module and radar module in a vehicle. Module-level reliability evaluates the reliability performance of solder joints on the component of interest. It is mounted on PCB with other components and clamped on the position where it should be under real application such as heatsink. In other words, it is board-level reliability when PCB is mounted in an electronic housing. Electronic systems such as automotive, airplane, or missiles contain a large number of PCBs and numerous ICs. This causes complexity of evaluation on its reliability performance. The failures that happened on circuits, components, or solder joints will induce failures in the final system. Therefore, evaluation on system-level reliability needs to rely on the reliability testing data from the lower levels such as module level and board level.
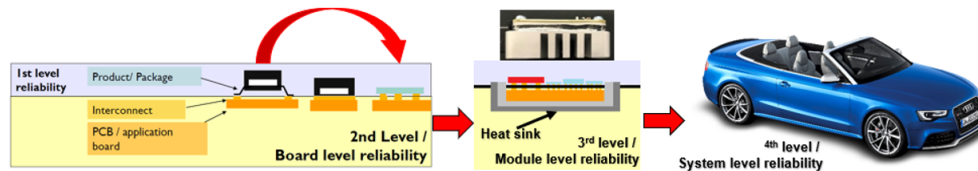
Figure 1.3: Reliability classification

1.2 VIBRATION TEST

The vibration test hardware comprises four major elements, including control system, amplifier, shaker, and accelerometer, to form a control feedback loop as described in figure 1.4. Besides this, a vibration fixture plate is bolted on top of the shaker armature. It acts as a mechanical adapter between the shaker and test board.
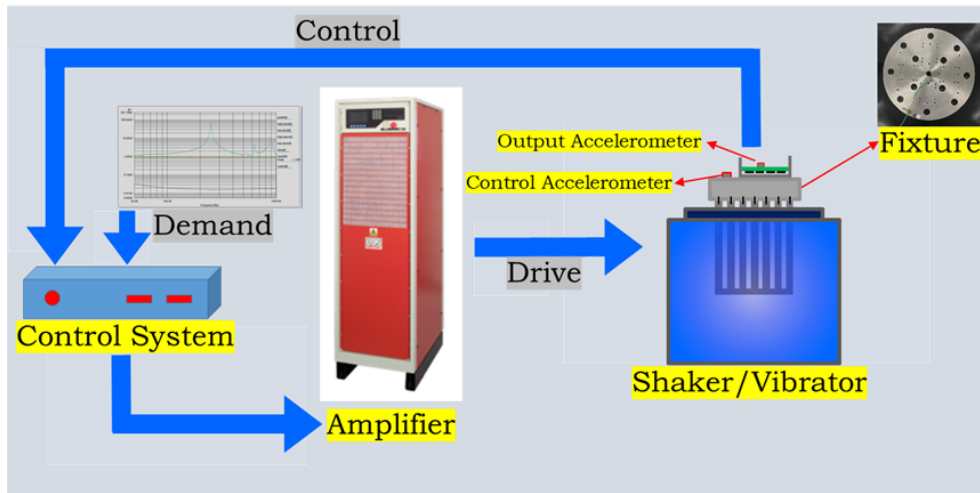
Figure 1.4: Vibration testing introduction

Vibration instructions or demands can be programmed by using the control software system. It is the demand assigning the amount of vibration energy which includes acceleration level, and vibration frequency range. Then, the control system translates the demand into the electronic signal (voltage) and drives the amplifier to deliver the required or demanded vibration intensity. A control accelerometer is installed on the vibration fixture which provides feedback to the control system. It confirms whether the acceleration level is corresponding to the demand on the fixture. This way, the control loop is able to maintain the required acceleration level experienced at the fixture plate during a vibration test. There are three common types of vibration stress methods, swept sine vibration test, random vibration test, and dwell vibration test. Swept sine vibration test is generally used for characterizing the dynamic response of the test setups. A determined frequency range, for example, 100Hz to 1000Hz, is swept with the assigned acceleration level which means a single frequency is excited at a certain moment. It can be used to characterize the resonance frequency and amplification factor of the board. However, an inappropriate input acceleration level will lead to inaccurate measurement due to the damage on the test board [29]. Therefore, it is important to select proper input when performing swept sine vibration test. Dwell vibration test is an extension application of swept sine vibration. The shaker is excited with a single frequency of interest. In random vibration tests, all vibration frequencies of interest are excited simultaneously. This technique can be used to excite multiple resonance modes of the test board at stressed at the same time.

1.3 VIBRATION THEORY OF PRINTED CIRCUIT BOARD

In vibration testing, acceleration, peak-to-peak displacement, resonance frequency, and strain on the board are important parameters of the PCB dynamic response. In this section, simplified formulas are derived under some assumptions.

Acceleration and Displacement:

The PCB vibration characteristics are measured by recording the PCB acceleration as a function of applied frequency at constant applied acceleration. The excitation is a controlled sinusoidal motion from the shaker that can be described by [33]:

$$x = X_{max} \sin(2\pi ft) \tag{1.6}$$

From the equation (1.6), level of velocity (v) and acceleration (a) can be derived in:

$$v = \frac{dx}{dt} = 2\pi f \cdot X_{max} \cdot \cos(2\pi ft) \tag{1.7}$$

$$a = \frac{dv}{dt} = -(2\pi f)^2 \cdot X_{max} \cdot \sin(2\pi ft) \tag{1.8}$$

From equation (1.7) and equation (1.8) the relation between displacement and acceleration can be expressed in:

$$a = -(2\pi f)^2 \cdot x \tag{1.9}$$

Peak-to-peak displacement d, $d = 2X_{max}$ is a more common way of expression than peak displacement of one side of PCB in vibration test. Also, the accelerometer is able to measure the acceleration, non-dependent of time, so we hereby have:

$$a = 2(\pi f)^2 \cdot d \tag{1.10}$$

If assuming the PCB under vibration loading acts like a single degree of freedom system, under this assumption, a relation between the displacement, acceleration, and frequency can be obtained:

$$d = \frac{a}{2\pi^2 f^2} \tag{1.11}$$

Resonance Frequency:

According to Steinberg [33], PCBs used in the electronic systems can be approximated as a flat rectangular plate. To derive the resonance frequency, a square plate is assumed to be simply supported on four edges as shown in figure 1.5.
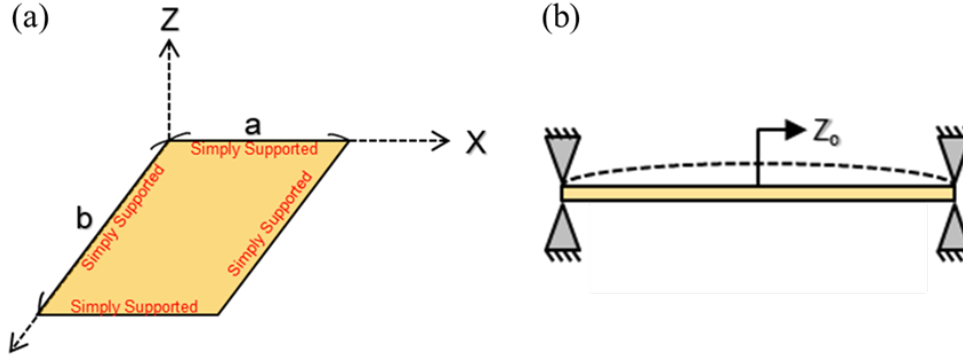
Figure 1.5: Boundary assumption of plate (a) top view (b) side view

Where a and b represent the width and length respectively and z_o is the maximum displacement in the middle of the plate. Simply supported means the deflection on the edge of the plate is equal to zero, but the slope of the edge depends on the loading. The displacement of the flat rectangular plate exciting at the first resonance frequency under the defined boundary condition. The displacement at any PCB location $z(x, y)$ can be simplified to the following equation (1.12) [33]:

$$z = z_o \times \sin(\frac{\pi x}{a}) \sin(\frac{\pi y}{b}) \tag{1.12}$$

The equation can be verified whether it complies the boundary condition by checking the displacement at the edge and slope of the plate in the middle. For example, if x and y are both equal to zero, the displacement calculated from the equation (1.12) is equal to zero which fulfills the boundary condition. Same check can be done by deriving the slop on the middle of the plate which is also equal to zero. Furthermore, if it is assumed that the energy does not dissipate from the board, the kinetic energy of the plate will be equal to the strain energy of the plate. Then the resonance frequency of the flat square plate can be described by equation (1.13):

$$f = \lambda \left(\frac{1}{a} + \frac{1}{b}\right) \sqrt{\frac{E \times h^3}{12 \times \rho \left(1 - v^2\right)}} \tag{1.13}$$

Where the λ is a constant depending on the clamping condition, E is Young's modulus, h is the thickness of PCB, ρ is the density of PCB and v is the Poisson's ratio.

Board Strain:

In order to roughly calculate the strain value on PCB with a measured level of acceleration when it is bent. The boundary condition of the two sides of the plate on the X-axis are changed to fully clamped (fixed). The displacement of the plate can be expressed in the following equation(1.14):

$$z = z_o \times \left[\cos(\frac{2\pi y}{b}) - 1\right] \times \sin(2\pi f t) \qquad (1.14)$$

To calculate the acceleration, differentiate Equation(1.14) in the time domain two times. Then, the acceleration of the board under this boundary condition can be described with equation (1.15):

$$Acceleration = -4\pi^2 f^2 z_o \times [\cos(\frac{2\pi y}{b}) - 1] \times \sin(2\pi f t) \qquad (1.15)$$

The curvature k along Y axis of the plate can also be calculated by differentiating the equation (1.14) twice with respect to y as shown in equation (1.16) [12]:

$$k = -\frac{4z_o \pi^2}{b^2} \times \cos(\frac{2\pi y}{b}) \times \sin(2\pi f t) \qquad (1.16)$$

In classic beam theory, the translation between curvature and strain of the plate can be illustrated in equation (1.17) [1]:

$$k = \frac{2 \times \varepsilon_{PCB}}{t_{PCB}} \qquad (1.17)$$

Where t_{PCB} is the PCB thickness and ε_{PCB} is the PCB strain. By combing equations from (1.16) to (1.17), the relationship between the level of acceleration and strain value on PCB can be shown in equation (1.18):

$$\varepsilon_{PCB} = \frac{t_{PCB} \times \cos(\frac{2\pi x}{b}) \times Acceleration(g))}{2 \times b^2 \times f^2 \times [\cos(\frac{2\pi x}{b}) - 1]} \qquad (1.18)$$

Additionally, the strain value formula can also be derived by analyzing three points bending setup figure 1.6. First, region AB can be derived from the static equilibrium equation:

$$\sum F_Y = \frac{F}{2} \times V = 0 \qquad (1.19)$$

$$\sum F_M = -\frac{F}{2} + M = 0 \qquad (1.20)$$

Where F is equilibrium force, V is shear force, and M is the moment of force and region BC can be derived:

$$\sum F_Y = \frac{F}{2} - F - V = 0 \tag{1.21}$$

$$\sum F_M = -\frac{F}{2} + FX - \frac{FL}{2} + M = 0 \tag{1.22}$$

From the equation (1.19) to equation (1.22), the maximum moment can be calculated as:

$$M_{max} = \frac{1}{4} FL \tag{1.23}$$

by bending stress σ_{max} equation the maximum stress can be derived:

$$\sigma_{max} = -\frac{M_z Y}{I_z} = \frac{3}{4} \times \frac{FL}{wt_{PCB}^2} \tag{1.24}$$

Where the I is the area moment inertia of Z-axis. The t_{PCB} is the thickness of the beam. By applying the stress-strain formula the stress can be converted into strain:

$$\varepsilon = \frac{\sigma}{E} \tag{1.25}$$

Where the E is the flexural modulus, which can be derived from the beam deflection theory [27]

$$E = \frac{FL^3}{48\delta_{max}I} \tag{1.26}$$

Where the δ_{max} is the displacement of the board. Combining formulas from equation(1.24) to equation(1.26), the maximum strain can be derived:

$$\varepsilon_{PCB} = \frac{6\delta_{max}t}{L^2} \tag{1.27}$$
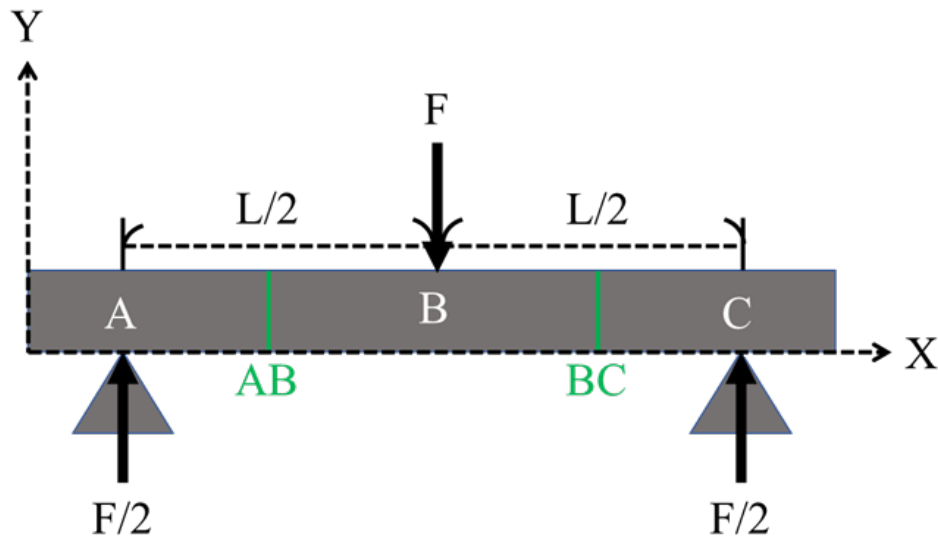
Figure 1.6: Three point bending beam structure

1.4 RECENT STUDIES ON BOARD AND MODULE LEVEL VIBRATION TEST SETUP

In this section, kinds of literature are summarized to show the state of art at board level and module level vibration test setup. It includes the industrial vibration test specifications, vibration measurement method, test fixture, module, electronic module, measurement sensor, and failure analysis techniques used.

1.4.1 Industrial Vibration Standards and Field Vibration Data

In the current study of vibration reliability tests, there are component level specifications and standards for an electronic product such as JEDEC standard [17] and ISO standard [26], but there is no board-level vibration test specification. To assess reliability risks for automotive radar sensor modules, at board level and module level, vibration test standards need to be reviewed by collating different vibration parameters. Therefore, existing vibration test standards will be summarized according to the type of vibration, test duration time, effective stress level, test frequency range, and application purposes in this section. In table 1.1, random vibration profiles from common industrial test specifications are summarized. The profile for device mounting on unsprung masses has a higher stress level than sprung masses in the same standard. The most stressful level is roughly equal to $13G_{rms}$. Besides, the lower and higher bound of vibration test frequency can be found from 5Hz to 2000Hz among all the profiles. While it is also noticeable that most of the vibration profiles in section A.1 have

lower stress levels after 1000 Hz. It is noted that the PCB design and test hardware are not mentioned in these standards.

Standard	Description	Axes	Test time (hrs/axes)	Stress level (G$_{rms}$)	Frequency (Hz)
IEC 60068-2-64 Spectrum A.3 Category 1	Automobile Chassis mounted	3	8	3.38	10 to 1000
IEC 60068-2-64 Spectrum A.3 Category 2a,2b,2c	Engine compartment Attached on body or radiator	1/1/1	8	1.1/0.67/1	5 to 200
ISO 16750-3 4.1.2.4	Attached on body	3	8	2.71	10 to 1000
ISO 16750-3 4.1.2.5	Attached on unsprung masses	3	8	10.73	20 to 2000
MIL-STD-810G Method 514.6	Wheel vehicles	3	2	2.24/1.4/1.9	5 to 500
GMW 3172 9.3.1.1	Attached on engine or transmission	3	44	12.96	10 to 2000
GMW 3172 9.3.1.2	Attached on Car/Truck sprung masses	3	16/36	2	10 to 1000
GMW 3172 9.3.1.3	Attached on Car/Truck unsprung masses	3	16/36	10.95	20 to 1000
JESD22-B103-B Condition A	Assess component level risk	3	0.5	6.27	20 to 2000

Table 1.1: Summary of industrial automotive random vibration profile [4-8]

In ISO 16750-3-4.1.2 [26], it states that the proposed sinusoidal vibration profile in IEC 60068-2-80 [32] should be performed for assessing engine effect. Also, in JIS-D-1601 [16] type 1 classification C and D, sinusoidal vibration test is also used for the device around the engine. The test frequency of both is lower than 1000Hz. In figure 1.7, it shows the automotive field vibration data which is measured by an accelerometer mounted on the engine. The effective stress level will increase with the car speed as shown in figure 1.7 (a) to (c). Also, it shows that the vibration power not only happens at low frequency ($< 100Hz$) but also happens at a higher frequency band which is over 1000 Hz. Comparing the industrial vibration standard and field vibration data indicates that the vibration specification cannot fully cover the risk in terms of the test range of frequency and effective stress level.
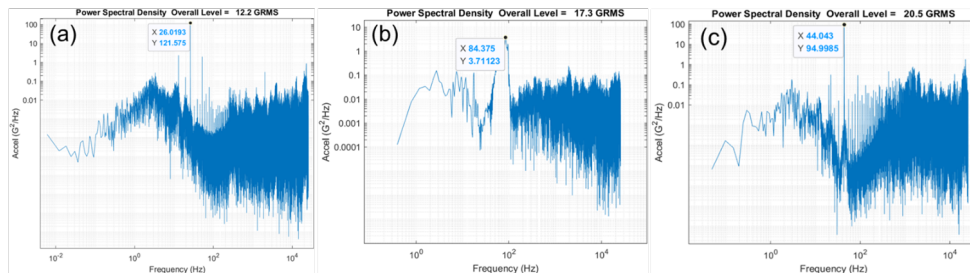
Figure 1.7: Automotive field vibration data (a) idle car speed (b) 50 kph (c) 70 kph

1.4.2 Vibration Measurement Sensor Used

In the current vibration testing, the piezoelectric accelerometer is the major measurement tool used in measuring PCB dynamic response [17-23]. An accelerometer consists of a piezoelectric crystal that is placed underneath a given mass. Vibration motion causes stretch and compression of the crystal element. The change in the amount of charge of the piezoelectric crystal can be converted into acceleration. In [21] the high-speed camera is used to record the motion of the PCB with Digital Image Correlation (DIC) technique under vibration. In [23], LASER Doppler Vibrometer (LDV) is used as the measurement tool for PCB dynamic response. LDV is able to measure the same parameter as the accelerometer. In [26-27] authors mount the strain gauge on the PCB to measure the shift in resonance frequency and the difference in strain under different temperatures. The stretch of the PCB changes the gird resistance of the strain gauge. The resistance change that causes the difference in voltage can be used to calculate the strain with the bridge circuit. These tools can be divided into contact-based and contact-less sensors. However, few kinds of literature assess the advantages, disadvantages, and accuracy of sensors. The comparison between strain gauge, accelerometer, and LASER will be discussed at both board level and module level vibration test in Chapter 2.

1.4.3 Electronic Module Structure Used for Automotive Radar Applications

In the electronics market, automotive radar sensor consists of several distinctive appearances and packages from different suppliers. To figure out common features of these automotive radar modules, radar products from Denso, Continental, Hella, BMW, and Bosch are shown in figure 1.8. First, all the modules comprise of board housing structure, which acts as a heatsink, supporter, and protector against dirt and water. The heatsink is used to dissipate heat generated by an electronic component. Second, the edges of the PCB are simply supported, and the corners are fixed. It can reduce the PCB motion which can decrease the stress level on PCB. Also, the PCB is placed in a box-like housing to protect it from environmental effects. Third, the electrical connection in a module is generally realized using the application-specific connector. In the end, a motion resistor is designed around the chip in the radar module from Denson to reduce the stress level under vibration. However, in some practical applications, the rib structure induces unexpected strain on the PCB [20].

Figure 1.8: Automotive radar sensor from markets [2, 4, 5, 6, 7]

To investigate the relevance of different housing structures with practical one, four heatsinks are designed in figure 1.9. Heatsink (a) is the original heatsink for the radar sensor used in this thesis. Not only the board vibration response will be investigated, but also the thermal interface material will be applied on the board. The boundary condition of the heatsink (b) is modified into a box-like housing with a hollow rectangular frame that can be used to clamp the PCB with four edges. Brass instead of aluminum is used to manufacture the heatsink (c). Besides, four M2 screw holes are designed for installing motion resistors to assess the risk induced under vibration stresses. Heatsink (d) is constructed by plastic and the small standoffs are mounted on the bottom of the heatsink for board fixation. Further discussion on the impact of heatsink structure will be made in Chapter 3.
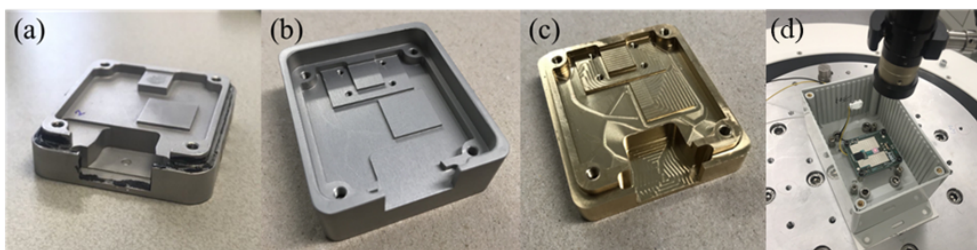
Figure 1.9: Different design of heatsink

1.4.4 Failure Monitoring Techniques Used During BL VIBR Tests

The Daisy chain is used to monitor the electrical failures in-situ during reliability experiments. A daisy chain structure comprises of un-

interrupted alternate electrical connection between the test package and PCB that is designed to cover all relevant failure modes. The resistance change is recorded by continuously monitoring the electrical voltage during reliability testing. The test pad then can be used to isolate failure location or section in order to ease out the failure analysis process.
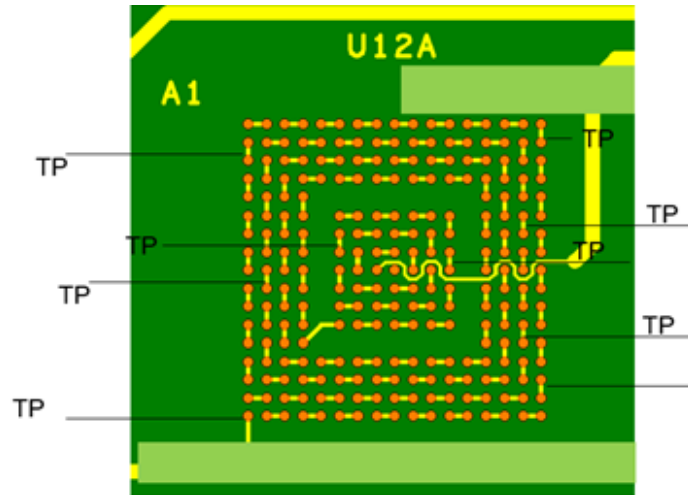
Figure 1.10: Daisy chain schematic

The circuit used in this research is the daisy chain detection circuit as figure 1.11 shown. As shown in the figure, two daisy chain packages are monitored in parallel. These daisy chain packages are electrically driven by a common voltage source and it connected in series to 1kΩ resistors. Finally, this is fed to the vibration controller channels that is used to monitor the voltages continuously during the test. Once the resistance of the daisy chain increases due to the crack formation in the solder joints, the voltage measured across the daisy chain also enhances. A resistance threshold limit of 1000Ω is set as a failure criterion, which is in line with the IPC-9701A test standard [28]. The vibration shaker equipment is programmed in such a manner that the vibration test is aborted once the resistance is equal to or more than 1000Ω.

In [38], the author divides the failure process under vibration test into four stages, which is no failure period (1st stage), crack fast initiate period (2nd stage), stable crack propagation period (3rd stage), and complete failure (4th period). In the 2nd and 3rd stages, the resistance value goes high and low which is caused by the crack opening and closing with PCB bending up and down.
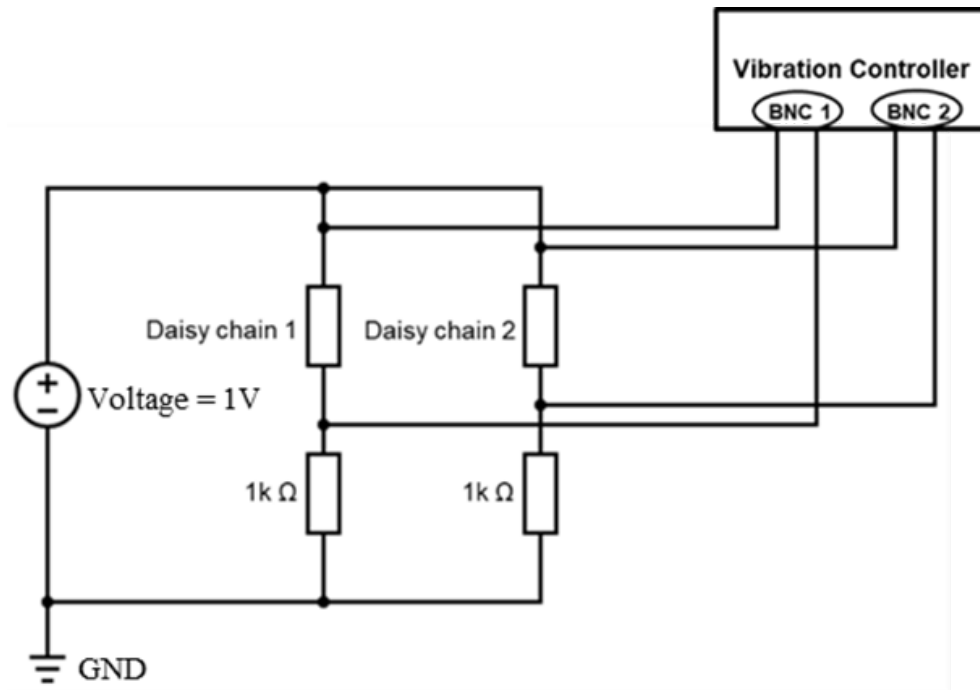
Figure 1.11: Daisy Chain failure detection circuit schematic

1.5 RECENT STUDIES ON BOARD AND MODULE LEVEL VIBRATION TEST SET UP

In general failure analysis techniques can be divided into non-destructive and destructive testing methods. The failure techniques used in this thesis are reviewed explicitly. Non-destructive Evaluation (NDE) methods such as C-mode Scanning Acoustic Microscopy (C-SAM), optical profiling, and Lock-in Thermography (LIT) are used to localize the abnormal sections, failure modes without applying physical damage or stress onto the component. After NDE, destructive evaluations such as decapsulation and micro sectioning (cross-section) are used to identify exact failure mechanisms and root causes.

C-mode Scanning Acoustic Microscopy (C-SAM): The acoustic wave is used to generate the images of the test specimen. When the acoustic wave propagates through a different medium and is reflected by the package, the amplitude of the wave will be amplified and mapped into the function of position. It is usually used for detecting delamination, cracks, and void.

Lock-In Thermography (LIT): LIT working principle is based on sensing the thermal response by using a thermography camera to sense the thermal response on the component of interest. A thermal wave is reflected and dissipated at a different rate at nonhomogeneous ma-

terial property locations that might be present in the form of defects such as cracks, delamination as shown in figure 1.12.
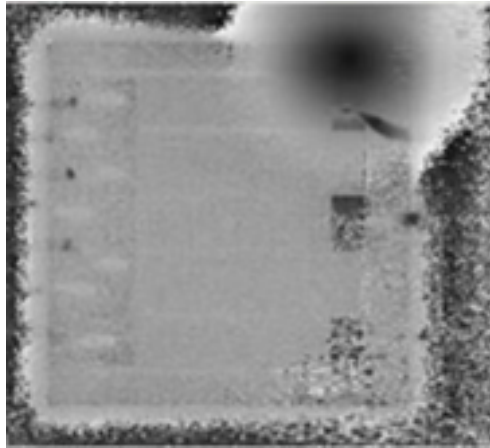
Figure 1.12: LIT thermal spot [36]

Micro Sectioning: Micro sectioning is a destructive failure analysis method. The component of interest is put into the epoxy resin to prevent additional damage and ensure the planarity. The sample will be ground to the interested area. It can provide the cross-sectional view of the solder joint at a selective plane as shown in figure1.13 to find out the failure mode and mechanism.
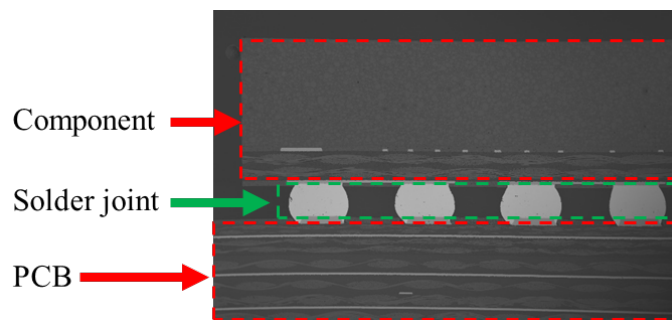
Figure 1.13: Micro sectioning view on component

1.6 RESEARCH MOTIVATION AND OBJECTIVES

In the current semiconductor industry, chip suppliers, modules, and system developers cooperate to build the product. All of these stakeholders take responsibility for their devices and system. It implies that module and system developers ask the supplier to assess the reliability risk of the product at a specific application level. For example, as an automotive radar chip supplier, radar module architects ask about the reliability risk of the component at the module level. There is no globally accepted industrial standard for board-level vibration
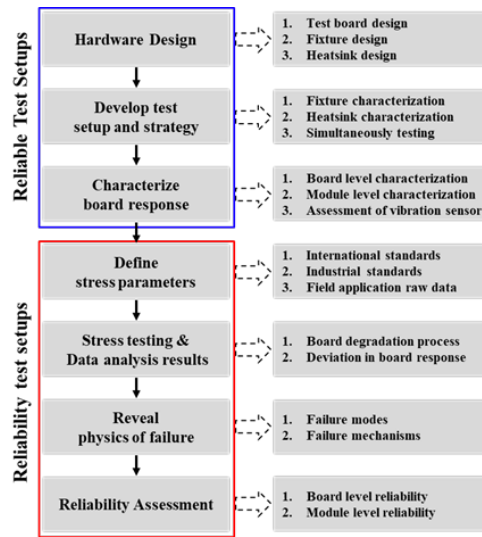
Figure 1.14: Vibration test flow and approach

specification. Similarly, there is also no vibration standard prescribed for radar application-based electronic modules. Most of the vibration test specifications such as IEC 60068-2-64 [25], ISO 16750 [26], and MIL-STD-810G [24] are stated for general electronic devices. It is obvious that there is a gap between board level, board module level, and application-level vibration test to determine the component reliability risk. Additionally, measurement sensors for vibration tests can induce the deviation in the measurement result. This deviation can cause inaccurate assessment on defining the vibration test strategy and reliability, while no specifications prescribe appropriate vibration measurement sensors for test setup at the board module level. A robust setup should be able to explore the interaction between housing and board under vibration. Also, the research has not been done on board degradation in terms of vibration parameters such as resonance frequency, peak-to-peak displacement, and board strain. This is expected to be an indicator of underlying failure or data source for training future application-driven vibration tests. When it comes to the failure, the translation from strain rate to failure mode observation is not available for vibration tests. In conclusion, vibration test specifications and test setup are not fully prepared to discover the reliability risk of the advanced automotive package and board characters at board level, board module level, and application-level vibration test. The main objective of this Master Thesis is to assess the risks of the automotive radar component under vibration loading at both board level and module application level. To achieve this goal, the following objects need to be delivered with the following development flow in figure 1.14.

Establish Robust Vibration Test Setups:
Robust vibration test setup includes hardware design and develop-

ment, and dynamic response characterization. The hardware such as fixture and heatsink is designed to be able evenly to transfer the pre-defined stress level from the shaker to them. The measurement sensor is currently available for board-level vibration but not for the module-level vibration test. Measurement sensors, such as accelerometer, LASER, strain gauge for will be assessed its availability at module level vibration.

Reliability Test Setup Preparation:
Appropriate stress parameters should be defined according to the board response, and furtherly correlate with vibration standards to evaluate vibration risks. By doing the stress test to induce failures, various failure analysis techniques should be able to provide a decent understanding of failure mechanisms. In the end, the reliability performance between board level and module level under vibration loading for this automotive radar component will be revealed.

Understand the impact of module design elements:
Electronic module elements such as electrical connectors, thermal interface material, and motion restrictors are designed according to the automotive radar module in the market. The impact of these elements is explored under vibration testing.

Vibration Sensor and Board Degradation Assessment:
In this automotive radar module vibration test, focuses are also put on the cause of deviation in board dynamic response. Different measurement methods and board degradation processes will be discussed, and the simulation model is used to correlate the experimental results. Finally, the impact of hardware design on the measurement method and board degradation process will be studied.

1.7 THESIS OUTLINE

- Chapter 2 explains the design of the fixture and the module used in this thesis. After that evaluation of results of vibration response measured on fixture and module is done for assessing whether the force from the shaker is able to correctly be transmitted to PCB. The Surface Mount Technology (SMT) is explained. Assessment on vibration measurement sensors, such as accelerometer, LASER, and strain gauge, is developed for this vibration testing.

- Chapter 3 discusses the result of PCB dynamic responses. The response measured at board level and module level vibration testing will be characterized with different types of PCB. Furtherly, the impact of module elements on the board dynamic response is discussed. In the end, board vibration at board level

and module level is compared in terms of strain and peak-to-peak displacement.

- Chapter 4 explains how vibration testing stress parameter is defined in this research. It follows with the reliability testing result comparison between board level and module level vibration testing. The proposed increment stress test results are correlated with the degradation process of board strain and resonance frequency. In the end, it will bring the failure analysis results after board and module level vibration reliability test and correlate with other mechanical testing methods.

- Chapter 5 concludes results from the vibration experiment and recommendations for the future development on vibration testing.

2 | DEVELOPMENT OF VIBRATION TEST SETUP

As shown in figure 2.1, the automotive application-specific vibration test landscape requires development in both hardware and software sectors. A reliable experimental test setup is needed to develop a well-characterized test methodology. Vibration test fixture, PCB under test, module, measurement method, simulation, and in-situ detection method, shown in figure 2.1, are crucial elements of vibration test methodology. In this chapter, further discussion and investigation will be done on these elements.
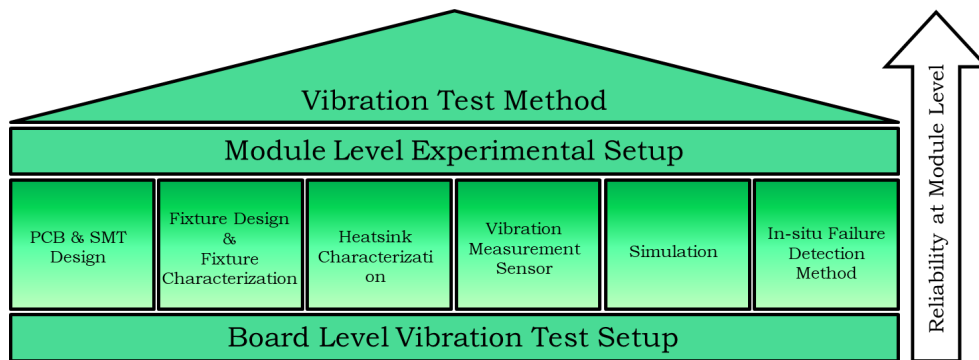
Figure 2.1: Vibration testing landscape

2.1 PCB LAYOUT AND SMT FLOW

As shown in table 2.1, B111A JEDEC PCB is generally designed to carry four components on one side only. It is used for reference purposes because there is a board and module level vibration standard prescribing the PCB type for vibration test. The customized PCB (board 1) is manufactured into a radar application board which is called PCB module as picture shown in figure 2.2. Two marked components, component 1 is a Fan-out Chip Scale Package (FOCSP) and component 2 is a BGA component with daisy chain for failure monitoring purpose.
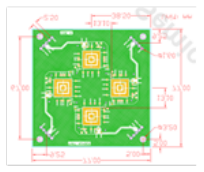
PCB	B111A [3]	Customized PCB (board 1)
Dimension (mm)	77*77	47*42
Thickness (mm)	1	1
Young's Modulus (GPa)	25	14
PCB Weight (grams)	16	5
Number of Layers	8	8
Layout		

Table 2.1: PCB details
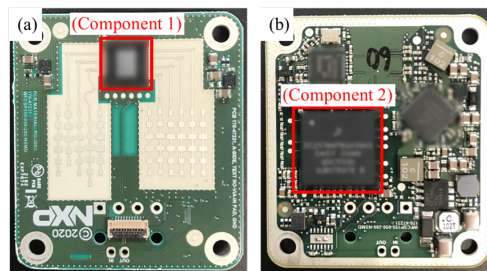
Figure 2.2: Customized electronic module layout [9]

SMT process for board 1 is shown in figure 2.3. First, the material quality is checked, and the solder paste prints on the bottom side of PCB. Then, an automated pick and place machine is used to place components at the target component locations defined on the PCB. Next, temperature reflow is performed. At the top side of the PCB, the same procedure will be done as the bottom side of the PCB. After components are soldered on the PCB, the resistance is measured on the daisy chain devices. X-Ray is performed at the end to check for unintended defects such as solder shorts.

Figure 2.3: SMT procedure of customized PCB (board 1)

Trial SMT run is performed before the final SMT production. During the resistance measurement step, high resistance was observed daisy chain of component 1. After cross-sectional analysis, PCB cracks are found on the Copper trace of the daisy chain. Root cause analysis showed that these cracks are introduced after the reflow step. It might be linked to the thermo-mechanical stresses that are introduced during the reflow process. Therefore, the cooling rate is decreased to reduce the effect of Coefficient of Thermal Expansion (CTE) mismatch between component and PCB copper trace. The board is successfully assembled and it will be mounted on the fixture with standoffs or heatsink.
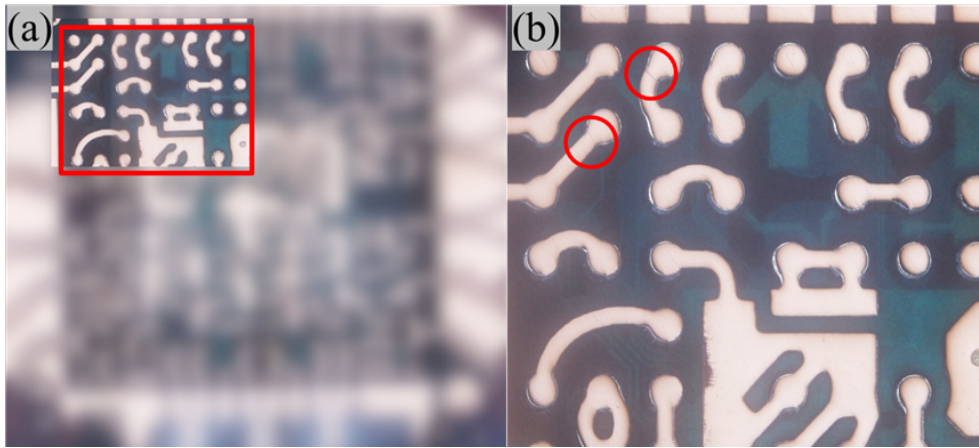
Figure 2.4: Optical scan on component 1 (a) entire daisy chain (b) zoom in the red zone

2.2 VIBRATION FIXTURE DESIGN CHARACTERIZATION

The fixture is a mechanical adapter screwed in between the shaker and test board that is mounted onto an electronic module as figure 2.5. The force from the shaker will be amplified depends on its transmissibility when an inappropriate fixture is designed and used in vibration tests. For example, a 5G sweep sine is required to be performed on the test board, and the test board is mounted on a fixture with transmissibility 10. The test board is possible to be stressed with 50G. This might lead to incorrect conclusions. In order to transmit the required total amount of force at the required frequency from the shaker to the test module, there are some recommendations described from Steinberg [10] that can be followed to design a good vibration fixture. Firstly, some of the current automotive vibration test specifications require the test that frequency range from 5Hz to 2000Hz. Also, it is necessary to avoid having a similar resonance frequency of the fixture as the test specimen. Therefore, the fixture is better to be designed with a resonance frequency at least 50% higher than the required test frequency. Secondly, it is better to have fewer sharp changes and a symmetric fixture which is helpful transmit the force from shaker to fixture equivalently at the whole surface. Finally, the fixture should be kept as rigid and low mass as possible. By reducing the mass, the resonance frequency of the fixture can be adjusted to a higher frequency range according to equation 1.13 which avoids the resonance falls into the common test frequency range which is lower than 2000Hz. When it comes to designing a rigid and light fixture, a stiffness-to-mass ratio is used to evaluate the material. One material

with a higher stiffness-to-mass ratio can be found lighter and more rigid. As the result, the fixture is chosen to use aluminum alloy.

Fixture Details				
Mounting Holes	11 (mm)	10-32 UNF	3.1 (mm)	M6
Quantity	12	13	36	4
Purpose	Fixation	Accelerometer mounting	Heatsink mounting	Pillar mounting
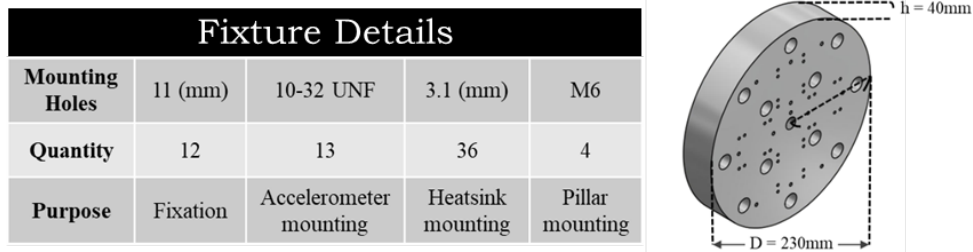
Figure 2.5: Details and schematic of fixture design

Two major measurement techniques, accelerometer, and LASER can be used to capture vibration acceleration levels. Both measurement units are employed to capture vibrations at the metallic fixture surface shown in figure 2.5. In figure 2.6, the normalized response measured by accelerometer and LASER on the center of the fixture shows the deviation between the two is within 5%. This indicates that the measurement tool can be used when the mass of the accelerometer is negligible comparing to the vibration object to be measured. Therefore, the accelerometer will be used for measuring the vibration response of the fixture at the Z-axis.
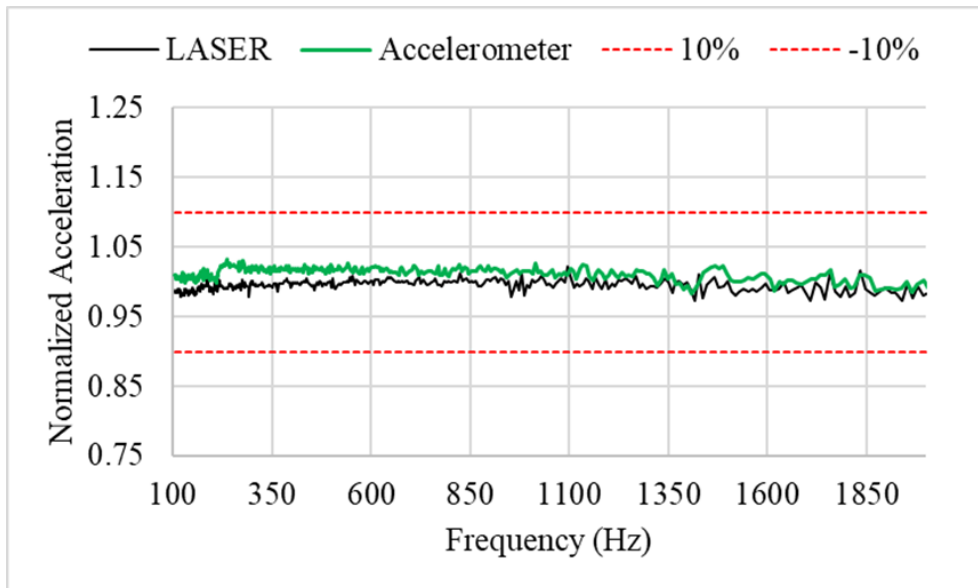
Figure 2.6: Comparison between Accelerometer and LASER in vibration response

Fixture vibration response at several possible test locations is characterized next. The acceleration level is used to assess the homogeneous transfer of the force from the shaker to the PCB that is placed in a module housing. Two accelerometers shown in table 2.1 are used in the

fixture vibration characterization test. In the characterization vibration test, the profile shown in table 2.2 is performed. The acceptable range of acceleration level measured on the fixture is ±10% of the input signal of the shaker.
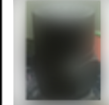
Picture	Mass (g)	Sensitivity (mV/g)	Fixation	Purpose
	3	101.5	Mounted with nut system	Control Acc.
	0.5	2.28	Mounted with wax	Measurement

Table 2.2: Accelerometer used in fixture characterization

Method	Swept sine
Input level of acceleration (g)	1
Frequency (Hz)	From 100 to 3500
Sweep rate (oct/min)	1

Table 2.3: Vibration profile for fixture and module characterization

This fixture used in this thesis is designed to mount 4 electronic modules as shown in figure 2.7. In this characterization vibration test, four test positions where it is in the center of the module will be measured.
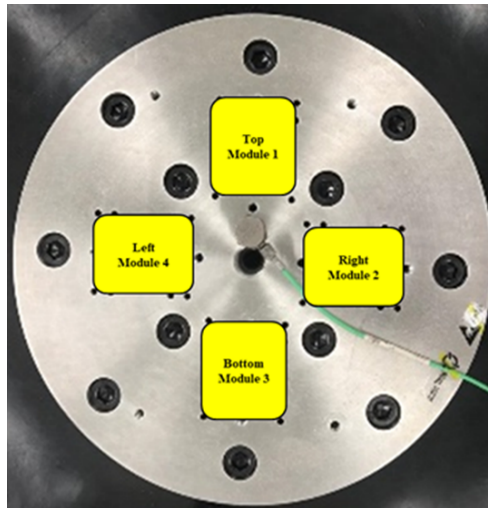
Figure 2.7: Module test positions on fixture

The vibration responses shown in figure 2.8 indicate that responses measured at the "Top", "Left", and "Bottom" side of the fixture are within 10% of the input signal. However, the response at the "Right" side of the fixture exceeds the 10% acceptable range at around 1400Hz. It means this fixture can do a vibration test with three electronic modules at the same time at the top, left, and bottom sides of the fixture.
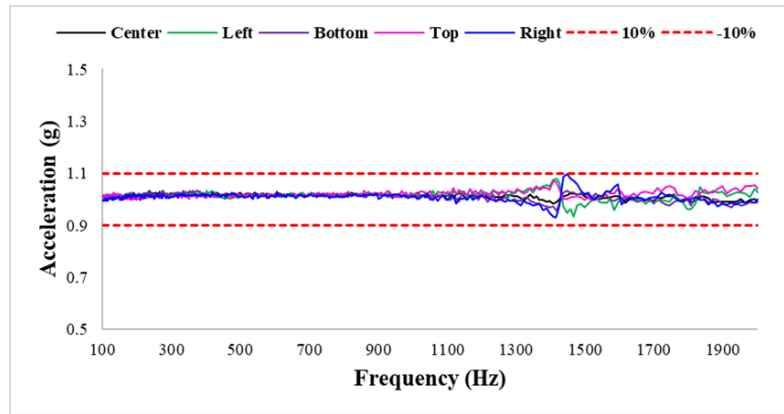
Figure 2.8: Fixture vibration characterization response at Z direction

However, to look into the cause of this deviated response, two possible hypotheses are proposed. Firstly, it might be related to the design of the fixture, and the other one is related to the shaker element structure. The second hypothesis is first considered. To prove the second hypothesis, characterization is done on the armature which is part of the shaker. The response, in figure 2.9, shows deviated signal at around 2350Hz. This can be explained as the root cause of deviated signal that happened on the fixture. Due to the mass of the fixture, the deviated signal is shifted to 1400Hz. However, it is the nature of shaker structure that cannot be changed and is inevitable.
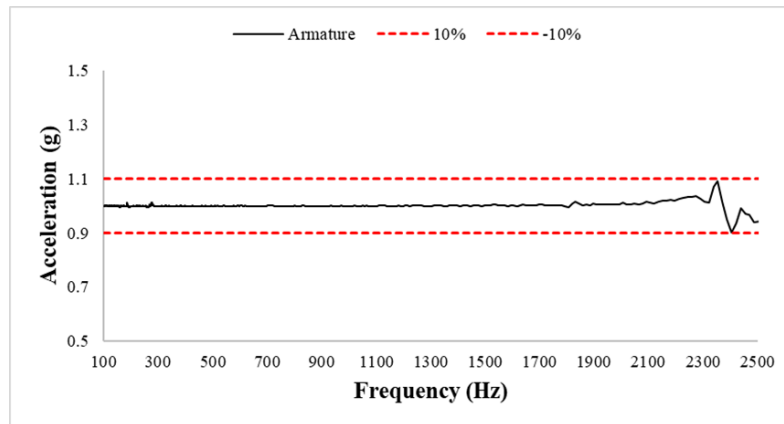
Figure 2.9: Armature vibration characterization response

2.3 MODULE DESIGN AND CHARACTERIZATION

The module here is referred to the housing structure part of the electronic sensor module which is also called heatsink. In the application, PCB is usually mounted onto a heatsink so that the heat generated by chips can be transferred to the heatsink. Heatsink increases the surface area in order to accelerate the heat dissipation process. As

the figure 2.10(b) shown, the bottom side of the heatsink used in this thesis has a cylinder structure for better thermal management. On the front side, there are two square areas that step higher than other areas. Thermal Interface Material (TIM) is applied on this square area and transfers the heat from the chip by directly contacting the PCB.
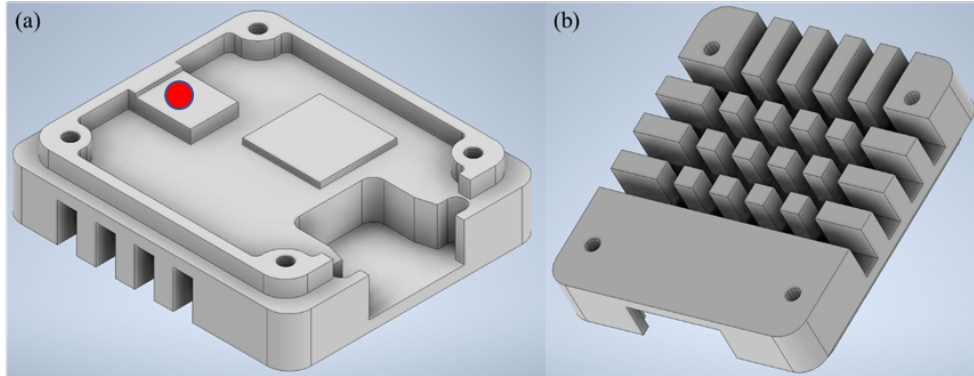
Figure 2.10: (a) Heatsink design schematic – front side (b) Heatsink design schematic – bottom side

The PCB is tested by mounting it onto the heatsink. To ensure the required vibration response received on the heatsink, vibration characterization must be performed on the bare heatsink itself. The same experimental setup and vibration profile will be used as section 2.2 Before characterization of the module, the torque applied on the heatsink fixation screws needs to be defined first. To determine the required torque, it is increased from 0.1N·m to 0.4N·m. As figure 2.11 shown, the acceleration level measured on the heatsink at Z direction is over 10% of the input signal at around 1300Hz. This rising acceleration indicates that the heatsink is stepping into the resonance frequency range and it doesn't show improvement with the increased torque.
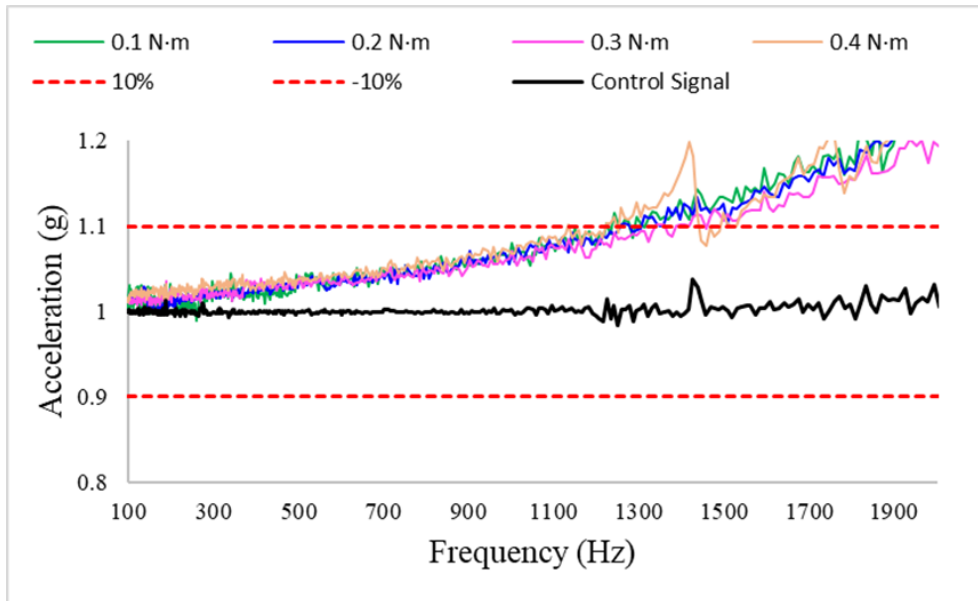
Figure 2.11: Heatsink vibration characterization response at Z direction

To improve this situation, four types of vibration motion dampers are introduced in between the heatsink and fixture. The damper can reduce vibration energy. In figure 2.12, it indicates that the increase in torque is able to increase the damping (vibration response of damper-1, 2, 4 can be found in appendices A.2). When the torque reaches 0.3 N·m and 0.4 N·m, it prevents two metallic plates from hitting one another vibration and this leads to a more damped and consistent vibration response. Without sufficient torque, the freedom is still given to the heatsink to oscillate. The torque with 0.4 N·m is chosen in the end.
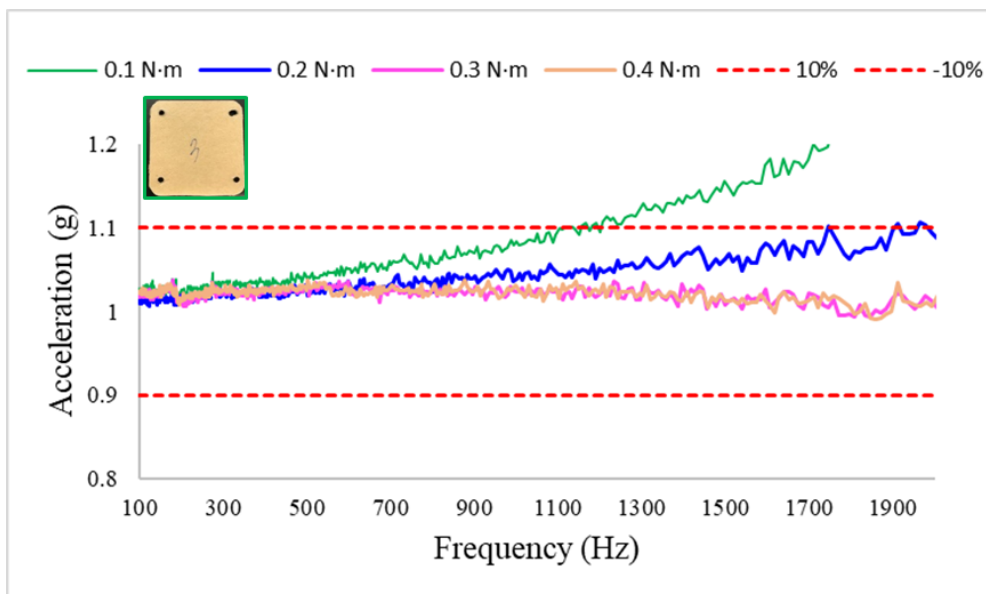
Figure 2.12: Heatsink vibration response at Z direction with damper-3

After discovering the appropriate experimental setup for heatsink installment, heatsink to heatsink variation is investigated. Since it is intended to use multiple heatsinks at the reliability test, the force transfer from shaker to heatsink needs to be similar. In figure 2.13, heatsinks are compared with the one used in the previous test. It shows deviations are within 10% which means these heatsinks should receive a similar vibration response with the same input acceleration level from the shaker.
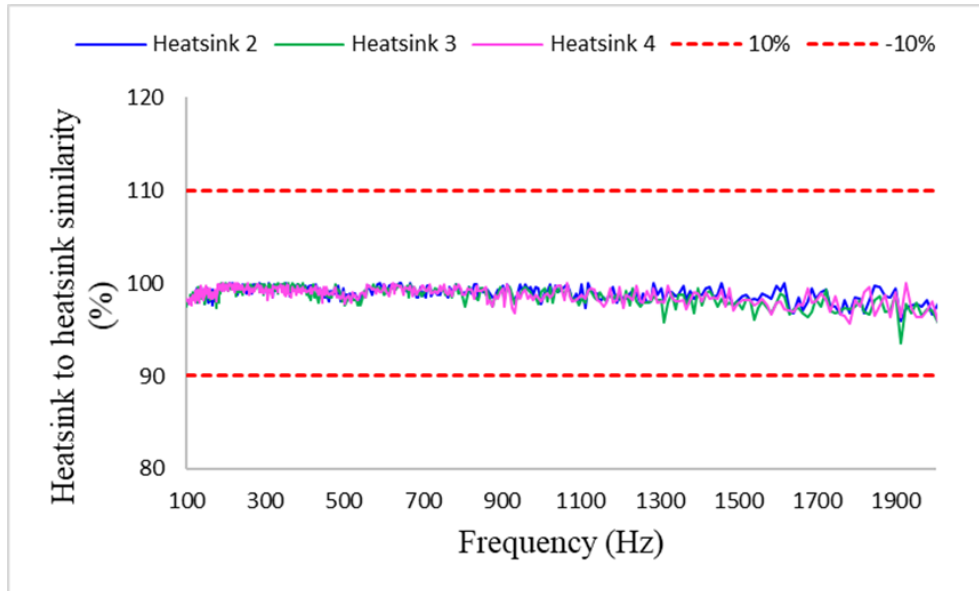
Figure 2.13: Heatsink to heatsink variation characterization at Z direction

Reliability stress-test strategy, involving simultaneous testing of multiple modules is characterized next. This can help in reducing the stress test time consumption. Four electronic modules are mounted on the fixture as figure 2.14.
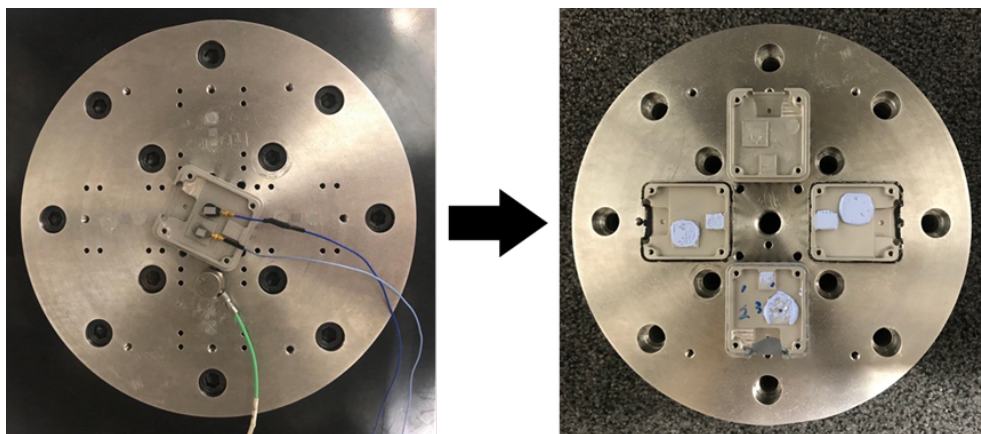
Figure 2.14: Single test to simultaneous test setup at Z direction

However, the response measured on the heatsink which is mounted on the right side of the fixture is marginally out of the specification

as shown in figure 2.15. Therefore, it will not be used for reliability stress test purposes, only three positions, top, left, and bottom side can be used in the further test.
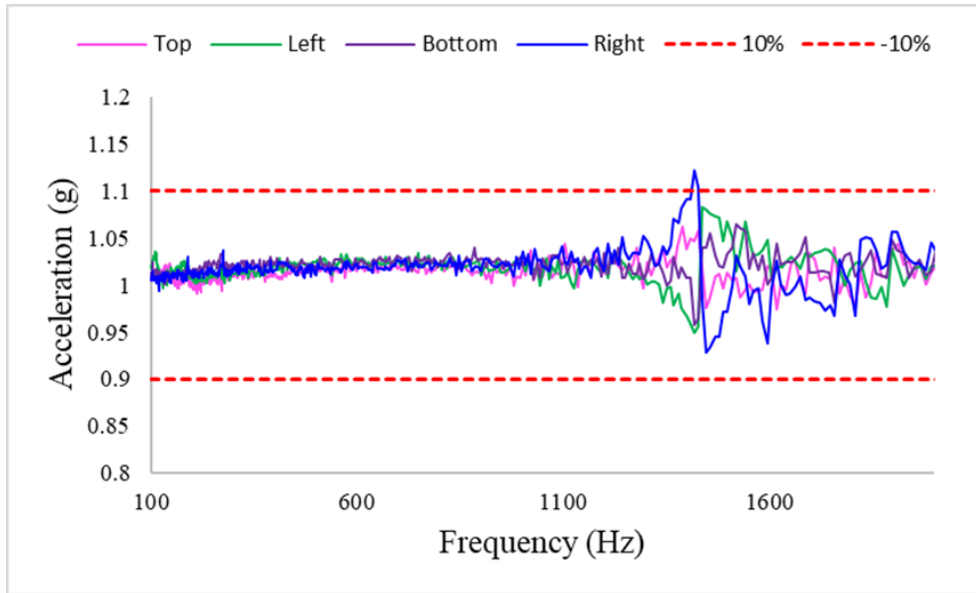
Figure 2.15: Simultaneous test characterization

2.4 VIBRATION MEASUREMENT SENSOR

In general, three measurement sensors, piezoelectric accelerometer, LASER, and MEMS based accelerometer can do the indirect stress measurement on PCB. However, MEMS based accelerometer is not able to be mounted freely because it needs an application board to drive ICs. Therefore, a proper measurement sensor will be selected between accelerometer and LASER by assessing the impact on the board vibration response at board level and module level with board 1 in table 2.1. Besides, a strain gauge is common a method to do direct strain measurement on the board. However, the deviation on strain is normally caused by the mounting process and experimental parameter selection. Therefore, an appropriate verification needs to be done for the strain gauge test setup. In this section, proposed measurement methods in figure 2.16 will be used to investigate the impact of the measurement sensor and verify the strain gauge measurement of other mechanical test methods, drop test, and bending test.
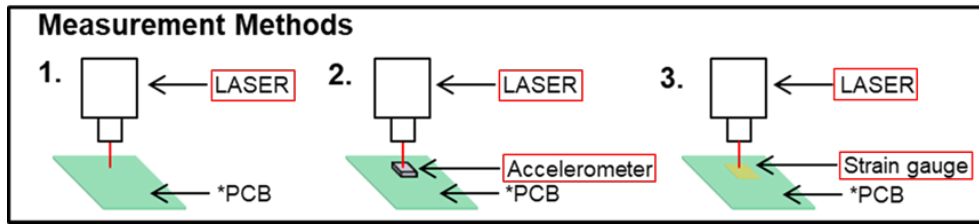
Figure 2.16: Proposed measurement methods

2.4.1 Vibration Test Setup

At board level vibration test, the customized PCB in table 2.1 will be mounted on 4 standoffs by four M3 screws with 0.45N·m as shown in figure 2.17 (a). The board at module level is mounted on the customized heatsink as shown figure 2.17 (b) with same screw and torque setting.
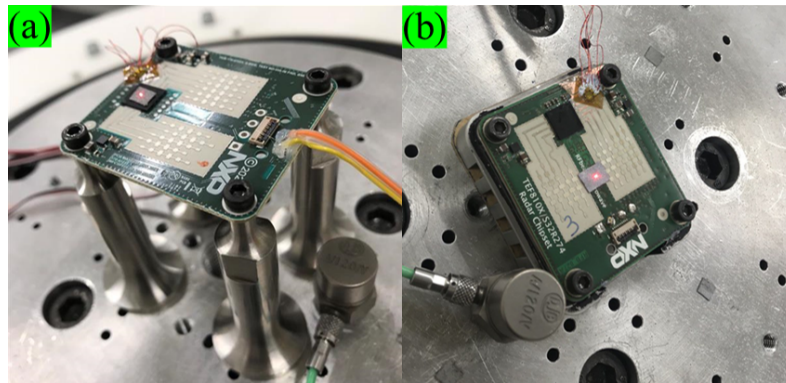
Figure 2.17: PCB vibration test setup (a) board level (b) module level

The vibration profile used to assess the impact of the measurement sensor is shown in table 2.4 and the measurement tools used in this section are listed in table 2.5

Method	Swept sine
Input level of acceleration (g)	1 and 5
Frequency (Hz)	From 100 to 2000
Sweep rate (oct/min)	1

Table 2.4: Vibration profile for assessing measurement sensor

The accelerometer which will be placed on PCB is weighted 0.2 gram as a recommendation in [34] to reduce the measurement deviation.

Picture	Mass (gram)	Sensitivity (mV/g)	Fixation	Purpose
	3	101.5	Mounted with nut system	Control Acc.
	0.2	0.24	Mounted with wax	Measurement
	contactless	Depends on measure conditions	Tripod	Measurement

Table 2.5: Measurement equipment used in PCB vibration characterization

To verify the test setup and parameter settings of accelerometer and LASER, Measurement Method 2 in figure 2.16 is applied on customized bare PCB with 1g swept sine vibration test. In figure 2.18, shows acceleration level measured by accelerometer and normalized by LASER signal. At the low frequency, the signal between both measurements seems to deviate. It can be due to the nature of this accelerometer, which is designed for measuring high acceleration levels, so it has higher sensitivity deviation when measuring low acceleration. At the frequency range between 1200 Hz to 1800 Hz which is also the resonance frequency of the bare PCB, the higher acceleration level happening which shows the limited deviation between both measurements. overall, the accelerometer and LASER signal has an acceptable 10% range.
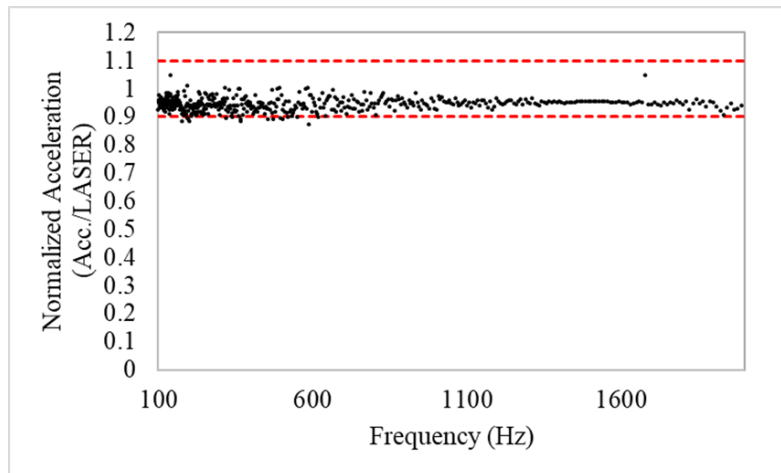
Figure 2.18: Normalized vibration response at bare PCB – Input 1G

2.4.2 Impact of Measurement Sensor

Vibration at Board Level

In figure 2.19, sine sweep vibration is performed on the bare PCB and the dynamic response is measured by LASER at different PCB locations. The resonance frequency measured on two positions has only 0.008 Hz shift which can be explained with the equation(1.13). The equation shows that the resonance frequency is determined by the PCB

material property such as Young's modulus, density, PCB dimension, and Poisson ratio. When using the LASER to measure the vibration response on the same PCB but at different PCB positions, there is no impact on these parameters which can cause a shift in the resonance frequency.
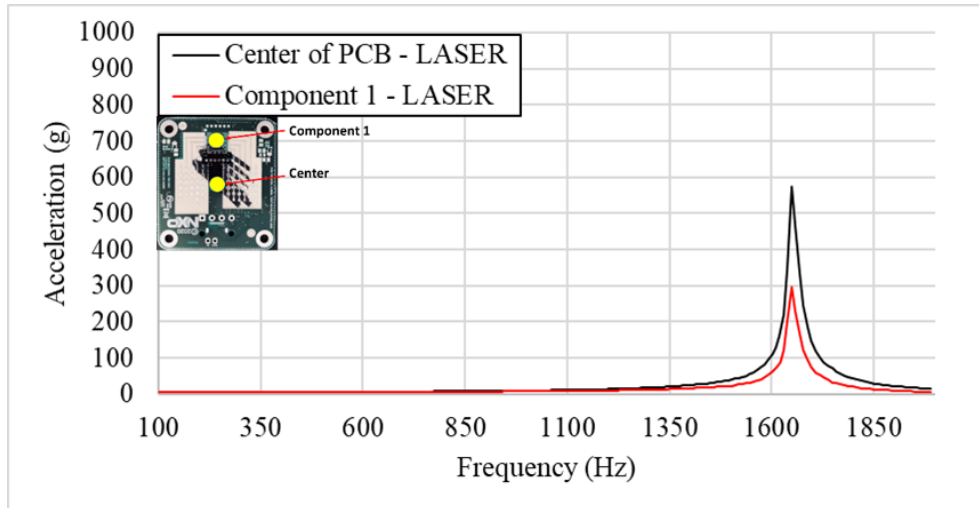
Figure 2.19: Bare PCB vibration response (Measurement Method 1) – Input 5G

However, the most common way of characterizing the PCB is using a lightweight accelerometer because it is cheaper and handier than other measurement sensors such as LASER. The location where the accelerometer is placed on the PCB is able to cause asymmetric loading and thereby influences the PCB vibration mode shape. In figure 2.20, the accelerometer is placed on component 1 location and center, the response of PCB is measured by LASER. The resonance frequency increases by 7% because the accelerometer is moved from the center to the edge.
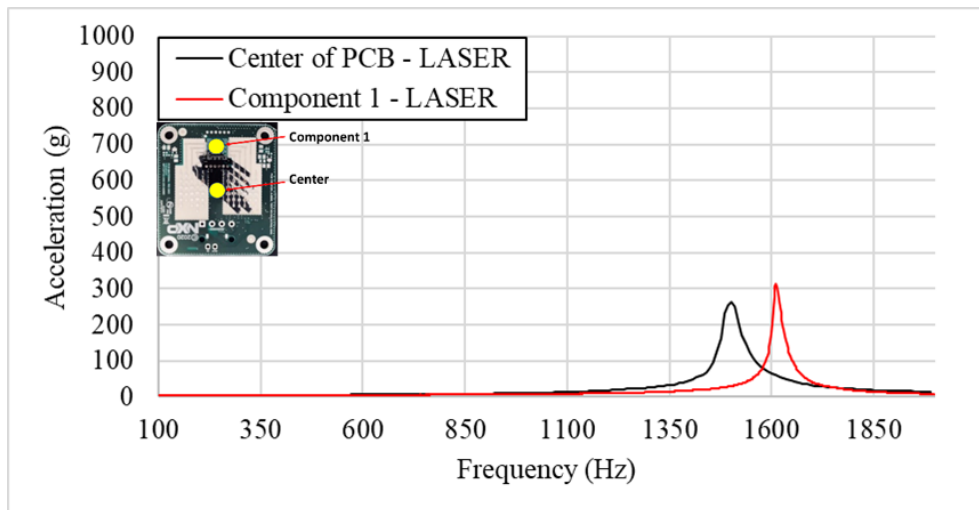
Figure 2.20: Bare PCB vibration response (Measurement Method 2) – Input 5G

Additionally, the mass of the accelerometer is also a crucial parameter to deviate the resonance frequency and peak acceleration level. The resonance frequency and peak-to-peak displacement recorded on a bare PCB with and without accelerometer are significantly different as shown in figure 2.21. The resonance frequency and peak-to-peak displacement when measured performing with LASER but without the accelerometer, is 1648Hz and 0.105mm, and the measurement with accelerometer is 1501Hz and 0.058mm. By comparing measurement methods 1 and 2, the resonance frequency and level of acceleration decrease by 9% and 52% respectively. It is due to the additional mass of the accelerometer. From equation(1.13), it can be derived that frequency is inverse proportional to the square root of the mass. The deviation in resonance frequency is larger in the experiment can be devoted to the formula is derived under the assumption that the board has homogeneous material.
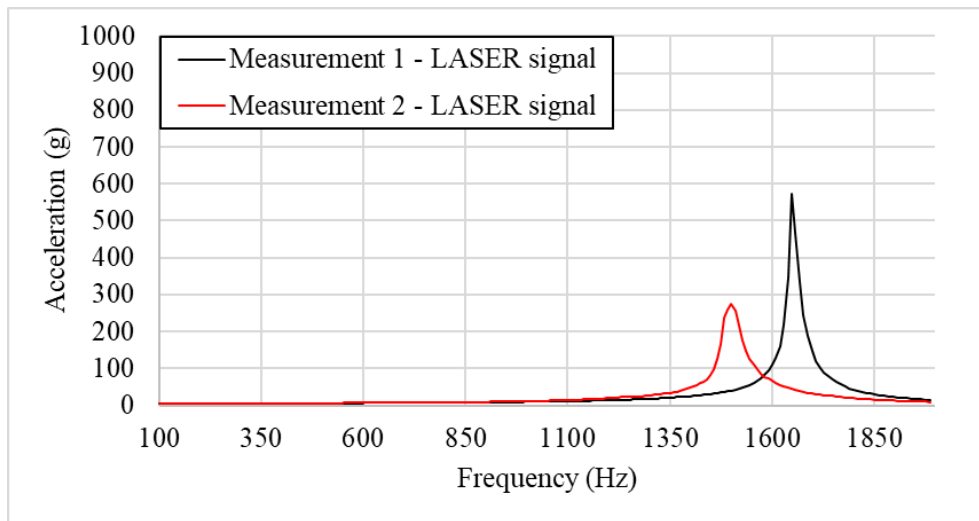
Figure 2.21: Impact of accelerometer on customized bare PCB dynamic response - Input 5G

Furthermore, the finite element model is built for customized PCB to investigate the effect of the accelerometer. However, the model will focus on the shifting trend of the resonance frequency rather than the absolute resonance values of the PCB because the difference in the absolute value of resonance frequency can be attributed to two main reasons. First, the model is built in homogenized material, but it is a hybrid PCB which is made of FR4 and ROGER in the actual situation. Second, the clamping in the model is perfectly firm, but it is 0.45N·m to prevent damage on the PCB and screw thread in the experiment. In figure 2.22, a similar trend is found in the simulation result. When the accelerometer is placed on the center of bare PCB, the resonance frequency is decreased by 10% due to the mass effect. When the accelerometer is placed on the component 1 location which is close to the edge, the mass effect still shifts the resonance frequency about 3%, while the amount of shift is relatively small compared to the condition in which the accelerometer is on the center. The amount of shift is decreased because the accelerometer brings a force pressing on the edge of PCB which can be taken as a change in boundary condition (λ in the equation(1.13) changed).
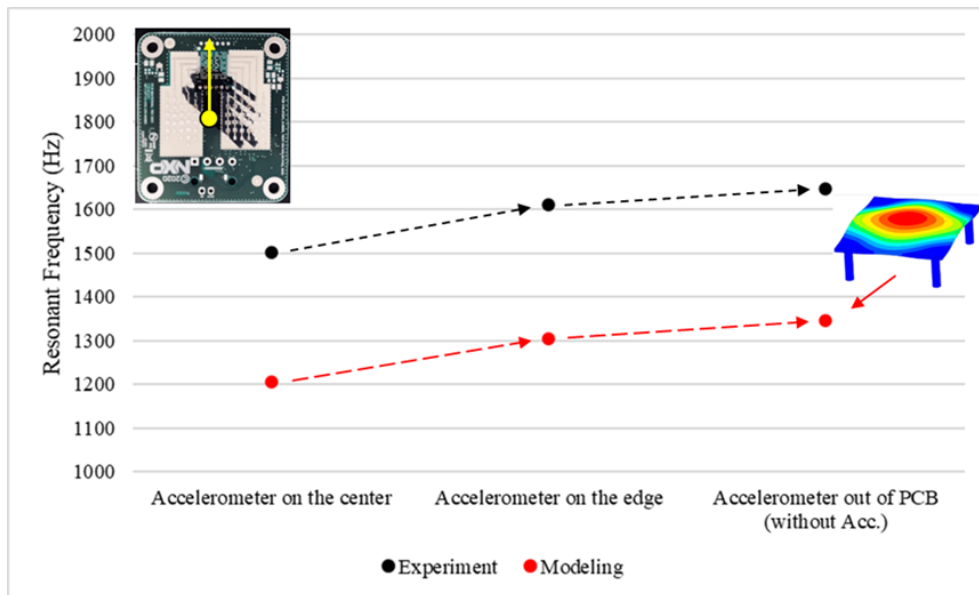
Figure 2.22: Impact of accelerometer on resonance frequency (experiment vs modeling)

Additionally, a MEMS based accelerometer with the specific driven board is also used to verify the measurement as shown in figure 2.23. The LASER is the point at a MEMS based accelerometer to verify whether it can detect resonance signal correlating to LASER in the time domain. The driven board is mounted on four standoffs by M3 screws with 0.45 N·m.
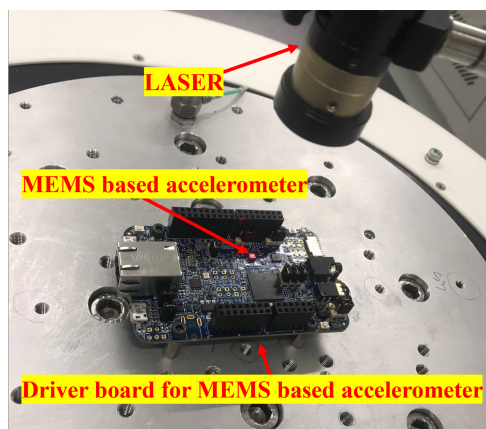
Figure 2.23: Vibration setup of driven board for MEMS based accelerometer

As shown in figure 2.24, when the LASER signal shows the resonance peak, the MEMS based accelerometer shows a similar trend, the only 0.3-second difference between two peaks. This time difference can be due to the synchronization of the measurement equipment, which is not expected to come from the measurement error. The result indicates that both measurement sensors can detect the resonance correctly. However, the MEMS based accelerometer needs a specific circuit

to read out the data, which cannot be used in this thesis for further research.
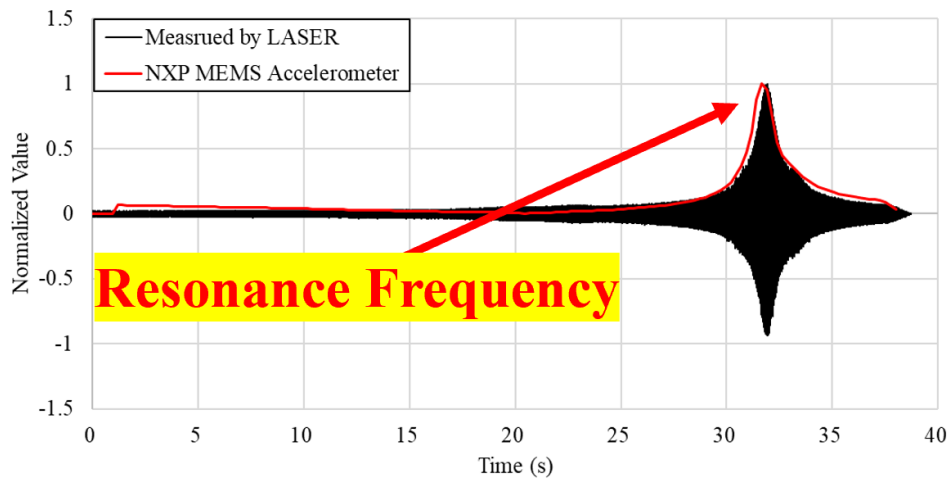
Figure 2.24: Comparison between MEMS based accelerometer and LASER in time domain - Input 1G

Vibration at Module Level

In figure 2.25(a), swept sine vibration with input acceleration 5G is performed on customized electronic module with heatsink. The LASER is used to measure the center of the board and component 1 position. A 0.6% decrease of the resonance frequency is observed (from 1728Hz to 1716Hz). According to the plate theory, a similar resonance frequency is expected on the same board at different measurement positions. This variation is expected to come from the interaction between PCB and housing or cause by measurement accuracy. In figure 2.25(b), the input acceleration is decreased to 1G which can reduce the vibration motion of the board. The value of the resonance measured on the center and component 1 location has only 0.3Hz shift. The result corresponds to the theory, and this will be used to assess the impact of the accelerometer.
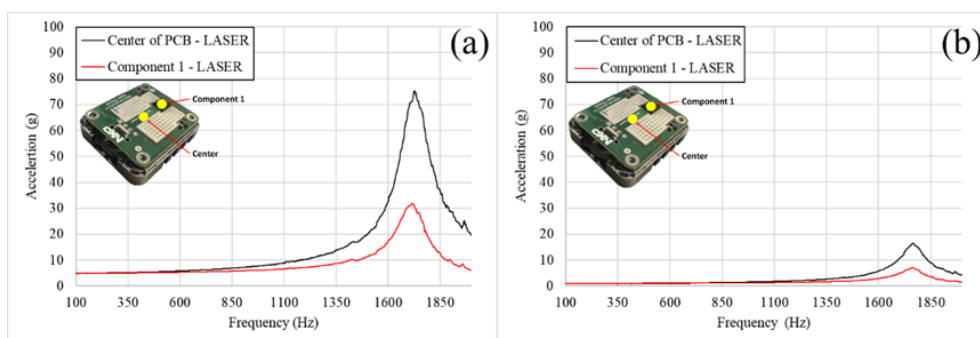
Figure 2.25: Bare PCB vibration response (a) Input 5G (b) Input 1G - Measurement Method 1

In figure 2.26, accelerometer is mounted at the PCB center and component 1 position at module level vibration test. LASER measures

acceleration level with respect to the frequency at the center of the PCB and component 1 location. The resonance frequency shifts 10% to a higher frequency (1564Hz to 1721Hz). This variation is due to the change in vibration mode shape perturbed by the accelerometer. The component 1 location where it is close to the edge of the board. An accelerometer is equivalent to an extra force that is added on the simply supported edge that alters the clamping condition of the board.
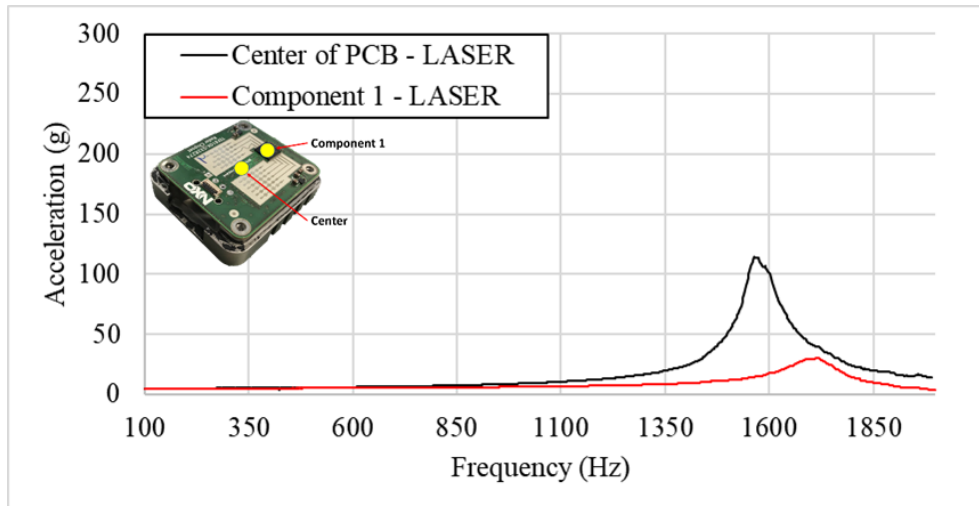
Figure 2.26: Bare PCB vibration response (Measurement Method 2) – Input 5G

Furthermore, an accelerometer is placed on the PCB to assess the impact on board dynamic response at the module level vibration test. It is observed that the resonance frequency shift backward from 1728 Hz to 1564Hz. The shift can be devoted to the mass of the accelerometer. However, the peak-to-peak displacement is increased by around 59%. This contradicts Newton's second law of motion when the same amount of force (same input acceleration) is applied to an object, the acceleration should decrease with an increase in mass.
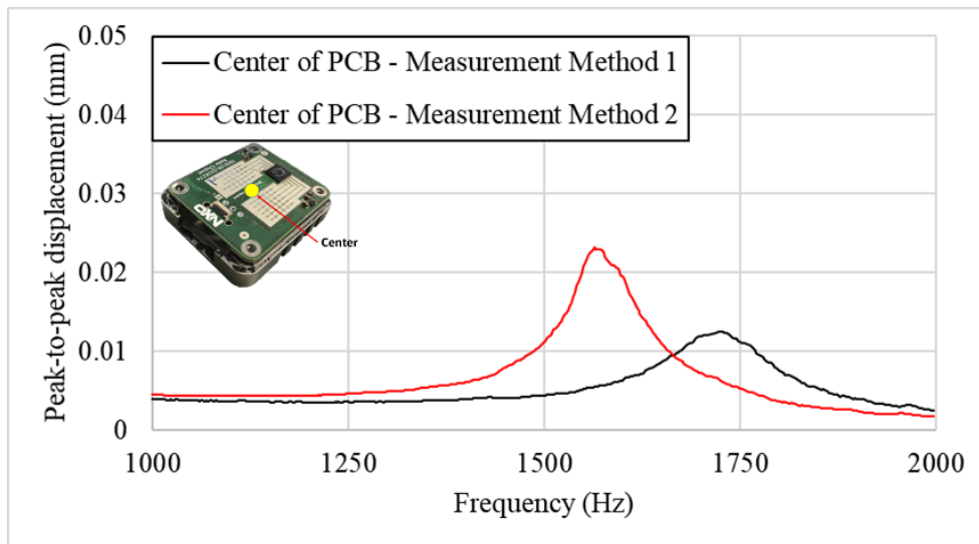
Figure 2.27: Impact of accelerometer on customized bare PCB dynamic response - Input 5G

Two assumptions can explain this phenomenon. First, the air pressure between the housing structure and the PCB reduces the motion of the board, when the extra mass is added to the board, it helps to resist the air pressure formed in between the PCB and heatsink. Second, the interaction between the housing structure and PCB increases the amplification factor. In figure 2.28 assembled PCB which is heavier than the bare PCB is tested at module level with heatsink structure. The mass is larger enough to resist the air pressure; therefore, the peak-to-peak displacement decreases 27% with the accelerometer mounted on PCB. To conclude, the above result shows that taking an accelerometer as a measurement tool is not the best option at this module-level vibration test, the further experiment at module level will be done in LASER.
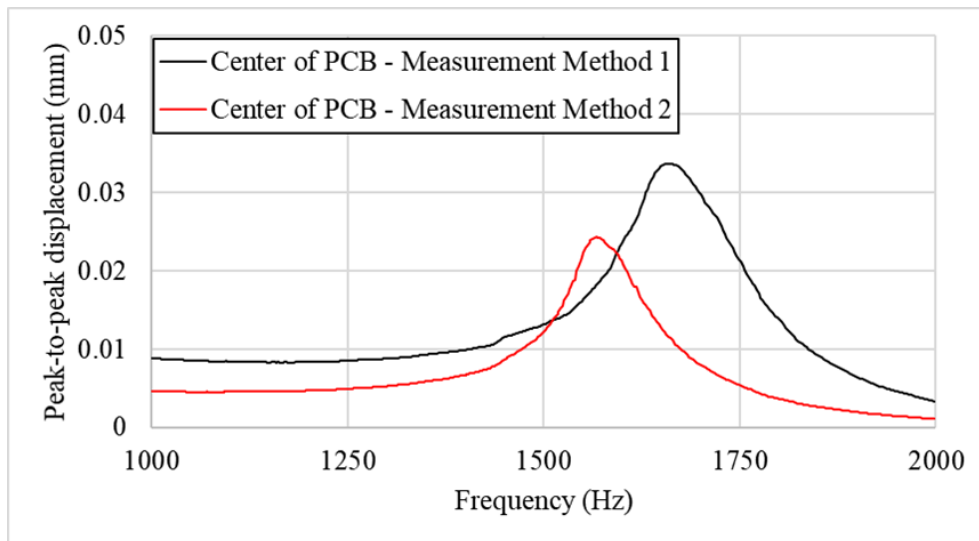
Figure 2.28: Impact of accelerometer on customized assembly PCB dynamic response - Input 5G

Vibration at Reference Board

The impact of the accelerometer on B111A reference board is shown in figure 2.29. Following the recommendation in [34], a small 0.2-gram accelerometer is used on B111A PCB, indeed, limited impact on resonance frequency for the first mode and second mode, but the level of acceleration and peak to peak displacement have more than 65% deviation.
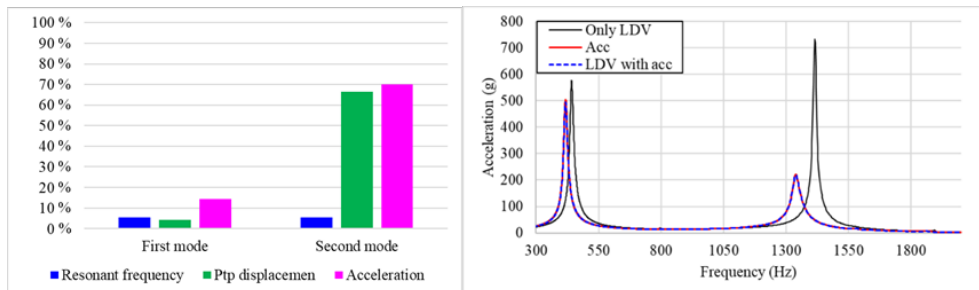
Figure 2.29: Deviation (%) between measurement method – measured by LASER

To summarize the impact of the accelerometer, it depends on the dimension of the PCB, material properties, and board clamping condition. The amount of deviation is higher on customized PCB than reference B111A because the PCB is lighter; therefore, the mass effect of the accelerometer is more significant. In this investigation, the accelerometer is not the best option for measuring the vibration dynamic response of the PCB at board level and module level. The further experiments will be conducted under LDV.

2.4.3 Strain Gauge

The strain gauge is generally made of a metal grid and attached to the PCB. The resistance of the metal grid will be slightly changed due to the deformation of the board under stress. This resistance difference can be furtherly calculated into board strain. In this section, the strain gauge experimental test setup complying with IPC/JEDEC-9704A [13] is implemented and verified. First, a $1.0mm^2$ and $2.0mm^2$ staked rosette ($45°/90°/180°$) which is a form of strain gauge containing three grids within the gauge sensor as shown in figure 2.30 is recommended. In this thesis, uniaxial and rosette strain gauges are used in the experiment. Normally, the strain value of the uniaxial strain gauge will be slightly lower than the rosette. The resistance of the strain gauge grid is either 120Ω or 350Ω. Under the same voltage level, the heat generation will be reduced with higher resistance so that the signal-to-noise ratio is improved.

Second, to measure the strain of the selected component, the intersection of the strain gauge grid needs to be placed 5 mm away from the corner of the component as shown in figure 2.30. The 45° grid should be perpendicular to the diagonal line of the package.
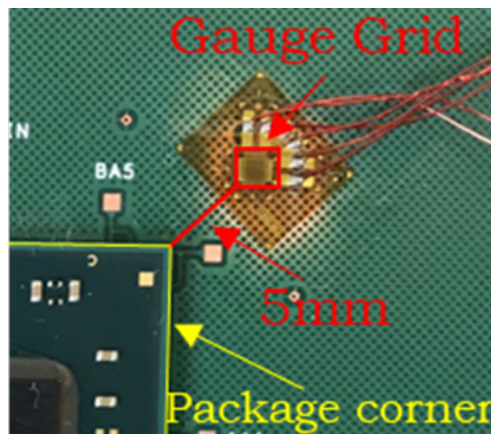
Figure 2.30: Recommended strain gauge placement and details

Third, the lead wire is recommended with 30 AWG and 1.5m to 2m wire length. The strain gauges used in this thesis are 1.5m. The thicker cable (24 AWG) is used, but the signal won't be enormously deviated once properly pre-heat the strain gauge. Fourth, the excitation voltage is recommended to be 2V, while it is mentioned that the supplier's suggestion (5V) should be followed. The sampling frequency is suggested with 500Hz to 2000Hz. However, the Nyquist theorem which the sampling rate needs to be 2 times of bandwidth must be fulfilled, the sampling rate needs to be increased to apply on vibration testing. Also, in [30] the author indicates that the minimum sampling rate should be addressed for different test setups. A vibration test is performed from 100 Hz to 2000 Hz on the B111A PCB with a different

sampling rate. A proper sampling rate where the strain value starts to saturate should be addressed. In figure 2.31, the strain value shows saturation at around 350 microstrains. Therefore, the sampling rate of strain gauge measurement should be over 5000Hz. In the further strain measurement, a sampling rate of 7500Hz will be used.
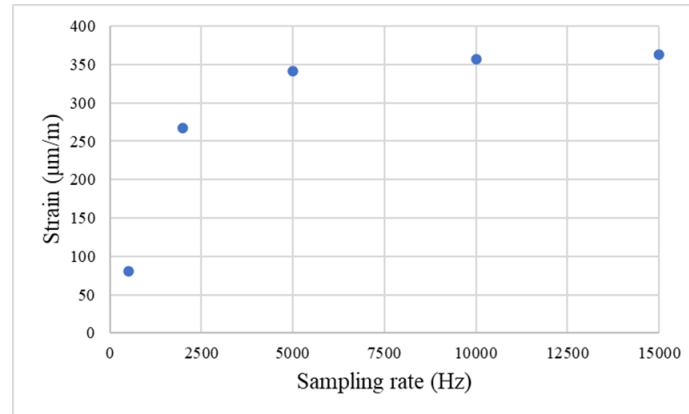
Figure 2.31: Impact of sampling rate on strain gauge measurement

In the end, two mechanical test methods, the board level drop test, and the board level bending test, are performed to verify the quantification of the measured strain value and compare it with the literature and simulation studies. Board level Drop tests are performed on the B111A PCB with similar test parameters as [37]. In figure 2.32 (a), SG1 value in blue is compared with the setup used in this thesis.
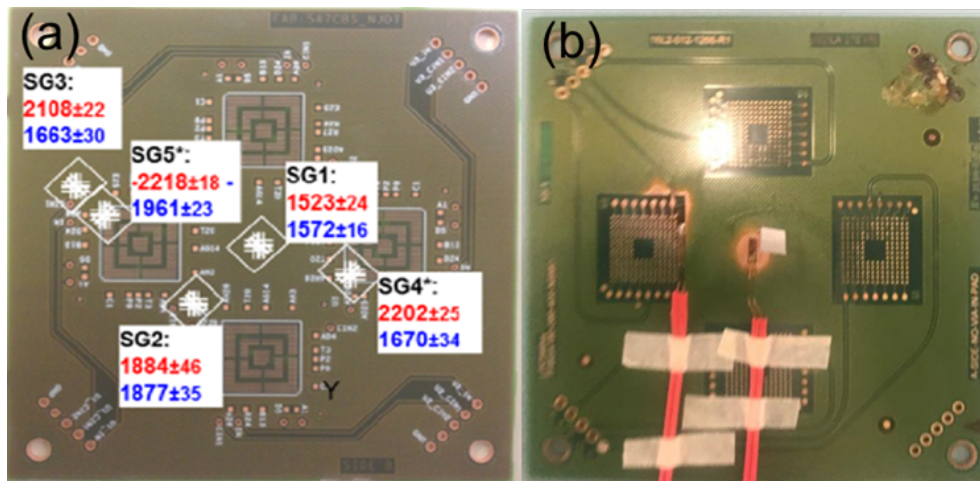
Figure 2.32: B111A PCB layout (a) strain value drop test [37] (b) PCB used in this thesis

Three drops are performed on the PCB in the figure 2.32 (b) with uniaxial strain gauge (120Ω grid resistance). The average maximum strain is 1503 ± 37 as shown in figure 2.33. It is similar to the values observed in the literature. The slight strain differences might be caused

by different PCB manufacturing batch and strain gauge mounting orientation.
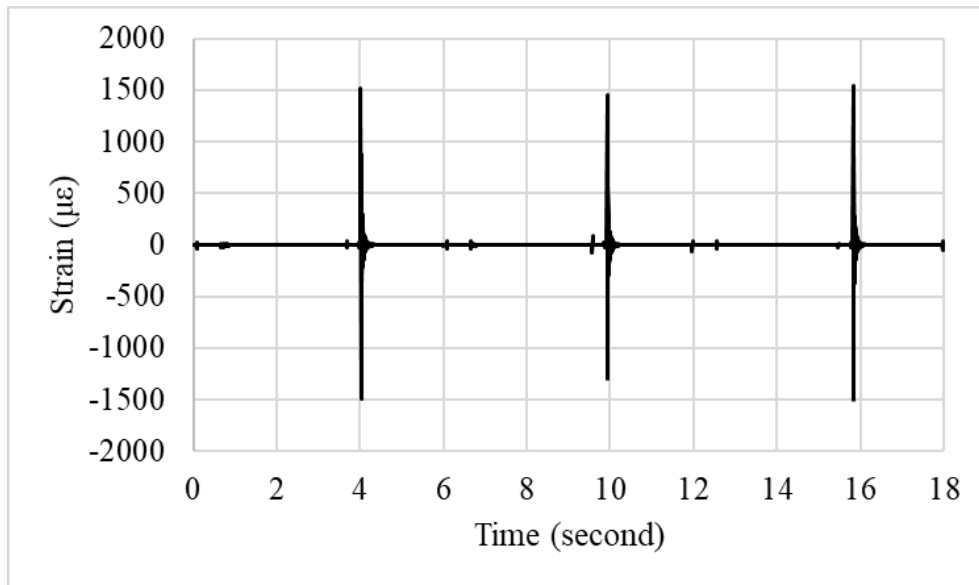
Figure 2.33: Strain value of JEDEC B111A under drop test

A monotonic Bending test is also performed on the B111A PCB and copper plate with the same dimension. A uniaxial strain gauge is mounted on the center of PCB, and the measured strain will compare with the numerical simulation results. As shown in figure 2.34, more deviation happens with the bending displacement increase. This can be caused by the assumption of PCB boundary condition in the model is different from the actual clamping condition and mounting orientation of the strain gauge. However, both simulation and experimental data show non-linearity on the copper plate once bending displacement exceeds 1.5mm. The deviation of strain value measured under 0.5mm displacement is within 10%.
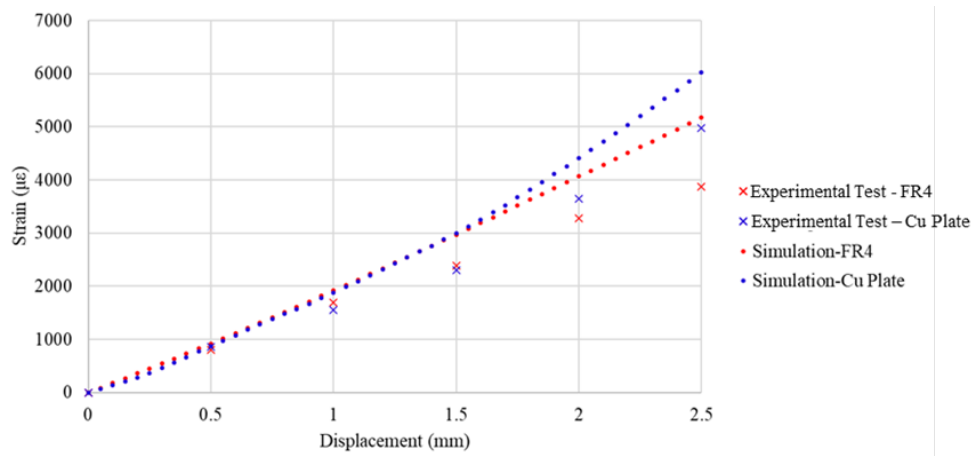
Figure 2.34: Stain value of JEDEC B111A under bending test and numerical simulation

Additionally, the strain data is processed by Fourier transform and compared with vibration acceleration data measured by LASER in terms of the resonance frequency. As figure 2.35 shown, the resonance frequency is similar with only 1Hz deviation. This again verifies strain gauge test setup is reliable.
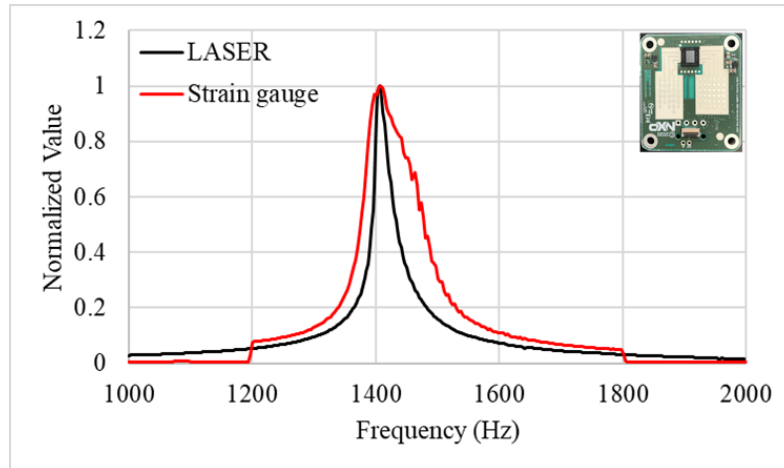
Figure 2.35: Comparison between strain gauge and LASER - Input 5g

In conclusion, the strain gauge acquisition system is implemented by complying with the IPC/JEDEC-9704A [13]. Different mechanical testing techniques are used to verify the quantification of the strain value. The strain measurement test setup can further be used for vibration testing.

3 | PCB DYNAMIC RESPONSE CHARACTERIZATION RESULT

3.1 BOARD LEVEL (TEST BOARD 1)

In the board level vibration characterization test, the radar sensor application boards are characterized in three different forms as shown in table 3.1. Three of them will be mounted on 4 standoffs by four M3 screws with 0.45 N·m as shown in figure 2.17 (a). To investigate features of this PCB, the vibration test will be performed under different test parameters [29]. The result will be recorded by the LDV.
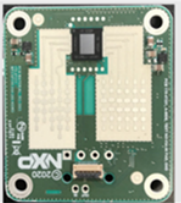
PCB Type	Bare PCB	Assembled PCB	Assembled PCB (connector)
Mass (gram)	4.9	7.8	11.3
Young's Modulus	Ref	+	++

Table 3.1: (a) bare PCB (b) assembly PCB (c) assembly PCB with connector

3.1.1 Board Level Vibration Characterization Result

Impact of Input Acceleration on PCB Dynamic Response
Experiment parameters and assembly processes that can affect the dynamic response of the application-specific bare PCB will also be characterized and investigated.
In the figure 3.1 the input acceleration of the shaker is changed between 1G and 20G, and the peak-to-peak displacement with respect to the frequency is measured. With the amount of input energy increasing, PCB peak-to-peak displacement is also increased by a factor of 19.6 times. In Chapter4, different levels of stresses will be correlated to the specific failure mode on a component or PCB. Also, the resonance frequency is found decreasing from 1658Hz to 1629Hz. It is not caused by the PCB but expected to come from the system setups including fixture and standoff [29].
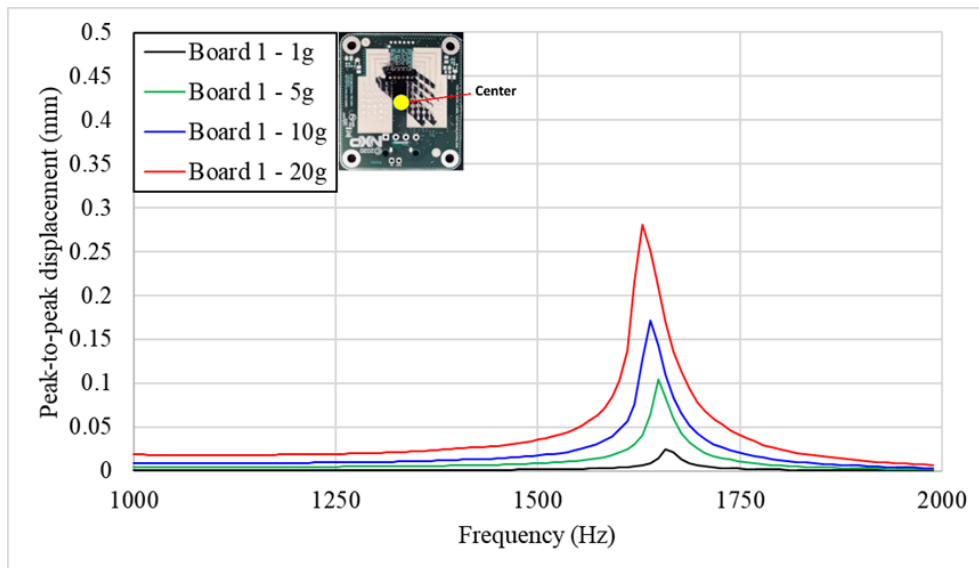
Figure 3.1: Influence of input acceleration on PCB vibration dynamic response

Impact of Assembling on PCB

The two types of assembly PCB are measured under 5G input vibration. In figure 3.2, the resonance frequency of assembly PCB and assembly PCB with connector (table 3.1 (b) and (c)) is 1405Hz and 1235Hz. In general, the connector is used to drive the ICs and for data communication in the radar module. The resonance frequency of assembly PCB is reduced by around 15% due to the combinational effect of mass and stiffness of the PCB. The weight of the PCB increases from 4.9 gram to 7.8 gram because of assembled components and solder joints. From the equation (1.8), the mass effect should decrease the value of the resonance frequency by 20%, but the solder joints increase the stiffness of the PCB which reduces the mass effect. Still, the mass effect is dominant because the resonance frequency decreases. A similar phenomenon happens when assembling the connector on the PCB. The mass of the board is gained from 7.8 grams to 11.3 grams, and the value of resonance frequency decreases from 1405Hz to 1235Hz. The amount of mass increase by the connector is higher than the amount of mass increase by components, while the resonance frequency reduces by 170Hz. The amount of the shift is reduced by 73Hz which is owing to the increase in stiffness, and it is expected to come from the connector.
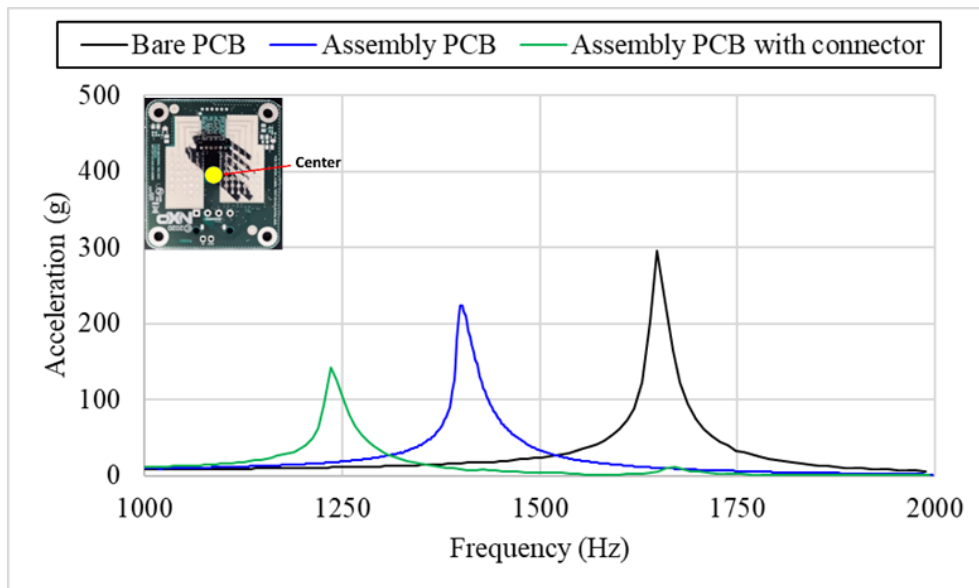
Figure 3.2: Influence of PCB forms on vibration response – Input 5g

In order to prove that the stiffness of the board is increased by the connector, swept sine test from 100Hz to 2000Hz with 20G input is performed. PCB assembly with soldered connector is stressed for analyzing the vibration response before and after the solder joint failure on the connector. The test board had already been characterized numerous times (N-1 times) with a lower input acceleration (1G and 5G), but it is not expected to cause failure on the connector and significant aging on PCB. The test with 20g input shows similar resonance frequency in the first two swept in the figure 3.3. In N+2nd and N+3rd runs, both resonance frequency decreases by 8Hz. Visual inspection on the fixing point of the connector and PCB is found to be loose. The connector solder joint cracks give the board freedom to move which decreases the stiffness (Yong's Modulus) of the board. In the further test, the resonance peak shows an unusual shape, and it was found that the connection pin and solder joints of the connector are broken. To summarize, before the crack initiation, the resonance frequency stays in similar values. However, when the crack forms, the bound between PCB and connector is broken which reduces the stiffness of the PCB, furtherly decrease the resonance frequency. After that, the full crack on the connector, the connector and PCB were hitting each other under vibration. This might cause the abnormal response on the PCB.
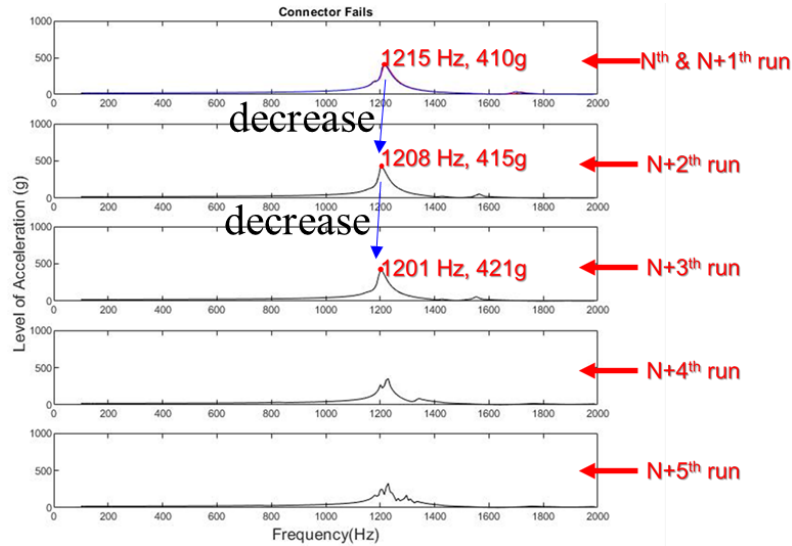
Figure 3.3: Influence of connector failure on vibration response – Input 20G

Impact of PCB Types

In the figure3.4, test board 1 is compared with the test board pre-scribed in JEDEC B111A at board level by analyzing parameters in equation (1.13). First, the dimension of board 1 is smaller than the B111A and the mass is also significantly lighter. Even though Young's modulus of B111A is higher than board 1, the mass and form factor is dominant (the a, b, and in equation (1.13) are higher) which causes a 1210Hz difference between resonance frequency of bare B111A and bare board 1. Besides that, B111A board is assembled with a 25mm×25mm and 2.5 gram BGA component in the center of PCB. On board 1 compo-nents including capacities, resistors, and chips with around 2.9 grams are double-sided assembled. Two boards show an inverse trend on resonance behavior after assembling components on the PCB. The res-onance frequency of board 1 is dominated by the mass effect rather than stiffness. However, the B111A shows a higher resonance fre-quency after the assembly process, which shows stiffness dominant. In [15], author states that this phenomenon is due to the parameter $\sqrt{E/\rho}$.

Mass Dominates	Stiffness Dominates
$\sqrt{E/\rho} > 1$	$\sqrt{E/\rho} < 1$

Next, the bending cycle at resonance frequency under swept sine is approximated with:

$$Bending\ cycle = \frac{\ln(\frac{f_H}{f_L})}{0.69} \times \frac{F}{s} \qquad (3.1)$$

Where f_H and f_L are the higher and lower range of the resonance, 10% of the maximum acceleration or displacement is chosen. The f

is the resonance frequency of the test board and s is the sweep rate (oct/min) of the swept sine. The bending cycle and time duration have been through the resonance are shown in the table below:

	Bare B111A	Assembly B111A	Bare board 1	Assembly board 1
Time duration (s)	9.6	7.6	10.6	11.9
Bending cycles	2161	1815	8798	8535

Table 3.2: Bending cycle and time duration under resonance mode
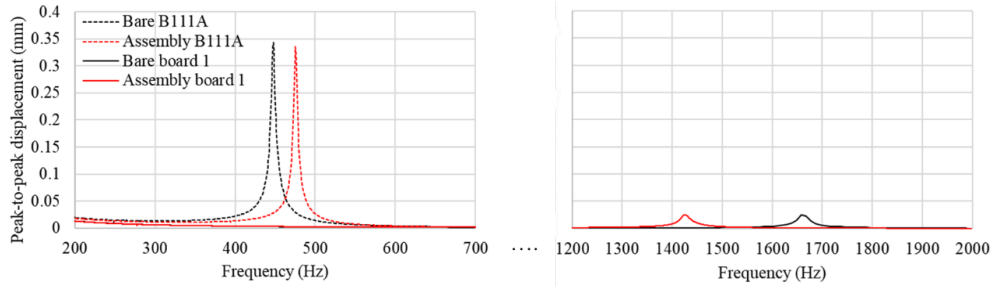
Figure 3.4: Impact of PCB type on board dynamic response – input 1G

To summarize, material property, dimension of the PCB has a great impact on peak-to-peak displacement and bending cycle of the test board. It is difficult to directly correlate these data to the solder joint reliability performance under the test on different PCB. However, it is expected to see the B111A is more critical than board 1.

Assessment on Stress Distribution
Component 2 is the largest package on this radar application board and is therefore selected to assess the stress distribution as a function of the component area. The dynamic response at four corners (Right-top (RT), Right-bottom (RB), Left-top (LT), and Left-bottom (LB)) of this package are measured using LASER. In figure 3.5, the stress can be ranked in $RT > RB \gg LT > LB$. The measured position is closer to the center, the acceleration is much higher. This can be explained by assuming that the PCB's motion is acting as a simple harmonic vibration. The equation of displacement with respect to time can be derived in:

$$Y = Y_o \sin(2\pi f) \tag{3.2}$$

The acceleration of the board is the second derivative:

$$Acceleration = \ddot{Y} = -(2\pi f)^2 Y_o \sin(2\pi f) = -(2\pi f)^2 Y \tag{3.3}$$

As the peak-to-peak displacement is smaller when approaching the edge of PCB. The acceleration also decreases. On component 2, the stress distribution is not symmetrical which higher stress level happens at the right side of it.
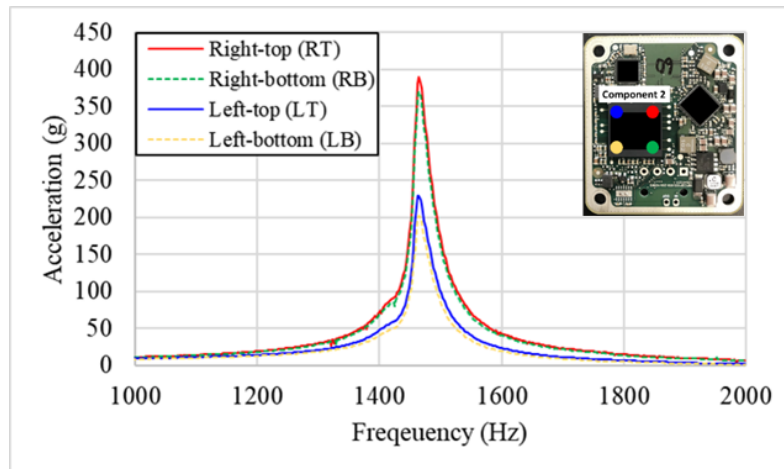
Figure 3.5: Dynamic response of the package corner – Input 5G

3.2 MODULE LEVEL (TEST BOARD 1)

In the module level vibration characterization test, the assembled PCB is mounted onto a customized housing structure. PCB module is clamped at the corners by M3 screws using 0.45 N·m torque. The four edges of the PCB are simply supported by the heatsink. To assess the impact of the housing structure on the PCB dynamic response, board vibration response at the module level, different housing design concepts will be discussed in this section. Same measurement units and PCB type will be used as shown in Section 3.1.

3.2.1 Module Level Vibration Characterization Result

Impact of Input Acceleration on PCB Dynamic Response
To assess the effect of the experimental parameter, the input acceleration is changed from 1G to 20G. The peak-to-peak displacement is found to increase from 0.002mm to 0.058mm (by a factor of 20). At the same time, the resonance frequency decreases from 1761Hz to 1681Hz with the input energy increase as shown in figure 3.6. This amount of shift is not expected to come from the PCB itself, but the system stiffness changes [29]. Besides, the vibration response signal at module level is not smooth as at board level response, this can be due to the interaction between the board and heatsink. It is found that this phenomenon becomes less with the input acceleration decreasing because less vibration energy is applied to the board and heatsink.
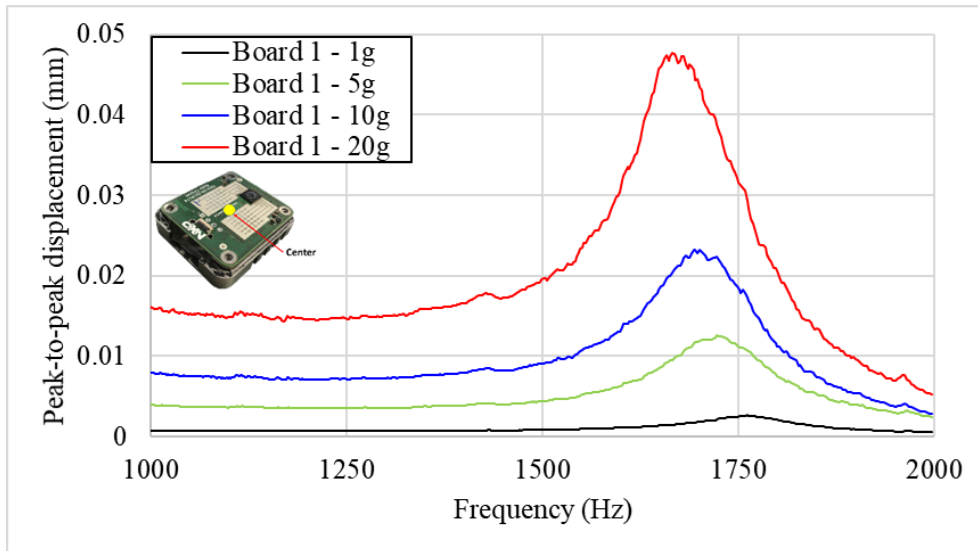
Figure 3.6: Influence of input acceleration on PCB vibration response

Impact of Assembling on PCB

In figure 3.7, two type of PCB assemblies (table 3.1(b) and (c)) are analyzed at module level vibration test to compare it with the bare PCB. The resonance frequency of the PCB assembly decreases by 2% when compared to the bare PCB. According to the numerical calculation equation (1.13), the resonance should decrease by 20% (if the stiffness effect were ignored). This shows that the resonance of the assembly PCB here is dominated by the mass effect more than the PCB stiffness. Besides that, there are three peak-to-peak displacement peaks of PCB assembly with connector are observed at 1402Hz, 1450Hz, and 1683Hz. The peak at around 1400Hz to 1450Hz is expected to come from the connector. The connector vibration motion is coupled with the vibration movement of the heatsink causing multiple peaks. Multiple peaks are not expected to come from the board itself, because it does not be seen in figure 3.2. Similarly, if the stiffness effect were neglected, the resonance of the PCB should decrease by 34% according to the numerical calculation equation (1.13). However, that is not the case here because the stiffness factor of the connector is decreasing the amount of shift that should be caused by the mass.
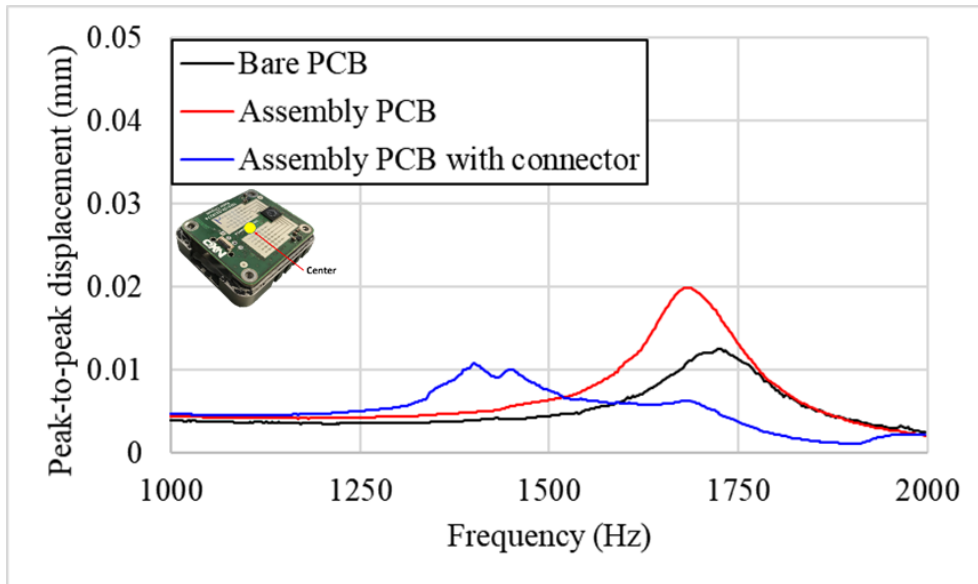
Figure 3.7: Impact of PCB type on vibration response at module level – Input 5G

3.3 IMPACT OF MODULE DESIGN PARAMETERS

In this section, different electronic module design parameters, including PCB clamping condition, housing or heatsink material, and housing construction mentioned in section 1.4.3 will be assessed by designing a similar structure for the electronics module used in this thesis.

3.3.1 Impact of housing structure and material

In the figure 3.8, the bare customized PCB is tested under three different housing as introduced in figure 1.9 It is observed that the increase in mass (from (a) to (c)) of the housing reflects on decrement of the resonance frequency. Also, the wall structure of the housing (b) changes the λ in the equation (1.13) causing the decrease in resonance frequency. This phenomenon can also be due to the difference in the amount of air in between the board and the heatsink. Air acts like a damper to alter the resonance behavior. As for peak-to-peak displacement, when the mass of the heatsink enhances, the momentum of the system also increases. This causes the board to show higher displacement. In conclusion, heatsink or housing is interacting with the PCB vibration motion, and it changes its response to vibration stresses. The stress of PCB can be effectively adjusted by modifying the construction or changing the material of the housing.
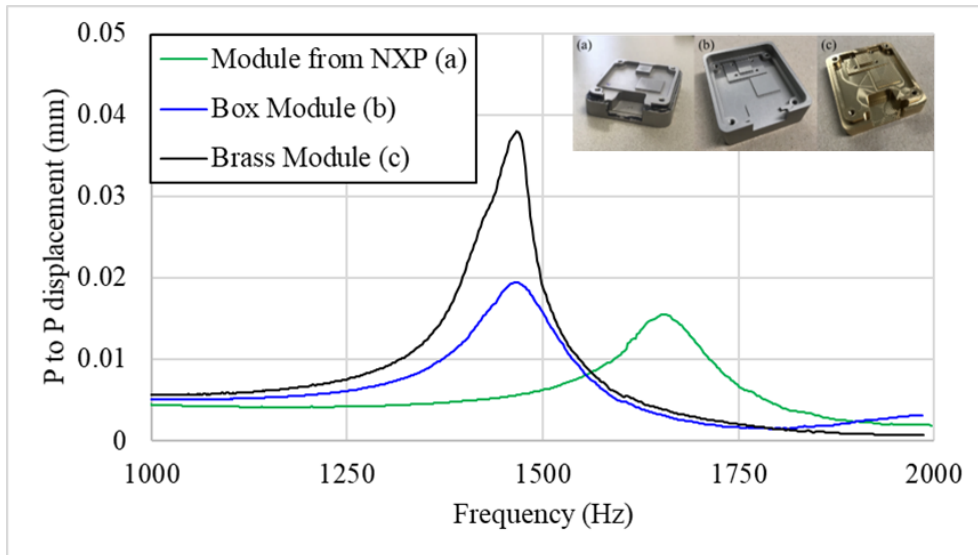
Figure 3.8: Impact of the housing construction

To show the influence of a not well-design housing structure, another customized electronic module is characterized under vibration test. The housing is constructed by two parts, the bottom plate, and the box. The bottom plate is for fixation and the box is for placing the board module. In figure 3.9, another customized electronics module is characterized with and without the housing structure, and the plastic housing is characterized under vibration test. In (A) the board is fixed at the corner by four M3 screws with 0.45 N·m torque on the vibration fixture which is close to the board level vibration setup. In (B) the board is fixed on the housing and the entire module is bolted on the vibration fixture by four M6 screws with 10 N·m that is a module-level test setup.
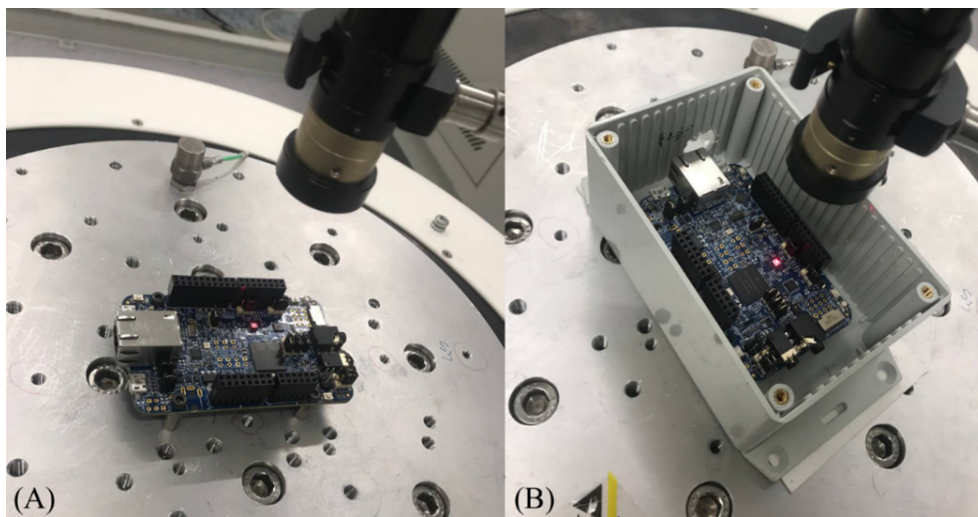
Figure 3.9: Customized electronic module 2 (A) without housing (B) with housing

The vibration signal is measured by LASER at the center of the plastic housing is shown using green line in figure 3.10. After a frequency of around 920Hz, the level of acceleration increases with the frequency rising. This is due to the motion of the bottom plate of the housing interacting with the vibration movement of the vibration fixture. When the frequency increases, the number of impacts occurs more frequently and thereby enlarges the stress level at components. If the board is mounted inside this housing structure, this interaction between them will be coupling. The board vibration response will be amplified. The board response measured at board level by LASER is plotted using black line in figure 3.10. The first resonance peak is found at 811Hz with an amplification factor of 7. Comparing the board response at the module level, the first resonance peak shows at 971Hz and the level of acceleration is 15G. Not only does the resonance frequency increase due to the change in the boundary condition, but also the acceleration peak increase by a factor of 2 because of the coupling effect. To summarize, this experiment shows that an inappropriate housing structure might lead to stresses being higher than the stress measured at the board level set up.
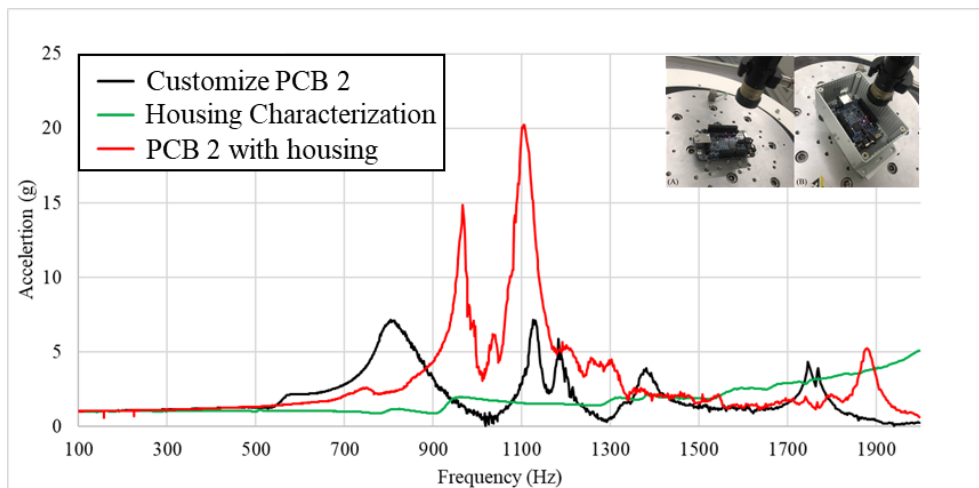
Figure 3.10: Board dynamic response of customized electronic module 2 – Input 1G

3.3.2 Impact of PCB Clamping Condition on Vibration Response

The PCB is fixed at four corners which is not the case in the electronic module as shown in figure 1.8. An aluminum frame with 3mm thick is placed on top of the PCB edges at electronic module as shown in figure 3.11. It changes the boundary condition of the board from four corners fixed with four simply supported edges to four fully clamping edges and corners with 0.45 N·m.
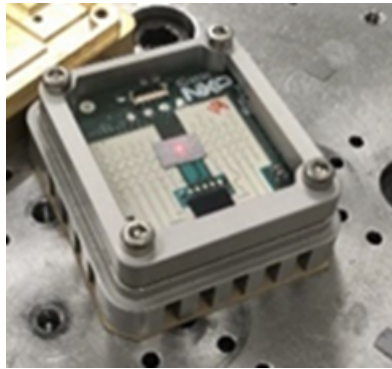
Figure 3.11: Clamping frame on electronic module

In figure 3.12, the dynamic response on assembled PCB is measured at module level. A 5G input acceleration is demanded from the vibration shaker. It is found that the resonance frequency increases by 8% when the boundary condition is changed to fully clamp which reduces the PCB length and width that is required to be excited. Also, the level of acceleration measured on the center of the board is an increase from 136G to 195G. This dynamic response change is due to the frame reduces the effective area of the board. In figure A.10, all the numerical equations of resonance frequency under different boundary conditions show that the increase in length and width of the board can effectively increase the resonance frequency. Also, the effective area of the board decrease, the same amount of energy transfer from the shaker to the test board will move the lighter board. This will increase the level of acceleration measured on the board.
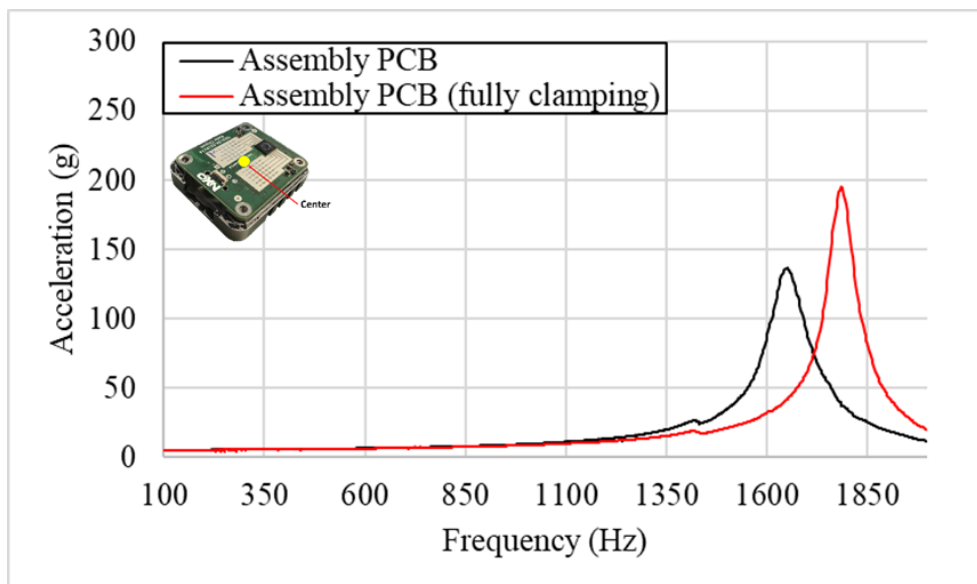
Figure 3.12: Impact of boundary condition on PCB dynamic response

In some electronic modules, a rib structure is added around the chip to constrain the motion of the PCB area surrounding semiconductor

chips (as shown in figure 3.13) or to maintain structural integrity. By doing this, the stress due to the vibration can be effectively reduced. However, this structure can also bring unexpected strain due to installation errors. Four M2 screws are mounted to fix the frame with 0.2 Nm, while visual inspection or advanced analysis such as optical profiling or strain gauge measurement is needed to assess if the board is not bent leading to extra strains in the component vicinity.
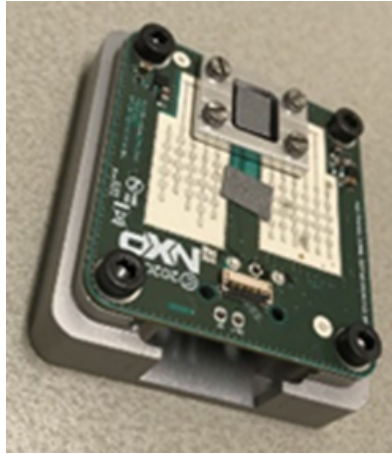
Figure 3.13: PCB motion restricting frame

In figure 3.14, board dynamic response on the assembled PCB at module level is measured. Input acceleration is set at 5G for the shaker. It is observed that the chip frame can significantly reduce the stress level introduced by the vibration. The effect of the rib can be taken as a mass that is added to the board. This causes the resonance peak to decrease to the lower frequency. Besides, the rib limits the board vibrating toward the +Z direction which leads to a low level of acceleration.
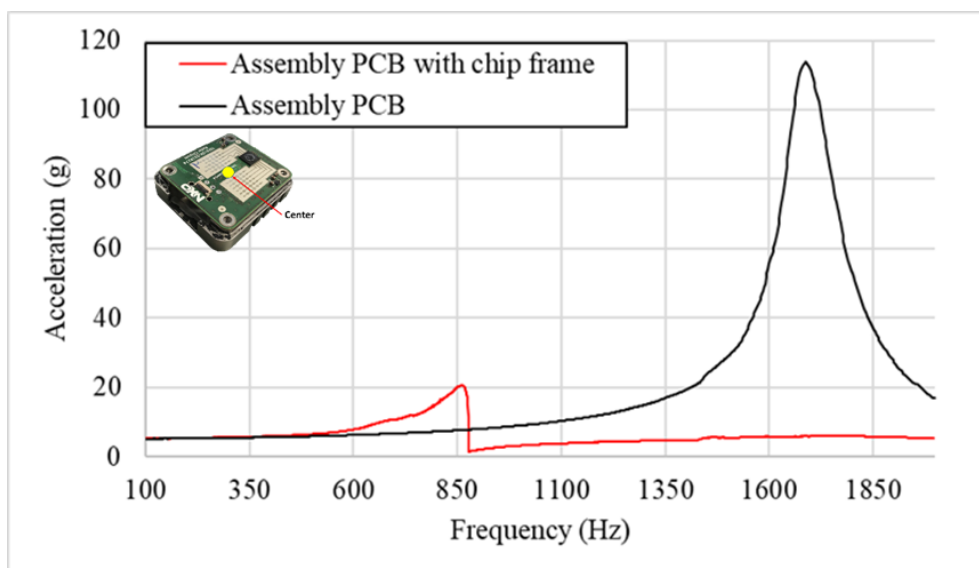
Figure 3.14: Impact of motion restricting frame on board dynamic response

3.3.3 Impact of Thermal Interface Material on Vibration Response

The housing structure of the electronic module normally contains a heatsink to transfer the heat generating from the device. The TIM made by high thermal conductivity material is placed between the board and heatsink to improve the efficiency of thermal conduction. In figure 3.15, thermal interface material is applied on the top of component 2 and the bottom side of component 1. The board vibration response will be investigated with two TIMs (Sil Pad [3] and Tflex 400 [8]).
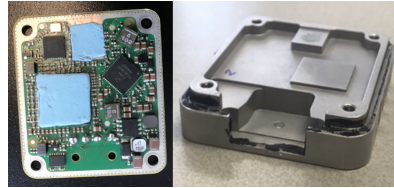
Figure 3.15: Assembly with thermal interface material (TIM)

In figure 3.16, board dynamic response on the assembly PCB at module level is measured. A 1G input acceleration is applied for the shaker. The thermal interface material is placed between the PCB and heatsink constrains the motion of the board vibrating toward -Z direction and damps the energy transfer from the shaker to the board. This causes a significant decrease in the stress level. It can be found that Tflex 400 shows a lower stress level than Sil Pad. It can be due to the 0.2mm thick difference between them which increase the damping. In conclusion, TIM can effectively reduce the stress level of the board under vibration and the effect is more obvious with TIM thickness increasing.
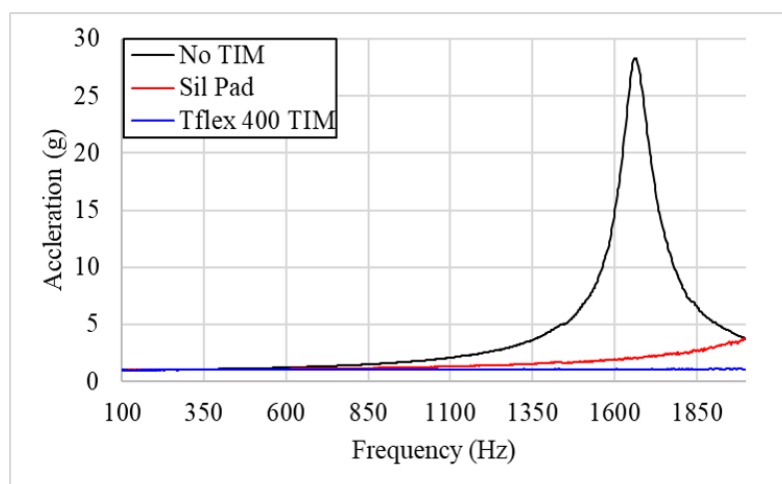
Figure 3.16: Impact of the thermal interface material on PCB dynamic response

3.4 CONCLUSION

According to the previous session of characterization results of the PCB at board level and module level vibration test, the heatsink changes the boundary condition of the board and it leads to differences in the stress level in terms of strain, resonance frequency, peak-to-peak displacement, and PCB peak acceleration. With these results the following conclusion can be summarized:

Dynamic Response of PCB

When the PCB boundary condition is changed from fixed at four corners to fixed at four corners and four edges simply supported, The motion of the board at the module level (with heatsink) is more restricted compared to at board level. As shown in figure 3.17, PCB at board level has higher peak-to-peak displacement than PCB at module level. However, the same input is given to the shaker which means similar energy is transfer to the module. The board at module shows lower peak-to-peak displacement but the bending cycle at resonance increases by 43%. To conclude, the vibration energy transfer to this board-level setup and module-level setup is constant. The vibration energy can be released on the board in two forms, peak-to-peak displacement, and bending cycle. On this board, higher displacement leads to a lower bending cycle under vibration or vice versa. As for the resonance frequency increases by 5% at module level when compared to the board level. This correlates to the formula in figure A.10 boundary condition 14 and condition 17 that more corners and edges are supported or fixed, the higher resonance frequency will show.
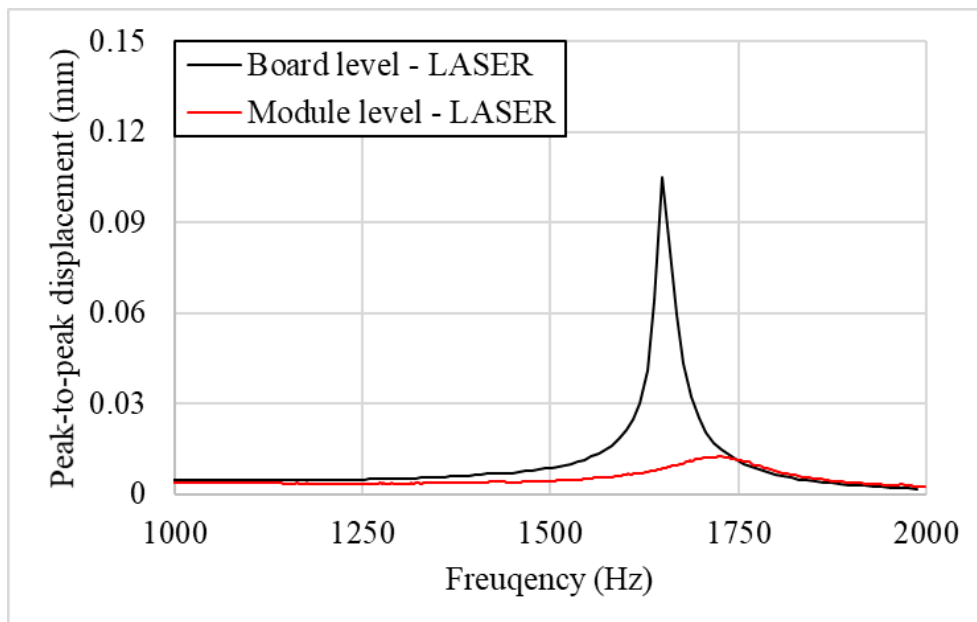
Figure 3.17: Comparison between board level and module level - bare PCB – Input 5G

Board Strain

In the equation (1.18) and equation (1.27), the PCB strain is proportional to acceleration and peak-to-peak displacement. In figure 3.18 the experiment result correlates with the numerical calculation. It is observed that the increased rate of strain and peak-to-peak displacement at the board level is 4 times larger than at the module level. Similarly, this is caused by the boundary condition of the board. The vibration energy releases in terms of the number of motions go up and down rather than the displacement. In other words, the heatsink acts as a damper between the board and fixture, this increases the damping and thus reduces the stress-induced on the board.
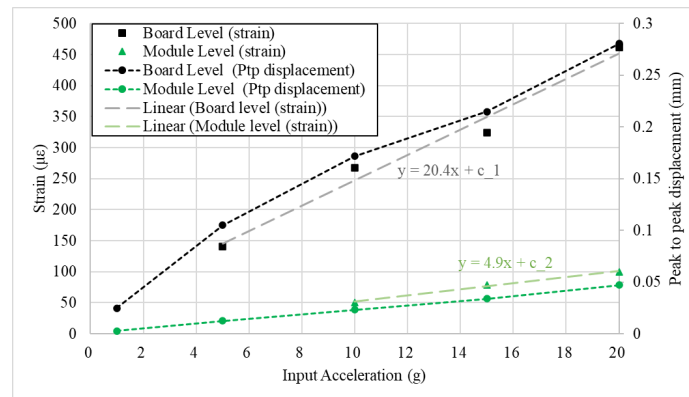
Figure 3.18: Strain and Ptp displacement comparison under vibration test

Impact of PCB Vibration Measurement Method

In the figure 3.19, it is found that the mass of the accelerometer is causing the decrease in resonance frequency. At the board level and module level, the value of the resonance decreases by 9%. As for the peak-to-peak displacement, the inverse trend is shown when mounting the accelerometer on the board. The peak-to-peak displacement decrease by 42% at the board level, while it increases by 58% at the module level. Therefore, it can be concluded that the impact of the accelerometer is larger at the module level than at the board level. However, a deviation that happens at both conditions may cause wrong assessment on reliability vibration profile such as wrong or less critical frequency range is selected.
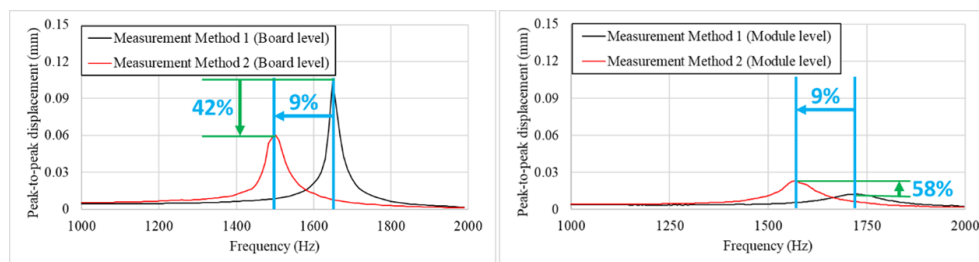
Figure 3.19: Comparison in impact of measurement at board level and module level

4 | BOARD MODULE LEVEL RELIABILITY AND FAILURE ANALYSIS RESULTS

4.1 DEFINE VIBRATION STRESS PROFILE

To define a vibration profile for the test board 1 in table 2.1, PCB dynamic response parameters need to be taken into account. An experimental approach is designed to find the appropriate stress level at which a component failure can be induced within a reasonable amount of test time. As shown in figure 4.1, reference data and pre-defined parameters will be used in the stress increment test and vibration test in a different orientation. Vibration test parameters, such as stress orientation, frequency range, acceleration level, type of vibration, and w/wo heatsink will be used to compose the final vibration profile. In this section, each vibration test parameter will be introduced and defined.
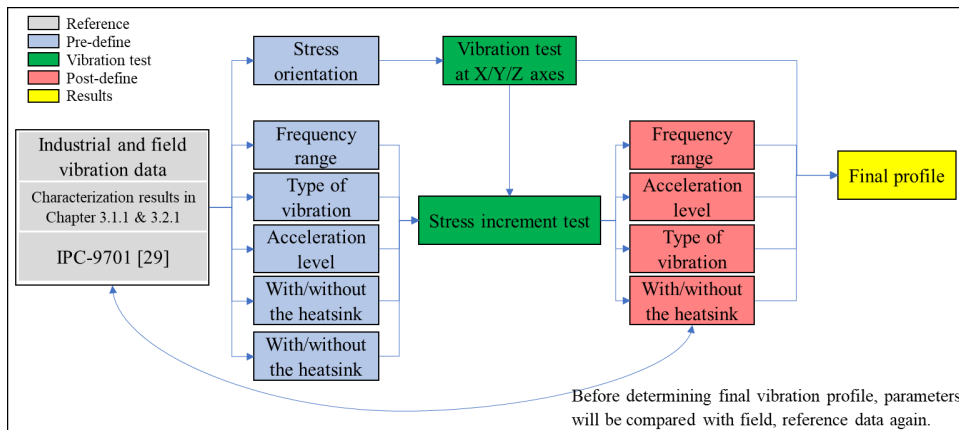
Figure 4.1: Test approach of defining vibration profile

- **Reference and pre-define:**

  1. Stress orientation
  In table 1.1, industrial standards state that the device should be tested at X, Y, and Z directions. In field application, radar module is commonly mounted in X and Y orientation as shown in figure 4.2. However, the possibility of mounting the module in Z orientation cannot be ignored. In this test, only the most critical stress orientation will be tested because the most critical orientation is able to cover the vibration risk for less stress orientation.

Therefore, the board stressed orientation is pre-defined at X, Y, and Z. The strain gauge is used to evaluate the stress level to determine the most critical test orientation.
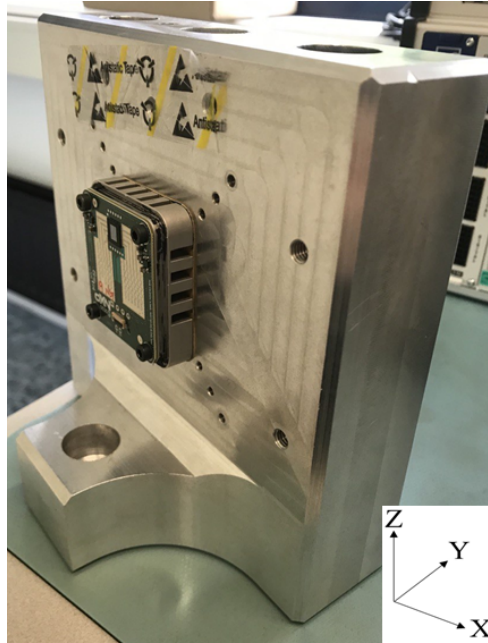
Figure 4.2: Vibration fixture of X and Y orientation

2. Frequency range

The characterization result shown in section 3.1.1 and section 3.2.1, the assembly PCB at board level and module level vibration test has resonant frequency at around 1500Hz and 1700Hz respectively. A restricted sinusoidal sweeping $\pm 300Hz$ (roughly $\pm 20\%$ [29]) is pre-defined to perform at the resonance frequency to stress the board at the most critical frequency range. As for the random vibration test, the minimum and maximum frequency test range in table 1.1 is taken into account which is from 5Hz to 2000Hz. However, the test starts from 10Hz due to the shaker limitation.

3. Type of vibration

In section 1.4.1, the industrial standards state that both swept sine and random test are performed for qualification test. Therefore, swept sine and random tests are pre-defined for the stress increment test, and the most critical one will be selected in the end.

4. Acceleration level

The test input acceleration level is following the stress increment test strategy. As shown in figure 4.3, the input for swept sine and for random test start from 5G and $5G_{rms}$. It steps 5G and $5G_{rms}$ in every 24hrs until 20G and $20G_{rms}$ due to the constrain

of the shaker. The final stress level will be selected at the level in which component 1 or component 2 fails, and one step of stress level lower will also be performed.
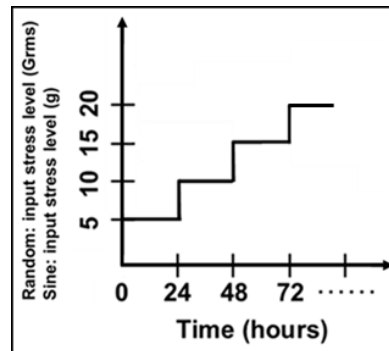
Figure 4.3: Stress increment test strategy and pre-defined parameters

5. With/without the heatsink
The board will be stressed with and without the heatsink in the stress increment test. In the end, the most critical condition will be selected in terms of component failure in the stress increment test.

- Vibration test result:
1. Vibration test at X/Y/Z direction
Strain gauge close to the component vicinity is applied here to assess the stress level under different vibration orientations of the module. In figure 4.4, a swept sine vibration with input 20G is performed on the module. As the strain value measured at different vibration orientations shown in figure 4.4, the highest strain is measured when PCB vibrate under Z direction which is selected to be the test orientation.
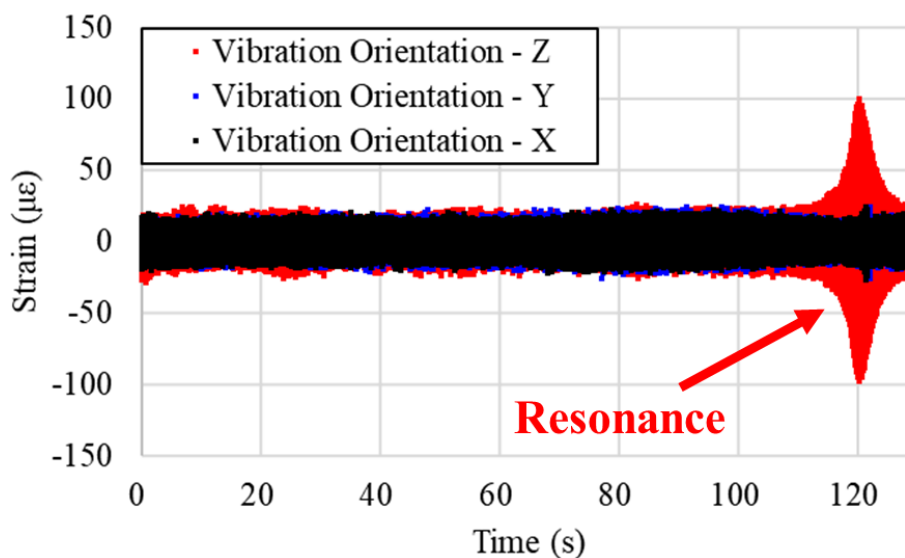
Figure 4.4: PCB Strain under different vibration orientation

2. Stress increment test

To find the failure margin in the suitable time frame, a test strategy is proposed in the figure 4.3. As the pre-defined parameters in the previous section, the stress increment test is performed by following the table 4.1. Additionally, the failure criteria of the test is set when the daisy chain resistance of component 1 or component 2 exceeds 1000Ω as mentioned in section 1.4.4

Pre-defined vibration parameters				
Type of vibration	Swept sine		Random	
With/without the heatsink	With	Without	With	Without
Stress orientation	Z	Z	Z	Z
Frequency range (Hz)	1400-2000	1200-1800	10-2000	10-2000

Table 4.1: Pre-defined vibration test parameters

As shown in table 4.2 and table 4.3, component 1 doesn't show failure during the stress increment test. Also, both component 1 and component 2 have no failure shown at the module level vibration test. However, component 2 is failed at the 15G sine sweep vibration test.

|	Component 1 (Board level)	Component 1 (Module level)	Component 2 (Board level)	Component 2 (Module level)
5G	No fail	No fail	No fail	No fail
10G	No fail	No fail	No fail	No fail
15G	No fail	No fail	Fail	No fail
20G	No fail	No fail	Not Tested	No fail

Table 4.2: Stress increment test result under sinusoidal sweep vibration

	Component 1 (Board level)	Component 1 (Module level)	Component 2 (Board level)	Component 2 (Module level)
5G	No fail	No fail	No fail	No fail
10G	No fail	No fail	No fail	No fail
15G	No fail	No fail	No fail	No fail
20G	No fail	No fail	No fail	No fail

Table 4.3: Stress increment test result under random vibration

- Post-define and results

1. Stress orientation

As shown in figure 4.4, the highest strain is measured when the electronic module is stressed at Z orientation. Therefore, Z orientation is chosen in the end.

2. Frequency range

As shown in figure 4.5 and figure 4.6, it is found that the board

degradation in resonance frequency is not out of the pre-defined frequency range at board level and module level. Therefore, the frequency range keeps the same as in the stress increment test for reliability test.
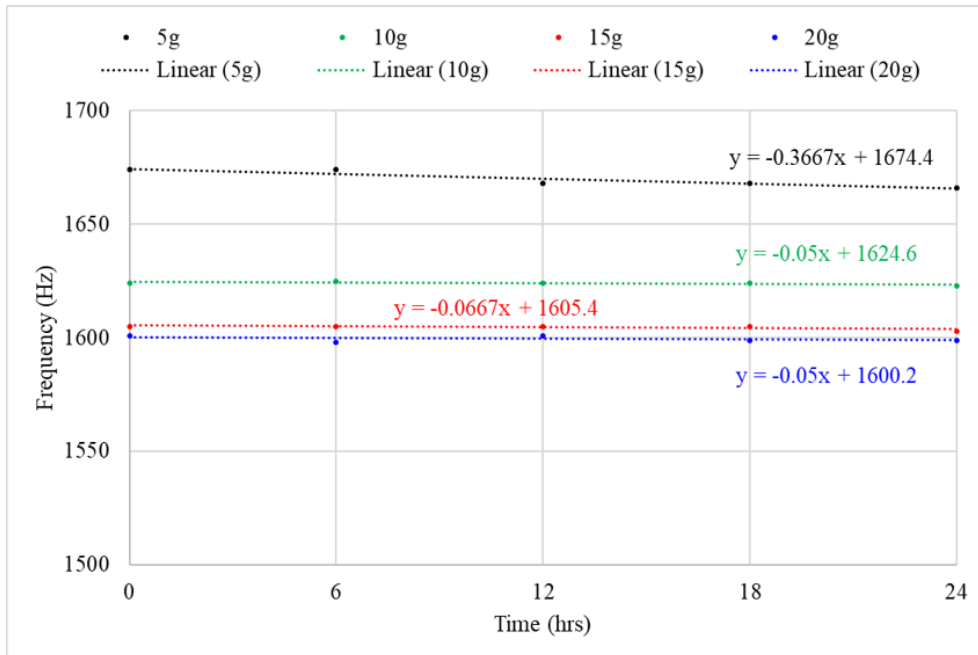
Figure 4.5: Aging process under vibration at module level
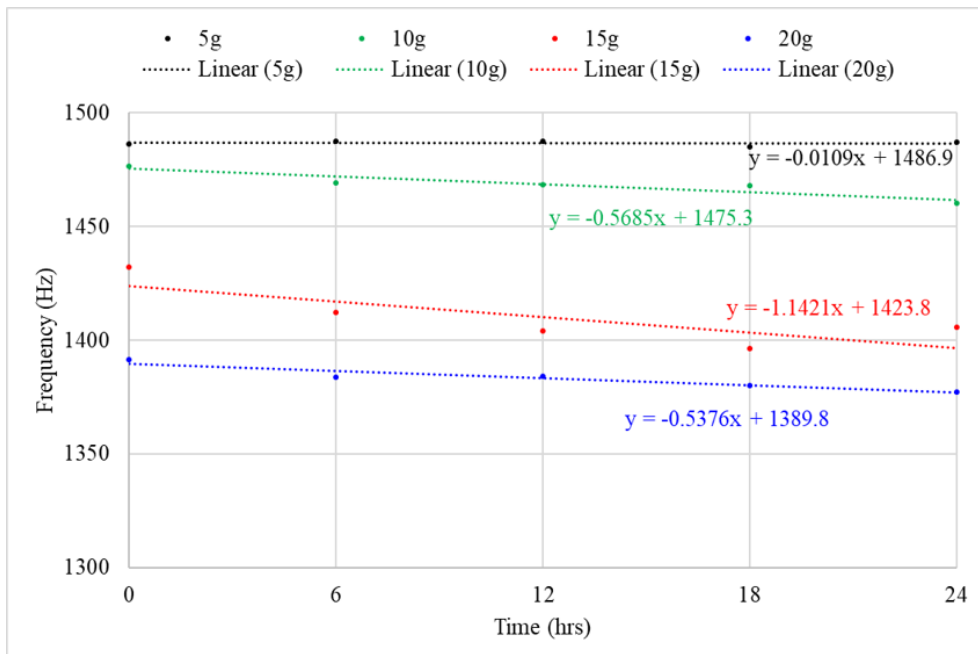
Figure 4.6: Aging process under vibration at board level

Besides this, it can be concluded that the degradation at the board level is more obvious than at the module level. The max-

imum degradation (22.5%) within 24 hours happens at board level swept sine 15G. This can be due to component failure causing the stiffness decrements. The results correlate with the strain degradation findings as shown in figure 4.7 and figure 4.8. The highest strain increase rate also happens at the board level with 15G input acceleration.
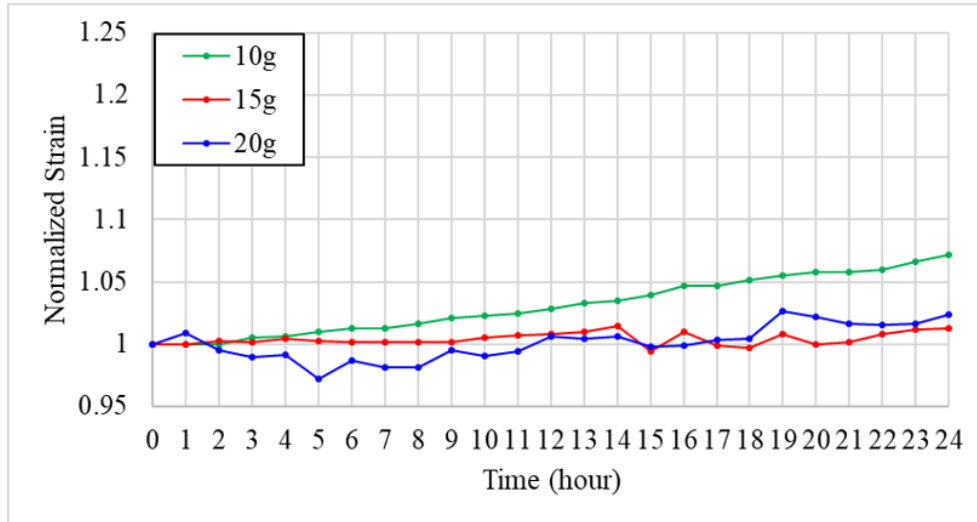
Figure 4.7: PCB strain degradation at module
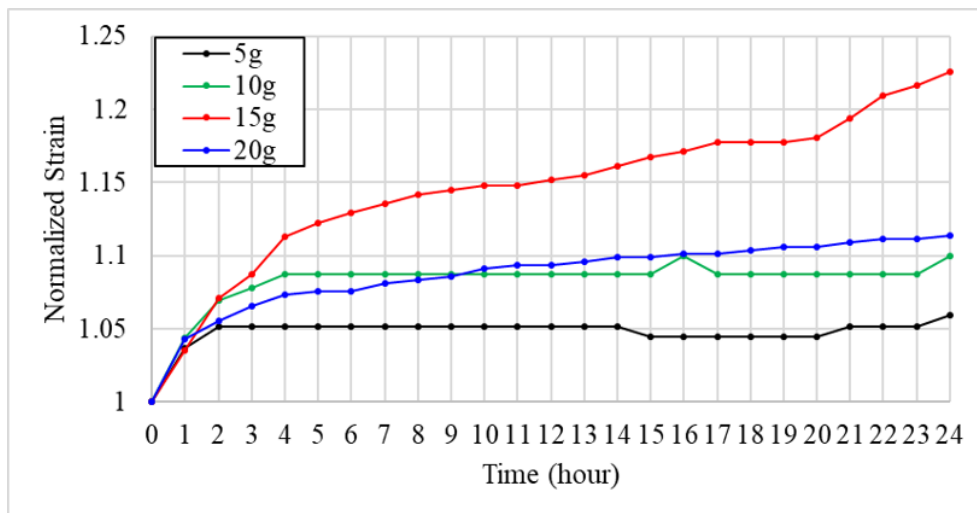
Figure 4.8: PCB strain degradation at board level

3. Type of vibration

As mentioned before, the most critical stress condition will be chosen for the reliability vibration test. In table 4.3, no failures at random vibration which can be summarized that the swept sine profile used on this board is more critical than the random profile. Therefore, swept sine is selected for the reliability test.

4. Acceleration level

In the stress increment test, component 2 fails at 15G input swept sine. As formerly mentioned, the stress level which failure happens will be selected for the reliability test, and one step lower for stress level will also be selected to perform the test.

5. With/without the heatsink

In table 4.2 and table 4.3, the failure is not found when the board is tested with heatsink. This can be due to that the board level vibration stress is higher than at module as shown in figure 3.17. As the result, the test will be performed without the heatsink.

4.2 RELIABILITY ASSESSMENT RESULTS

In the reliability test, 15 and 12 samples are tested under 10G and 15G input until component 1 or component 2 fail. The failure criteria are set at the resistance of the daisy chain over 1000Ω. The Weibull distribution is done for both component 1 and component 2. As shown in figure 4.9, 10G input has the $\beta = 0.86$. The shape factor here at 10G is low which is at the transition from early failure to random failure. At 15G input, the result shows that $\beta = 1.5$, similarly, this shape factor is low which is at the transition from random failure mechanism to wear-out failure mechanism. The characteristic life of component 2 at 10 G is at least enhanced by a factor of 20 compared to at 15G.
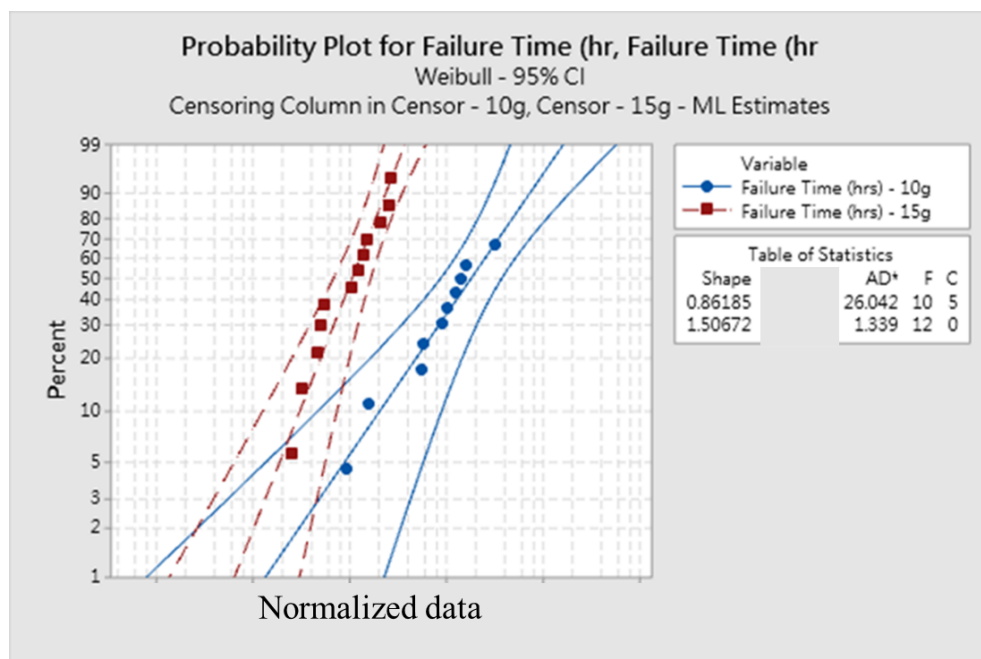
Figure 4.9: Weibull distribution of component 2 at 10G and 15G test result

In the 10G and 15G vibration tests, no failures occurred on component 1. In figure 4.10, the Weibayes analysis, characteristic lifetime estimation with 90% of the confidence bound is done for the component 1 at 10G and 15G input acceleration. According to the above results, it can be concluded that stress under 15G vibration is more critical than 10G vibration for both component 1 and component 2, and the risk for component 1 can be covered by component 2.
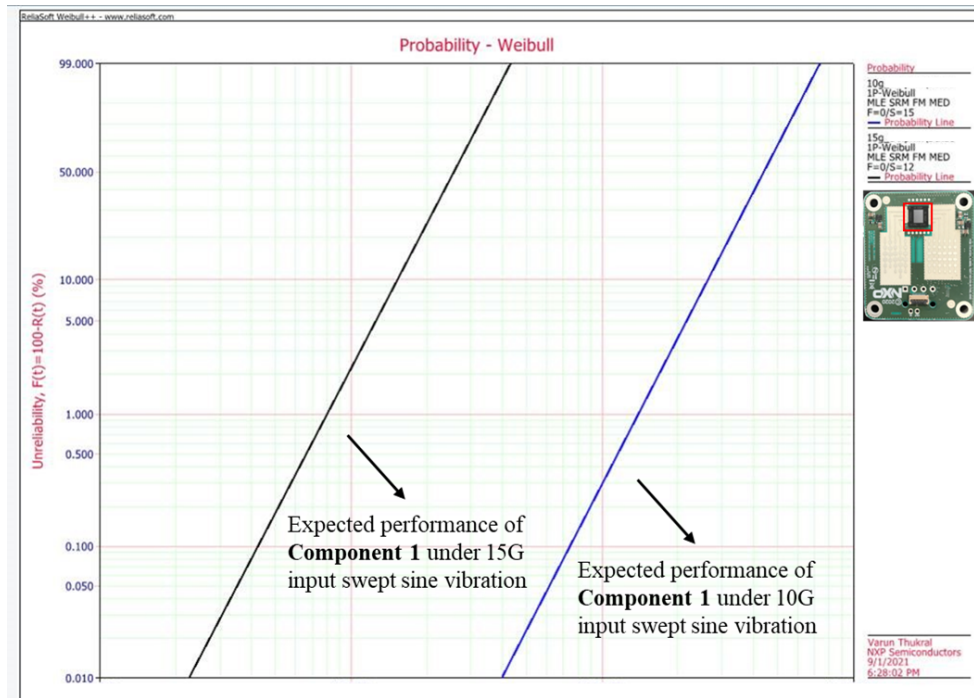
Figure 4.10: Weibayes distribution of component 1 at 10G and 15G input

4.3 FAILURE MODES AND MECHANISMS

The failure analysis is performed with the following techniques: C-SAM, LIT, and Cross-sectioning. As shown in figure 4.11 C-SAM and LIT will be done first to address the failure localization of the component. After the weakness of the component is localized, the cross-sectioning will be done on the sample from the first fail, and the last fail in the reliability test to explore the transition of failure mode.
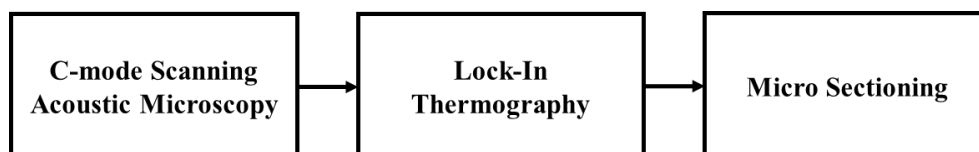
Figure 4.11: Failure analysis flow

In the C-SAM no component is found delaminated between the epoxy molding compound and die. In LIT analysis, an unstressed and passing component is used as a reference to obtain the signature of the components. As the figure 4.12 (B) shown, the color of the image took by thermography is evenly distributed on the package. The red spot is where the voltage fed into the component (Test Pad) which is not caused by failure.
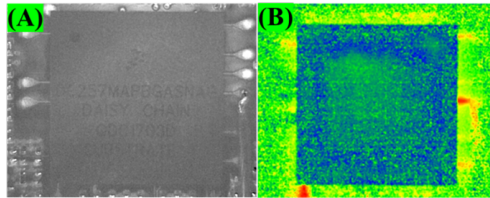
Figure 4.12: Reference board under LIT – component 2 (A) component view (B) LIT

The sinusoidal sweep at module level with step stress test from 5G to 20G shows no failure. As figure 4.12 shown, an evenly distributed color seen under LIT implies no failure found.
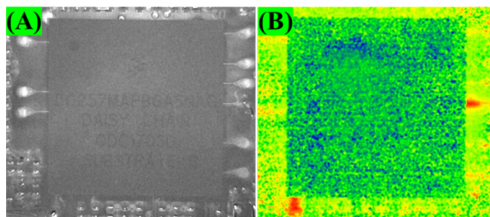
Figure 4.13: Component 2 test under step stress test at module level (A) component view (B) LIT

In figure 4.14 and figure 4.15, the failure component shows hot spot at the top right corner and bottom left corner. This hot spot may cause by the failure of the solder joint or PCB trace cracks. Therefore, the cross-section will be done on the first column on the right side and the first raw on the bottom side.
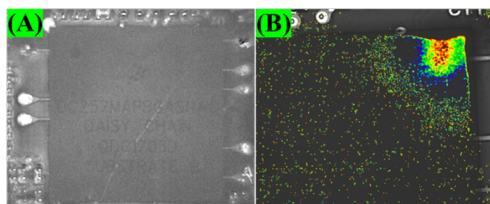
Figure 4.14: Component 2 test under step stress test at board level (A) component view (B) LIT
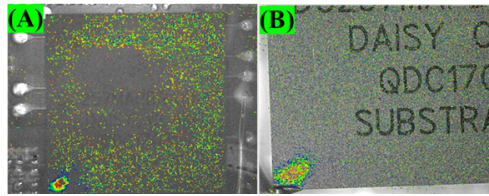
Figure 4.15: (A) LIT spot of 10G vibration reliability test (B) LIT spot of 15G vibration reliability test

In planar lapping, under 10G reliability test no PCB cracks are found as figure 4.16. Under the 15G reliability test, the first failure sample also has no PCB Cu trace cracks found.
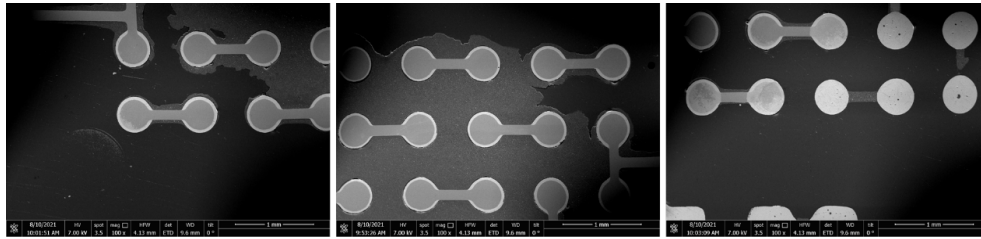
Figure 4.16: Planar lapping - 10G reliability test

Under cross-section, last fail sample from 15G reliability test three type of failure modes, solder crack and Intermetallic composites (IMC) crack both at the component side and PCB trace cracks are found in figure 4.17.
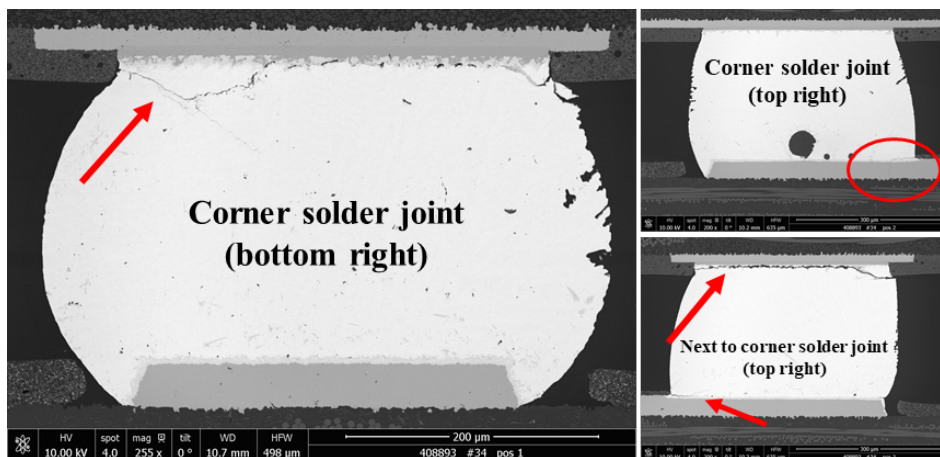
Figure 4.17: Cross-sectioning – Input 15G

However, a partial fracture within bulk solder was found on the samples under the 10G reliability vibration test as shown in figure 4.18. The possible failure mode is solder crack according to the results. Further failure analysis should be done to investigate the failure in the future.
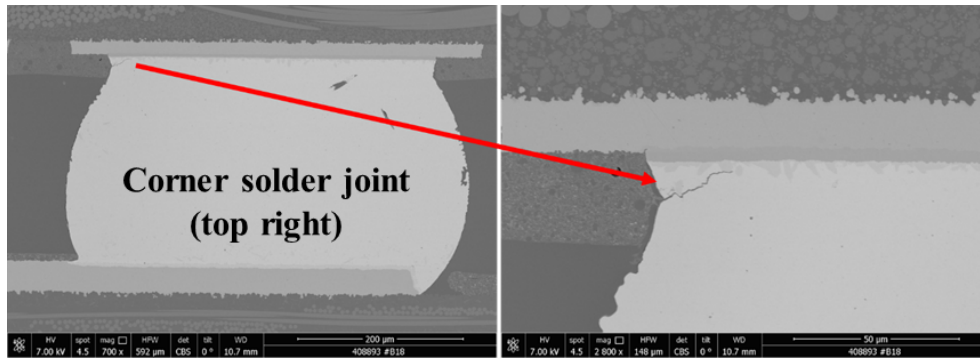
Figure 4.18: Cross-sectioning – Input 10G

In conclusion, the board is tested under 10G and 15G swept sine vibration. No PCB crack is found from the first fail sample at both stress levels. The last fail component at 10G is found partial fracture at bulk solder (possible to have complete solder crack) but no PCB crack. At 15G, mix fracture through IMC layer and bulk solder, and PCB trace crack is found in the last fail sample.

4.4 CORRELATION TO OTHER MECHANICAL TEST METHODS

Monotonic bent test and drop test are also performed on component 2. The drop test setup in [35] test method C is referred to. As the figure is shown, the PCB trace cracks are found in the bending test with strain 7485 and strain rate $0.005s^{-1}$. In the drop test, the complete fracture within IMC is found with strain rate $5.66s^{-1}$ in figure 4.20.
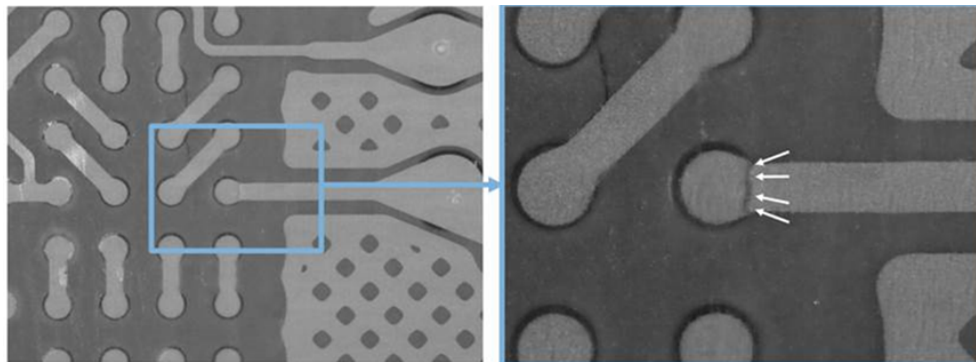
Figure 4.19: Cross-sectioning of component 2 under Monotonic bend testing
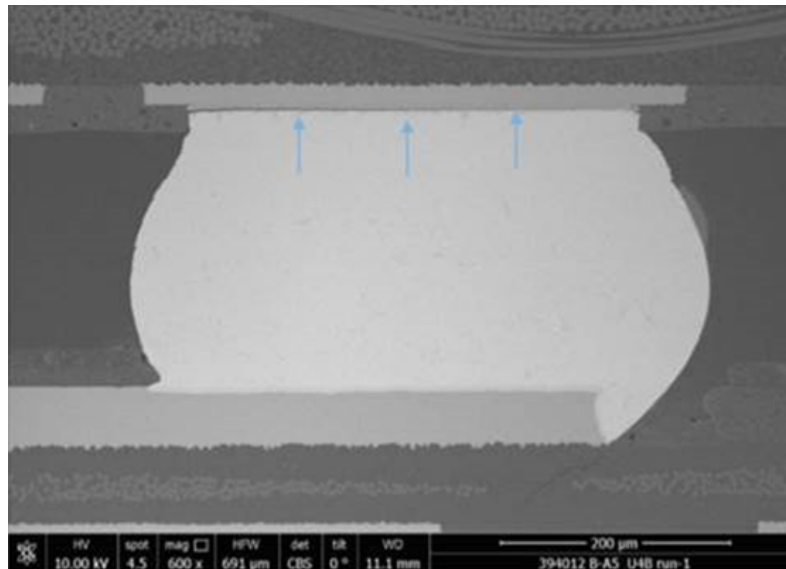
Figure 4.20: Cross-sectioning of component 2 under board level drop test

As the result shown above, it can be concluded that the transition in failure mode from solder crack to IMC crack with the strain rate and strain increasing. This can be due to the IMC is normally a brittle material. The strength will decrease with the strain rate increase. A similar phenomenon is found in the [22].

	Bending test	15G vibration	Drop test
Strain rate	0.005	2.6	5.7
Strain	7485	325	2175
Failure mode	1. PCB trace cracks	1. Mix fracture through IMC layer and bulk solder at package side. 2. PCB trace cracks.	1. IMC cracks at package side.

Table 4.4: Summary of mechanical test result of component 2

In figure 4.21, the strain rate is observed that increases with the input acceleration level rising. Also, in session 3.1.1, it is mentioned that the acceleration measured on the PCB increases with the input acceleration increasing. Therefore, it is convincing that the acceleration measured on the board higher will show a larger strain rate on the board. The failure mode will tend to happen with IMC for this package.
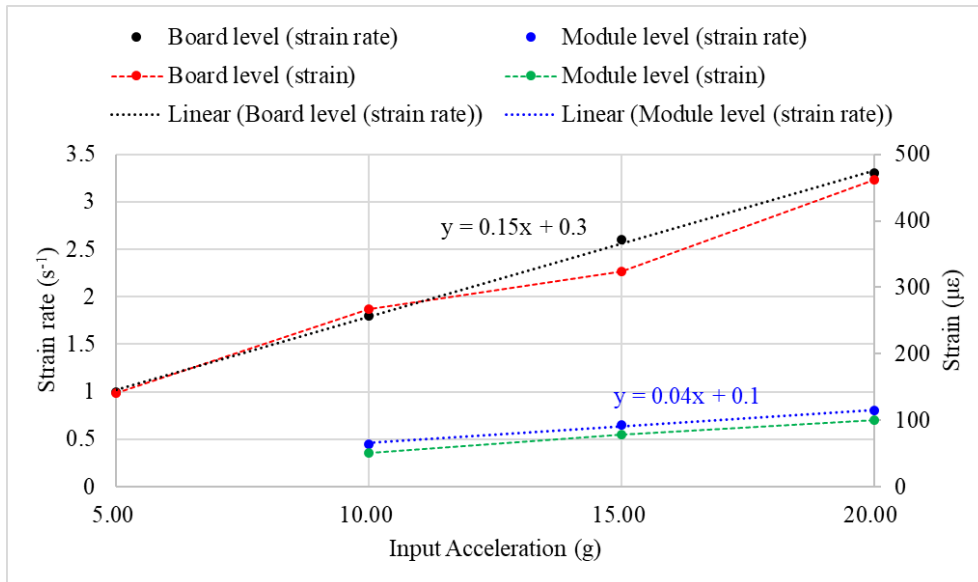
Figure 4.21: Strain rate and strain at different input acceleration

The plastic housing structure in figure 3.9 which has a larger amplification factor. The customized board 1 is also tested in that plastic housing structure. As expected, the level of acceleration is amplified due to the housing structure. This will cause a higher strain and strain rate as the conclusion from the previous session.
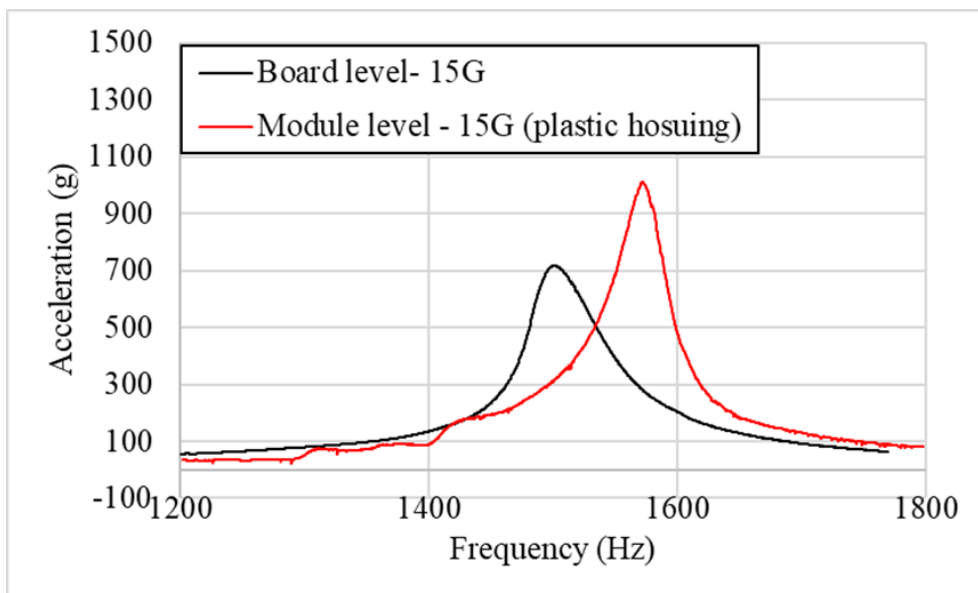
Figure 4.22: PCB vibration dynamic response in customized housing 2

As figure 4.23 shown, not only complete solder crack is found at the component side in the corner solder joint, but also complete IMC crack is found at the PCB side. Also, some partial fractures initial from the IMC. This correlates to the previous conclusion.
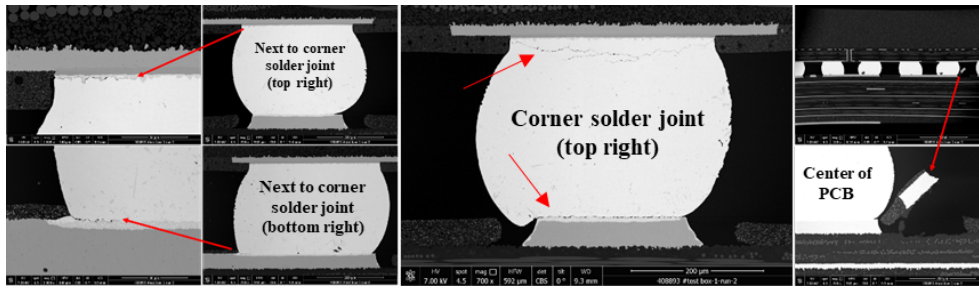
Figure 4.23: Cross-sectioning of component 2 in customized housing 2

5 | CONCLUSION AND FUTURE WORK

5.1 CONCLUSION

Revolutionary changes in the automotive industry toward fully connected electrical vehicles are changing the world of board-level reliability (BLR) vibration testing. It is taking BLR tests beyond board level to board module level. From this thesis, the impact of sensors such as MEMS-based accelerometer, LASER, piezoelectric accelerometer, and strain gauge are demonstrated. The influence of module elements on board vibration response is also introduced. In the end, the board degradation during the vibration is explored by different sensors. According to these results, the following conclusions are summarized:

- This study can be used as a reference for chip suppliers to answer the module developers' questions related to vibration risks. Also, it shows that housing induces the maximum impact on vibration response.

- Using the accelerometer, contact-based measurement method on this application-specific PCB in this thesis is not the most appropriate sensor to measure the board dynamic response. LASER can measure the board response without perturbing the motion at both board level and module level. The strain gauge is another reliable measurement method that can be used on this board under vibration.

- Module elements, housing structure, TIM, motion restricting frame and boundary frame are crucial especially for the product will be stressed under vibration. Some of these design elements can decrease the stress level, but some can induce more stress on the board. To conclude, TIM, a motion restricting frame can effectively reduce the stress level on the board. A housing structure can either amplify or reduce the response on the board as shown in figure 3.9 and figure 3.17.

- The selected reliability test condition is expected to cover the vibration risk for vibration measured in the field application.

- This automotive PCB radar module degrades more when tested under board level swept sine experiment (maximum at 15G).

The reliability margin for component 1 is bigger than component 2 and the transition in failure mode from solder crack to IMC crack with the strain and strain rate increasing.

5.2 RECOMMENDATIONS AND FUTURE WORK

The research done in the thesis investigates the reliability performance and PCB mechanical behavior under vibration loading at board level and module level. The following recommendations and future works can be furtherly explored:

- In section 2.4, the impact of the accelerometer is discovered that it is not a proper measurement method for the board used in this thesis. However, various PCBs are used for different purposes of reliability tests in different companies. There is no guidance in terms of PCB weight, dimension, and material property (Young's modulus and Poisson ratio) to indicate whether the accelerometer will cause a significant impact on the measurement result. Upcoming board-level specification is recommended to include the instruction of measurement method. The correlation between measurement method and PCB characteristics should be evaluated.

- An electronic radar module can have various constructions. In this thesis, the impact of thermal interface material, motion restricting from, housing material, and edge frame on the board vibration response have been discovered. The influence from other elements such as stacked PCB configuration, sealant, and radome, etc. should be assessed in the future.

- In section 4.1, vibration experimental parameters are recorded and analyzed during the reliability test. However, the environmental parameters such as temperature, humidity, and air pressure haven't been considered in the test. The degradation of board shift in resonant frequency, changes in strain measured on the PCB is expected to be different. Besides, the construction of the module can also play an important role under vibration stresses. The correlation between board degradation and module construction should be furtherly studied.

- The purpose of investigating and collecting the vibration data in different structures aims at a bigger picture. In current technology, it is still a challenge that the failure that happened on a device cannot be precisely predicted. Data-driven vibration reliability brings up a potential solution. The vibration response

can be recorded by MEMS based accelerometer and processed by a machine learning algorithm. Once the board character parameters are out of the normal range, the failure should be capable of detecting. However, a parameter that can effectively be related to the failure must be furtherly explored.

- The vibration data should be collected on more critical housing construction and in the field during car operation. This data can furtherly be used in the lab to simulate the vibration risk and to develop board-level vibration standards.

BIBLIOGRAPHY

[1] R. A. Amy, G. S. Aglietti, and G. Richardson. "Board-Level Vibration Failure Criteria for Printed Circuit Assemblies: An Experimental Approach". In: *IEEE Transactions on Electronics Packaging Manufacturing* 33.4 (2010), pp. 303–311. DOI: 10.1109/TEPM.2010.2084092.

[2] Aptiv Corp. *SRR6 Family of Corner/Side Radars*. URL: https://www.aptiv.com/images/default-source/advanced-safety/srr-product.tmb-customimg.jpg?sfvrsn=ce53163d_3.

[3] Bergquist Corp. *Sil Pad 2000*. URL: https://docs.rs-online.com/3a07/0900766b8038a183.pdf.

[4] Bosch Corp. *Long-range radar sensor*. URL: https://www.bosch.com/stories/making-the-most-of-car-time/.

[5] Continental Corp. *Advanced Radar Sensor - ARS510*. URL: https://www.continental-automotive.com/getattachment/bc2cd747-8874-4a9f-86cf-eba031c7d747/attachment.aspx?width=500.

[6] Denso Corp. *Submillimeter-wave Radar Sensor*. 2017. URL: http://psce.pw/3pukqf.

[7] Hella Corp. *Forth generation Hella radar sensor*. URL: https://www.hella.com/partnerworld/us/Product-range/Electronics/Radar-sensors-6088/.

[8] Laird Corp. *TflexTM HD400 Series Thermal Gap Filler*. URL: https://www.micro-semiconductor.com/datasheet/5e-A17713-06.pdf.

[9] NXP Semiconductors Corp. *TEF810x Fully-Integrated 77 GHz Radar Transceiver*. 2019. URL: https://www.nxp.com/products/radio-frequency/radar-transceivers/tef810x-fully-integrated-77-ghz-radar-transceiver:TEF810X.

[10] General Motors Corporation. *General Specification for Electrical/-electronic Component Analytical/development/validation (A/D/V) Procedures for Conformance to Vehicle Environmental, Reliability, and Performance Requirements*. General Motors Corporation, 2007. URL: https://books.google.nl/books?id=TV2AYgEACAAJ.

[11] G.R. Ed. Blackwell. *The Electronic Packaging Handbook*. 2000.

[12] Jie Gu, D. Barker, and M. Pecht. "PROGNOSTICS OF ELECTRONICS UNDER VIBRATION USING ACCELERATION SENSORS". In: 2008.

[13] IPC - Association Connecting Electronics Industries. *Printed Circuit Assembly Strain Gage Test Guideline (English Language), 9704A*. IPC International, 2012. ISBN: 9781611930368. URL: https://books.google.nl/books?id=2qx%5C_zgEACAAJ.

[14] Institute for Interconnecting and Packaging Electronic Circuits. *Implementation of Flip Chip and Chip Scale Technology*. Joint industry standard. IPC, 1996. URL: https://books.google.nl/books?id=H-zltgAACAAJ.

[15] J. Jalink et al. "Effect of PCB and Package Type on Board Level Vibration Using Vibrational Spectrum Analysis". In: *2017 IEEE 67th Electronic Components and Technology Conference (ECTC)*. 2017, pp. 470–475. DOI: 10.1109/ECTC.2017.146.

[16] *JAPANESE INDUSTRIAL STRANDARD: Vibration testing methods for automobile parts (JIS D 1601)*. Japanese Standards Association, 1995.

[17] *JESD22-B103-B: Vibration, Variable Frequency*. JEDEC Solid State Technology Association, 2006.

[18] K.C. Kapur and M. Pecht. *Reliability Engineering*. Wiley Series in Systems Engineering and Management. Wiley, 2014. ISBN: 9781118140673. URL: https://books.google.nl/books?id=GI8NAwAAQBAJ.

[19] Hocheol Kwak and Todd Hubing. *An Overview of Advanced Electronic Packaging Technology*. Mar. 2007.

[20] A. Falk L. Marsavina and O. Pop. "Analysis of Printed Circuit Boards strains using finite element analysis and digital image correlation". In: *Frattura ed Integrità Strutturale*. Vol. 14. 51. 2019, pp. 541–551.

[21] Pradeep Lall, Vikas Yadav, and David Locker. "Sustained High-Temperature Vibration Reliability of Thermally Aged Leadfree Assemblies in Automotive Environments". In: Feb. 2020, pp. 1–18. DOI: 10.23919/PanPacific48324.2020.9059339.

[22] Minyi Lou et al. "The effect of strain rate and strain range on bending fatigue test". In: *2008 International Conference on Electronic Packaging Technology High Density Packaging*. 2008, pp. 1–5. DOI: 10.1109/ICEPT.2008.4607132.

[23] P. Matkowski and I Brabandt. "Modal analysis of board vibration during mechanical reliability tests of lead-free solder joints". In: *2012 4th Electronic System-Integration Technology Conference*. 2012, pp. 1–7. DOI: 10.1109/ESTC.2012.6542092.

[24] *MIL-STD-810: Environmental Engineering Considerations and Laboratory Tests*. US Military. US Military, 2000. URL: https://books.google.nl/books?id=-FTlcQAACAAJ.

[25] Polska. Polski Komitet Normalizacyjny. *Environmental Testing - Part 2-64: Tests -Test Fh: Vibration, Broadband Random and Guidance*. PKN, 2008. ISBN: 9788325168810. URL: https://books.google.nl/books?id=32gbuAAACAAJ.

[26] Internationale Organisation für Normung. *Road Vehicles - Environmental Conditions and Testing for Electrical and Electronic Equipment: Part 3: Mechanical Loads*. International standard. ISO, 2012. URL: https://books.google.nl/books?id=hfiojwEACAAJ.

[27] E P Popov (Egor Paul), Sammurthy Nagarajan, and Z A Lu (Zung An). *Mechanics of materials*. Englewood Cliffs, N.J. : Prentice-Hall, 1976.

[28] IPC. Product and reliability committee. STM attachment reliability test methods task group. *Performance Test Methods and Qualification Requirements for Surface Mount Solder Attahments: IPC-9701A*. IPC, 2006. URL: https://books.google.nl/books?id=3QY8oAEACAAJ.

[29] Roucou R. et al. "Effect of Environmental and Testing Conditions on Board Level Vibration". In: *2016 IEEE 66th Electronic Components and Technology Conference (ECTC)*. 2016, pp. 1105–1111. DOI: 10.1109/ECTC.2016.184.

[30] Hong-Bin Shi and Toshitsugu Ueda. "Investigation on the optimum sampling rate of strain measurement during printed circuit board (PCB) system assembly". In: *2011 IEEE 13th Electronics Packaging Technology Conference*. 2011, pp. 579–584. DOI: 10.1109/EPTC.2011.6184487.

[31] Richard van silfhout et al. "Designing for 1(st) and 2(nd) level reliability of micro-electronic packages using combined experimental - Numerical techniques". In: vol. 2006. Jan. 2006, 7 pp. ISBN: 1-4244-0152-6. DOI: 10.1109/ECTC.2006.1645774.

[32] Malaysia. Jabatan Standard. *Environmental Testing: Tests - test FI: vibration - mixed mode (IEC 60068-2-80:2005, IDT)*. Malaysian standard 2-80. Department of Standards Malaysia, 2011. URL: https://books.google.nl/books?id=U-w0ngEACAAJ.

[33] D.S. Steinberg. *Vibration analysis for electronic equipment*. John Wiley and Sons, 2000.

[34] Varun Thukral et al. "Assessment of Accelerometer Versus LASER for Board Level Vibration Measurements". In: *2019 IEEE 69th Electronic Components and Technology Conference (ECTC)*. 2019, pp. 1339–1346. DOI: 10.1109/ECTC.2019.00208.

[35] Varun Thukral et al. "Understanding the Impact of PCB Changes in the Latest Published JEDEC Board Level Drop Test Method". In: *2018 IEEE 68th Electronic Components and Technology Conference (ECTC)*. 2018, pp. 756–763. DOI: 10.1109/ECTC.2018.00117.

[36] M. Vellvehi et al. "Lock-in Infrared Thermography: A tool to locate and analyse failures in power devices". In: *2017 Spanish Conference on Electron Devices (CDE)*. 2017, pp. 1–4. DOI: 10.1109/CDE.2017.7905234.

[37] Dongji Xie et al. "Duplicable and effective — A new drop test for BGA assemblies". In: *2015 IEEE 65th Electronic Components and Technology Conference (ECTC)*. 2015, pp. 417–424. DOI: 10.1109/ECTC.2015.7159626.

[38] Liu Yang et al. "Harmonic vibration test for accelerated reliability assessment of board level packaging". In: *2012 7th International Forum on Strategic Technology (IFOST)*. 2012, pp. 1–5. DOI: 10.1109/IFOST.2012.6357731.

A | APPENDICES

A.1 INDUSTRIAL VIBRATION SPECIFICATION DETAILS

IEC 60068-2-64 Spectrum A.3:

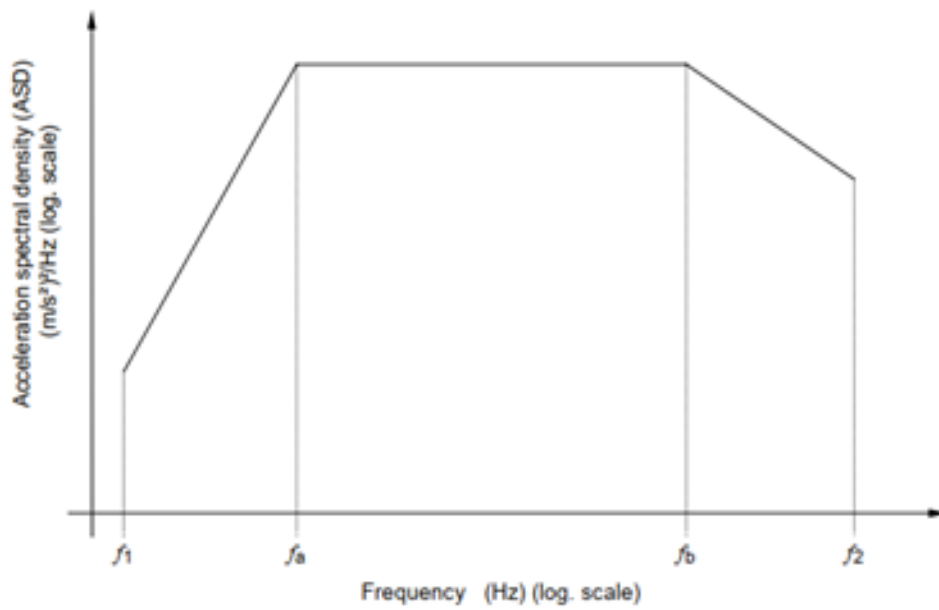**Figure A.1:** Vibration profile - equipment in wheeled vehicles [25]

Category	f_1	$ASDf_1$	f_a	$f_{\text{-}b}$	$ASDf_a,f_b$	f_2	$ASDf_2$	a_{rms}
No.	Hz	$(m/s^2)^2$/Hz	Hz	Hz	$(m/s^2)^2$/Hz	Hz	$(m/s^2)^2$/Hz	m/s^2
1	10	10	10	50	10	1000	0.1	33.8
2a	5	0.4	11	15	4	200	0.1	11
2b	5	0.15	12	18	0.9	200	0.07	6.7
2c	5	0.15	10	15	1.9	200	0.15	10

Table A.1: Break points for spectrum of - equipment in wheeled vehicles [25]
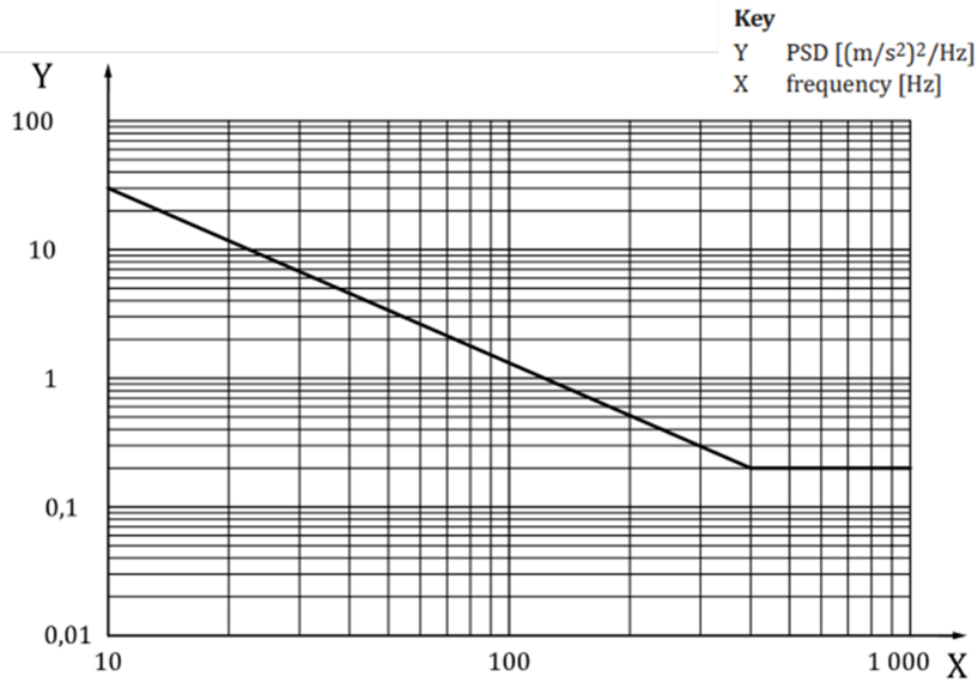
ISO 16750-3 4.1.2.4:

Figure A.2: Vibration profile – Passenger car, sprung masses [26]

Frequency (Hz)	PSD [(m/s^2)^2/Hz]
10	30
400	0.2
1000	0.2

Table A.2: Break points for spectrum of ISO 16750-3 4.1.2.4 [26]

ISO 16750-3 4.1.2.5:
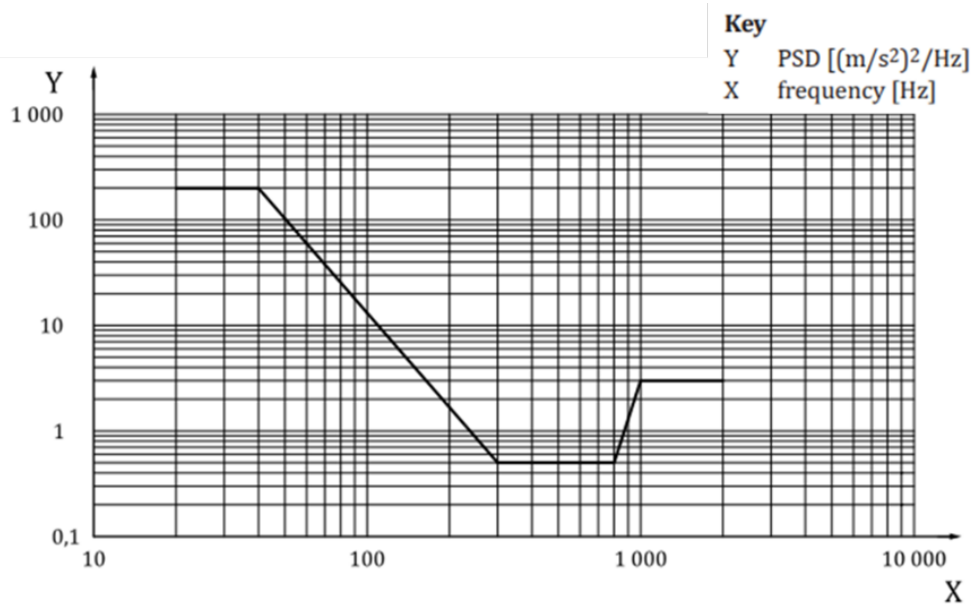
Figure A.3: Vibration profile – Passenger car, unsprung masses [26]

Frequency (Hz)	PSD [(m/s²)²/Hz]
20	200
40	200
300	0.5
800	0.5
1000	3
2000	3

Table A.3: Break points for spectrum of ISO 16750-3 4.1.2.5 [26]

ISO 16750-3 4.1.2:

Key

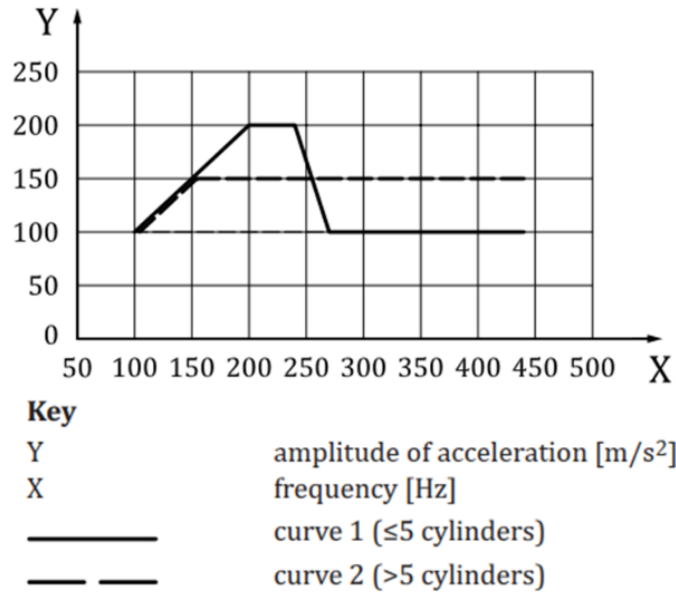| Y	amplitude of acceleration [m/s²]
X	frequency [Hz]
———	curve 1 (≤5 cylinders)
—— ——	curve 2 (>5 cylinders)

Figure A.4: Vibration profile – Passenger car, engine [26]

MIL-STD-819G Method 514.6 Annex C:
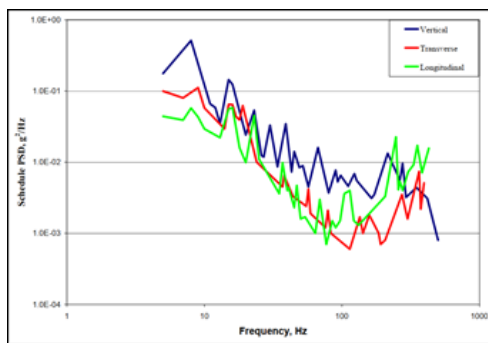
Figure A.5: Vibration profile – wheeled vehicle vibration exposure [24]

Vertical		Transverse		Longitudinal	
Frequency, Hz	PSD, g²/Hz	Frequency, Hz	PSD, g²/Hz	Frequency, Hz	PSD, g²/Hz
5	0.2252	5	0.0736	5	0.0521
8	0.5508	6	0.0438	7	0.1046
10	0.0509	7	0.0761	8	0.1495
13	0.0253	13	0.0130	13	0.0140
15	0.0735	15	0.0335	16	0.0503
17	0.0501	16	0.0137	18	0.0200
18	0.0319	21	0.0102	19	0.0342
19	0.0402	23	0.0268	20	0.0160
20	0.0566	25	0.0090	23	0.0378
43	0.1004	28	0.0090	27	0.0079
50	0.0508	30	0.0137	30	0.0208
102	0.0740	34	0.0055	32	0.0100
109	0.1924	37	0.0081	33	0.0267
117	0.0319	46	0.0039	35	0.0065
138	0.0869	51	0.0068	51	0.0040
150	0.0286	55	0.0042	53	0.0081
190	0.0605	106	0.0033	56	0.0035
263	0.0613	108	0.0045	59	0.0066
332	0.0097	111	0.0033	63	0.0037
360	0.0253	148	0.0030	65	0.0127
452	0.0053	163	0.0054	73	0.0026
500	0.0045	175	0.0023	93	0.0117
		235	0.0013	109	0.1635
		262	0.0028	120	0.0180
rms = 4.43 g		265	0.0025	132	0.0320
		317	0.0016	138	0.0738
		326	0.0057	153	0.0236
		343	0.0009	158	0.0549
		384	0.0018	164	0.0261
		410	0.0008	185	0.0577
		462	0.0020	257	0.0062
		500	0.0007	280	0.0032
				304	0.0068
		rms = 1.30 g		323	0.0045
				343	0.0193
				386	0.0014
				444	0.0054
				476	0.0018
				490	0.0046
				500	0.0014
				rms = 2.86 g	

Table A.4: Break point of spectrum of MIL-STD-819G Method 514.6 Annex C [24]
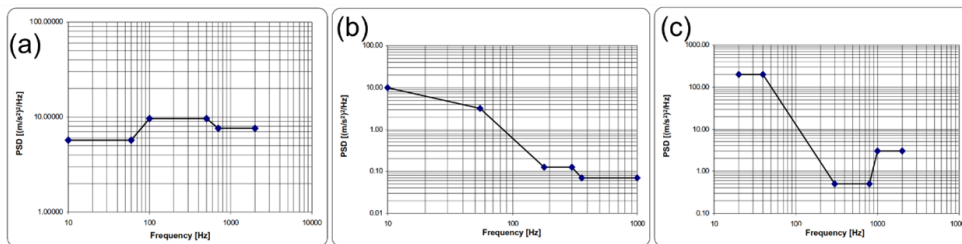
GMW 3172:

Figure A.6: Vibration profile – (a) 9.3.1.1 (b) 9.3.1.2 (c) 9.3.1.3 [10]

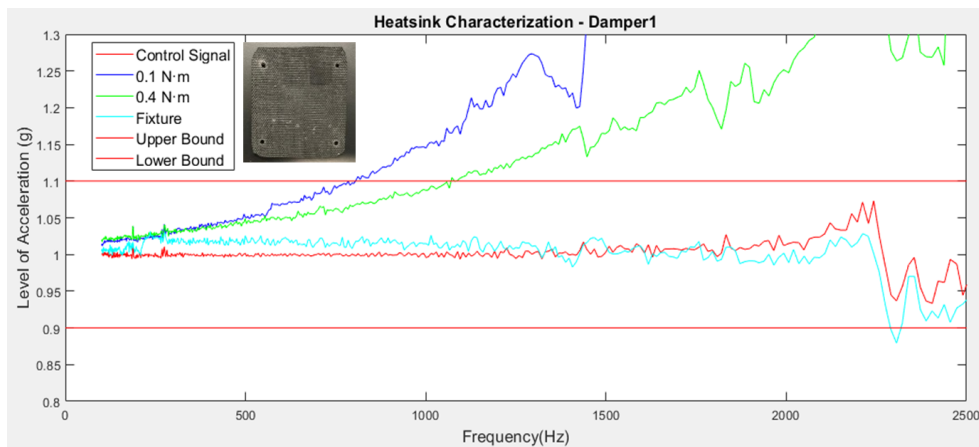## A.2 ELECTRONIC MODULE VIBRATION CHARAC– TERIZATION WITH DAMPER

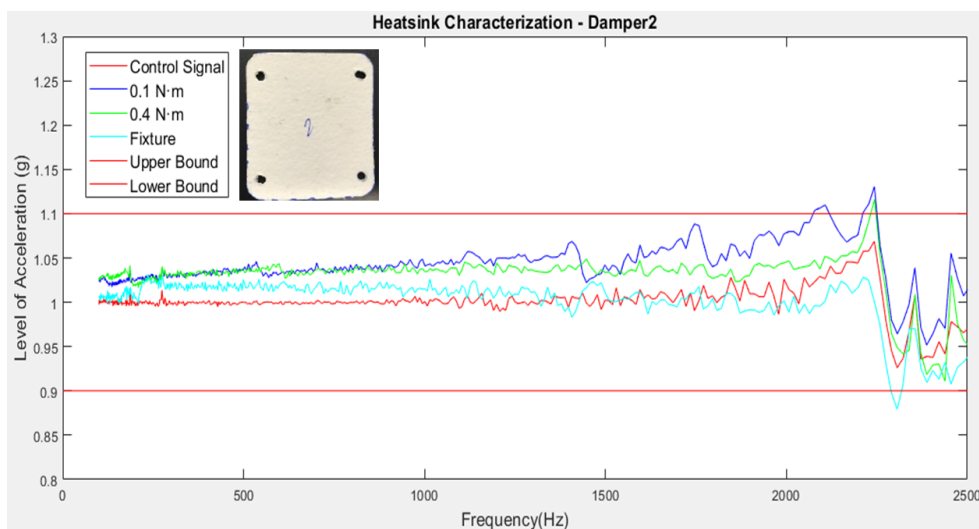**Figure A.7:** Heatsink vibration response with damper-1

Figure A.8: Heatsink vibration response with damper-2
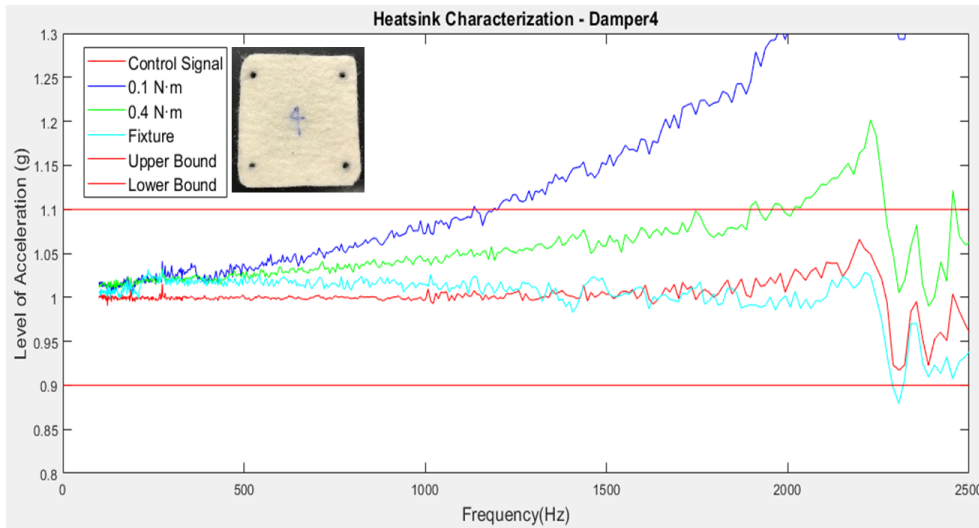
Figure A.9: Heatsink vibration response with damper-4

A.3 ADDITIONAL INFORMATION

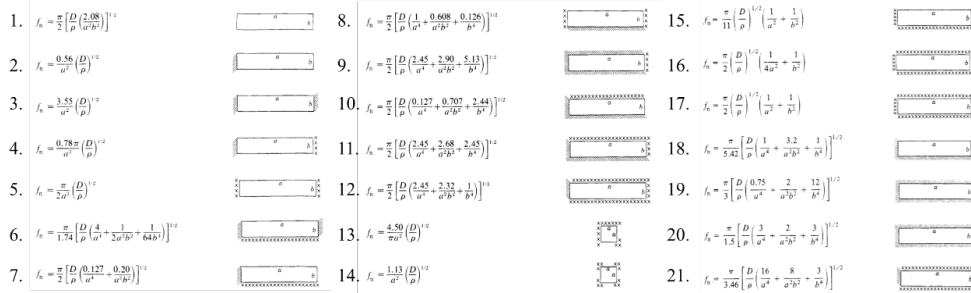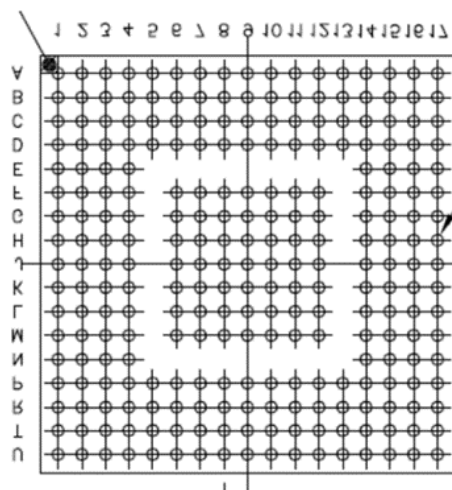**Figure A.10:** Resonant frequency equations for uniform plates [33]

Figure A.11: Numbering solder joints for component 2